

# AUS Repository

## Low Power Wireless Subcutaneous Transmitter

Item Type	Thesis
Authors	Ali, Mai
Download date	2026-03-07 06:02:08
Link to Item	<a href="http://hdl.handle.net/11073/2723">http://hdl.handle.net/11073/2723</a>

LOW POWER WIRELESS SUBCUTANEOUS TRANSMITTER

A THESIS IN ELECTRICAL ENGINEERING  
*Master of Science in Electrical Engineering*

Presented to the faculty of the American University of Sharjah  
College of Engineering  
in partial fulfilment of  
the requirements for the degree

MASTER OF SCIENCE

by  
MAI ALI  
B.S. 2008

Sharjah, UAE  
December 2010

©2010

MAI ALI

ALL RIGHTS RESERVED

---

# LOW POWER WIRELESS SUBCUTANEOUS TRANSMITTER

Mai Ali, Candidate for the Master of Science Degree

American University of Sharjah, 2010

## ABSTRACT

Low power wireless transmitters are finding applications in diverse fields. A field that is expressing a noticeable growth is biomedical telemetry, where a wireless transmitter accompanied with sensors is used to measure different physiological parameters. The design of low power transmitters, especially when intended for biomedical applications, is limited by a set of constraints ranging from signal interaction with biological tissues, ensuring biocompatibility of design materials, design complexity to power supply methodology.

The objective of this thesis is to design a low power wireless subcutaneous transmitter that can be used for biotelemetry applications. The novelty of this work resides in using low power system and circuit techniques to achieve the objective of low power consumption. The RF signal interaction with biological tissue under investigation i.e. subcutaneous tissue is characterized. The loss in signal power due to propagation through the skin is determined as well as maximum energy absorption that complies with the defined safety limits. In order to compensate for the signal power loss, an efficient class E power amplifier (PA) is designed. A direct modulation transmitter architecture is proposed that incorporates the carrier generation and data modulation into a single unit which not only decreases the system power consumption but also reduces its complexity to achieve the goal of miniaturization. An inductive link is proposed for power supplying the implantable transmitter for which another class E PA was designed to from a class E power transmitter.

---

## PUBLICATIONS

- [1] M. Ali, L. Albasha, and H. Alnashash, "A system study of a wireless subcutaneous transmitter," *Int. Symp. Mechatronics and its Applications*, Sharjah, pp. 1-6, Apr. 2010.
- [2] M. Ali, L. Albasha, H. Alnashash, "A Bluetooth low energy implantable glucose monitoring system", submitted for publication, *European Microwave Conf.*, Manchester, Oct., 2011.

---

## CONTENTS

ABSTRACT.....	iii
PUBLICATIONS .....	iv
LIST OF ILLUSTRATIONS .....	vii
LIST OF TABLES.....	ix
ACKNOWLEDGEMENTS.....	x
INTRODUCTION .....	1
1.1 DEFINITION OF LOW POWER WIRELESS TRANSMITTERS .....	1
1.2 APPLICATIONS OF LOW POWER WIRELESS TRANSMITTERS.....	1
1.3 MOTIVATION .....	2
1.4 CHALLENGES WITH IMPLANTABLE TRANSMITTERS DESIGN .....	3
1.5 OBJECTIVE.....	4
1.6 THESIS CONTRIBUTION AND OUTLINE .....	5
LITERATURE REVIEW .....	7
2.1 BRIEF HISTORY OF MEDICAL IMPLANTS COMMUNICATION .....	7
2.2 DESIGN CONSTRAINTS OF IMPLANTABLE DEVICES .....	8
2.2.1 <i>Ultra Low Power Consumption</i> .....	8
2.2.2 <i>Low Power Implantable Wireless Transmitter Requirements</i> .....	9
2.2.3 <i>The Human Body as a Medium</i> .....	12
2.2.4 <i>Communication Methods</i> .....	13
2.3 LOW POWER TRANSMITTERS SYSTEM ARCHITECTURE TRENDS .....	16
2.3.1 <i>Ultra Wideband Transceivers</i> .....	16
2.3.2 <i>RFID, Subsampling and Super-Regenerative Architectures</i> .....	17
2.3.3 <i>Spread Spectrum Systems</i> .....	18
2.4 STATE OF THE ART OF IMPLANTABLE TRANSMITTERS .....	19
2.4.1 <i>Glucose Sensors</i> .....	20
2.4.2 <i>Commercially Available Continuous Glucose Monitoring Systems</i> .....	22
SYSTEM ARCHITECTURE .....	24
3.1 FREQUENCY REGULATION .....	25
3.1.1 <i>FCC requirements for ISM bands</i> .....	27
3.1.2 <i>Wireless Protocols in 2.4 GHz ISM Band</i> .....	29
3.1.3 <i>Bluetooth Low Energy Protocol</i> .....	30
3.2 TRANSMITTER DESIGN PRINCIPLES .....	31
3.2.1 <i>Design Methodology</i> .....	32
3.2.2 <i>Transmitter Architectures</i> .....	33

---

3.2.3	<i>Direct Modulation Implementation</i> .....	34
3.2.4	<i>Phase Locked Loop (PLL)</i> .....	36
3.3	SYSTEM ARCHITECTURE .....	37
3.3.1	<i>Bluetooth Low Energy Transmitter</i> .....	38
3.3.2	<i>Power Amplifier Design</i> .....	41
3.3.3	<i>Low Power Circuit Techniques</i> .....	42
3.3.4	<i>Power Supply Methodology</i> .....	44
	TRANSMITTER DESIGN AND SIMULATION RESULTS.....	46
4.1	RF SIGNAL –BIOLOGICAL TISSUE INTERACTION .....	47
4.1.1	<i>Energy Absorption</i> .....	47
4.1.2	<i>Signal Propagation and Attenuation</i> .....	50
4.2	CLASS E PA CIRCUIT DESIGN .....	52
4.2.1	<i>Design Parameters</i> .....	53
4.2.2	<i>Circuit Simulation and Results</i> .....	56
4.3	EXTERNAL POWER UNIT .....	66
4.3.1	<i>Distinction between Near and Far Fields</i> .....	66
4.3.2	<i>Simulation Results</i> .....	69
4.4	DIRECT MODULATION ARCHITECTURE.....	71
4.4.1	<i>PLL Design</i> .....	72
4.5	LOW POWER TRANSMITTER SIMULATION AND RESULTS.....	83
4.5.1	<i>Spectrum Mask Test</i> .....	87
4.6	SYSTEM FUNCTIONALITY SCENARIO .....	87
4.6.1	<i>Maximum Detection Range</i> .....	90
	CONCLUSION AND FUTURE WORK .....	92
	REFERENCES.....	94
	Appendix .....	99
	Bluetooth Low Energy Technical Details .....	99
	VITA.....	100

---

## LIST OF ILLUSTRATIONS

FIGURE 2.1: ILLUSTRATION OF A PACEMAKER WHICH COMMUNICATE BY INDUCTIVE COUPLING.....	13
FIGURE 2.2: THE BUILDING BLOCKS OF AN IMPULSE BASED UWB TRANSCEIVER .....	17
FIGURE 2.3: FREQUENCY PRE-DISTORTION-BASED FH TRANSMITTER .....	19
FIGURE 3.1: WIRELESS TRANSMITTER MODEL .....	32
FIGURE 3.2: DIRECT CONVERSION TRANSMITTER ARCHITECTURE .....	33
FIGURE 3.3: DIRECT MODULATION TRANSMITTER ARCHITECTURE .....	34
FIGURE 3.4: FSK DIRECT MODULATION TRANSMITTER TOPOLOGY .....	35
FIGURE 3.5: BASIC PLL TOPOLOGY .....	36
FIGURE 3.6: SYSTEM LEVEL ARCHITECTURE .....	37
FIGURE 3.7: GENERAL FHSS TRANSMITTER .....	39
FIGURE 3.8: BLUETOOTH LOW ENERGY TRANSMITTER .....	39
FIGURE 4.1: DIELECTRIC PROPERTIES OF SKIN TISSUES BETWEEN 1M AND 10GHZ .....	48
FIGURE 4.2: ELECTRIC FIELD (V/M) VERSUS SKIN THICKNESS (M) AT 2.4 GHZ.....	51
FIGURE 4.3: POWER ATTENUATION AT 2.4 GHZ.....	51
FIGURE 4.4: BASIC CLASS E PA SCHEMATIC .....	52
FIGURE 4.5: CLASS E RF WAVEFORMS (A) SWITCHING CURRENT, (B) SHUNT CAPACITOR CURRENT, AND .....	52
FIGURE 4.6: CLASS E DESIGN CHART FOR CONDUCTION ANGLE ( $\phi$ ) .....	53
FIGURE 4.7: DESIGN PARAMETERS FOR CLASS E PA, AS A FUNCTION OF THE CONDUCTION ANGLE .....	54
FIGURE 4.8: 2.4 GHZ CLASS E POWER AMPLIFIER SCHEMATIC.....	56
FIGURE 4.9: IV CURVE MEASUREMENT SETUP .....	57
FIGURE 4.10: TRANSISTOR IV CURVE .....	57
FIGURE 4.11: CLASS E PA SIMULATION SCHEMATIC .....	58
FIGURE 4.12: OUTPUT VOLTAGE ( $V_o$ ) VERSUS OUTPUT CURRENT ( $I_o$ ).....	59
FIGURE 4.13: DC TO RF EFFICIENCY AT 2.4 GHZ.....	59
FIGURE 4.14: POWER ADDED EFFICIENCY AT 2.4 GHZ .....	60
FIGURE 4.15: POWER GAIN .....	60
FIGURE 4.16: GAIN AND EFFICIENCY VERSUS GATE BIAS VOLTAGE .....	61
FIGURE 4.17: AM –AM , AM-PM AND GAIN .....	62
FIGURE 4.18: TWO TONE PORT USED IN TWO TONE TEST .....	64
FIGURE 4.19: INTERMODULATION DISTORTION .....	64
FIGURE 4.20: OUTPUT POWER OF FUNDAMENTAL AND IM3 VERSUS INPUT POWER.....	65
FIGURE 4.21: EXTERNAL POWER UNIT .....	67
FIGURE 4.22: ELECTRIC FIELD (V/M) VERSUS SKIN THICKNESS (M) AT 13.56.....	68
FIGURE 4.23: POWER ATTENUATION AT 13.56 MHZ.....	68
FIGURE 4.24: EXTERNAL POWERING UNIT CLASS E PA .....	69
FIGURE 4.25: OUTPUT VOLTAGE Vs OUTPUT CURRENT .....	70
FIGURE 4.26: POWER GAIN AT 13.56 MHZ.....	70
FIGURE 4.27: EFFICIENCY AT 13.56 MHZ.....	70
FIGURE 4.28: THIRD ORDER LOOP FILTER TOPOLOGY.....	73
FIGURE 4.29: PLL DESIGN PROCEDURE .....	75
FIGURE 4.30: PLL LOCK TIME FOR 10 KHZ LOOP FILTER.....	77
FIGURE 4.31: PLL LOCK TIME FOR 15 KHZ LOOP FILTER.....	78
FIGURE 4.32: PLL LOCK TIME FOR 20 KHZ LOOP FILTER.....	78
FIGURE 4.33: OPEN LOOP FREQUENCY RESPONSE FOR 10 KHZ LOOP FILTER.....	79
FIGURE 4.34: CLOSED LOOP FREQUENCY RESPONSE FOR 10 KHZ LOOP FILTER .....	79

---

FIGURE 4.35: OPEN LOOP FREQUENCY RESPONSE FOR 15 LOOP FILTER .....	80
FIGURE 4.36: CLOSED LOOP FREQUENCY RESPONSE FOR 15 KHZ LOOP FILTER .....	80
FIGURE 4.37: OPEN LOOP FREQUENCY RESPONSE FOR 20 KHZ LOOP FILTER .....	80
FIGURE 4.38: CLOSED LOOP FREQUENCY RESPONSE FOR 20 KHZ LOOP FILTER .....	81
FIGURE 4.39: OPEN LOOP GAIN AT 15 KHZ .....	81
FIGURE 4.40: SYSTEM DIAGRAM USED IN PLL SIMULATIONS .....	81
FIGURE 4.41: PLL OUTPUT SPECTRUM .....	82
FIGURE 4.42: DIRECT VCO MODULATION .....	82
FIGURE 4.43: FREQUENCY MODULATED DATA AT THE OUTPUT OF THE VCO .....	83
FIGURE 4.44: POWER SPECTRUM OF VCO MODULATED OUTPUT.....	83
FIGURE 4.45: TRANSMITTER TEST BENCH .....	83
FIGURE 4.46: OUTPUT SPECTRUM BEFORE AND AFTER PA .....	84
FIGURE 4.47: FREQUENCY HOPPING OF BLUETOOTH LOW ENERGY.....	84
FIGURE 4.48: SIGNAL CONSTELLATION AFTER THE PA .....	85
FIGURE 4.49: SIGNAL CONSTELLATION AFTER AWGN CHANNE.....	85
FIGURE 4.50: RECOVERED SIGNAL .....	86
FIGURE 4.51: EYE DIAGRAM OF SIGNAL AT PA OUTPUT .....	86
FIGURE 4.52: BIT ERROR RATE (BER).....	86
FIGURE 4.53: MONITORING SYSTEM FUNCTIONALITY DIAGRAM .....	88
FIGURE 4.54: ULTRA LOW POWER WAKE-UP PROCEDURE .....	89
FIGURE 4.55: SIGNAL AFTER PA AND AFTER ATTENUATOR .....	90

---

## LIST OF TABLES

TABLE 2.1: DIELECTRIC PARAMETERS OF HUMAN TISSUE AT 403.5MHZ. ....	12
TABLE 2.2: WIRELESS STANDARDS IN ISM BAND.....	14
TABLE 2.3: FEATURES OF THE REAL-TIME CONTINUOUS GLUCOSE MONITORING SYSTEMS .....	23
TABLE 3.1: FCC REQUIREMENTS FOR ISM BANDS .....	27
TABLE 3.2: DSSS VERSUS FHSS SUMMARY .....	29
TABLE 3.3: BOUNDS FOR TRANSITION FROM WEAK TO MODERATE AND FROM MODERATE TO STRONG INVERSION .....	43
TABLE 4.1: BASIC RESTRICTIONS FOR TIME VARYING ELECTRIC AND MAGNETIC FIELDS FOR FREQUENCIES UP TO 10 GHZ..	49
TABLE 4.2: REFERENCE LEVELS FOR GENERAL PUBLIC EXPOSURE TO TIME-VARYING ELECTRIC AND MAGNETIC FIELDS .....	49
TABLE 4.3: DIELECTRIC PROPERTIES OF SKIN TISSUE AT 2.4 GHZ .....	50
TABLE 4.4: DIELECTRIC PROPERTIES OF SKIN TISSUE AT 13.56 MHZ .....	68
TABLE 4.5: CLASS E PAS PERFORMANCE CHARACTERISTICS.....	71
TABLE 4.6: PLL SYSTEM PARAMETERS .....	76
TABLE 4.7: LOOP FILTER COMPONENT VALUES.....	77
TABLE 4.8: BLUETOOTH LOW ENERGY TRANSMITTER SPECTRUM MASK.....	87

---

## ACKNOWLEDGEMENTS

بِسْمِ اللَّهِ الرَّحْمَنِ الرَّحِيمِ

First and foremost, I thank Allah the Most Gracious, the Most Merciful, for his blessings and for giving me the will to complete my thesis research, and allowing me to pass through such an experience where not only do you acquire the academic skills of research, but you also learn other qualities such as patience and perseverance.

Next, I would like to express my sincere gratitude to my research advisors, Dr. Lutfi Albasha and Dr. Hasan Alnashash for their continuous guidance, support and encouragement throughout the different stages of this research. I would also like to show my appreciation to Dr. M. Abdel-Hafez, Dr. Naser Qaddoumi, Dr. M. El-Tarhuni, Dr. M. Hassan, and Dr. Taha Landolsi who taught me during my master's study, for all the knowledge they provided me with. I would also like to thank Ms. Salwa Mohamed, the graduate programs coordinator who helped me and made it easier for me during my first days here. I am also grateful to all my friends and colleagues at UOK and AUS for their priceless encouragement.

I am particularly grateful to my family, my sister and brothers, my aunt and uncle who have inspired me, supported me, and treasured me through it all. At the end comes the most important force in my life, my parents, my father, to whom I owe everything I am now, my mother, who indulged me with her care and exceptional patience. Thank you for your generosity, kindness and unconditional support.

Thank you,

---

*To my parents,*

---

## CHAPTER 1

### INTRODUCTION

This chapter gives a brief introduction of the scope of this thesis. It starts by a definition for low power wireless transmitters and then introduces their application areas. Biomedical telemetry (Biotelemetry) applications are rapidly growing with wireless transmitters being one of the fundamental components. However, transmitter design for biotelemetry applications incorporates several challenges. These challenges are highlighted. Finally the objective and contribution of this thesis is clarified and the general outline of the thesis is provided.

#### 1.1 Definition of Low Power Wireless Transmitters

In general a low power transmitter can be defined as the transmitter that can operate for long periods without need for battery replacement. It might also employ a power autonomy scheme by using an energy scavenging technique (solar, vibration, etc). The operating range for these transmitters is between two to ten meters. They are expected to have power consumption in the low microwatt range with data rates of kilo bits/sec. To achieve system miniaturization and low complexity, high level of integration is needed. Techniques to reduce overall transmitter power are employed such as the implementation of deep sleep mode with on demand “turn off” and “wake up”.

#### 1.2 Applications of Low Power Wireless Transmitters

The marketplace for wireless connectivity is increasing steadily. A number of standards have been developed to satisfy the needs of various parts of this market. Examples of these standards include: Wi-Fi, ZigBee, and Bluetooth for wireless links and networks, ISO 15693 for Radio Frequency Identification (RFID) tags. While these active and passive solutions are well fitted to the requirements of a wide range

---

---

of applications, there is still a gap between them and a certain region of applications. This gap is in the region of low data rate communications for applications such as ambient intelligence, sensor networking and Biotelemetry applications. Low power/low data rate transmitters entail a new architectural approach, compared to moderate and high speed multimedia wireless links; in order to elongate battery life since battery replacement might not be feasible in certain applications such as implantable transmitters [1].

Low power wireless transmitters find use in diverse disciplines. Wireless sensor networks (WSNs) which are composed of a number of interconnected sensor nodes comprising low power transmitters are found in many fields. In the environmental field they are used in metrology for studying the atmosphere and weather forecasting. The irrigation process in the agriculture field also makes use of wireless sensor networks to optimize the process and save resources. WSNs are also widely used in home automation and smart environment. The area that is finding growing interest and applications for WSNs and low power transmitters is the field of health applications. They are used in interfaces for the disabled, communicating medical implants, swallowable camera capsules and telemonitoring of health data in real time. Many other applications are found in industrial and military fields.

### 1.3 Motivation

Standard medical diagnosis relies heavily on the measurement of various physiological parameters such as temperature, blood pressure, glucose level and biopotentials like the electrocardiograph. The use of these standard systems requires attaching sensors or electrodes to the patient and then connecting these electrodes to bulky equipment powered by a main supply. This is usually an acceptable procedure for short term patient monitoring. However, for long term monitoring, this approach is neither comfortable nor durable. Examples of long term monitoring include monitoring patients in the intensive care unit, home monitoring of the elderly, monitoring of mobile patients, multielectrode neural recording for research purposes, recording signals in brain computer interface experiments or continuous recording of signals from unrestrained or untethered lab-animals.

Fully implantable subcutaneous wireless systems can have many useful applications. Among those applications is glucose level measurement for diabetics.

---

---

Diabetes is a major health concern. According to the statistics published in year 2009 by the international diabetes federation, there are more than 250 million people around the world with diabetes. Unfortunately, there is still no known permanent cure for diabetes. However, one solution to this problem is to continuously measure blood glucose level and close the loop with appropriate insulin delivery. Statistics published by the UK Prospective Diabetes Group demonstrate that continuous glucose monitoring can reduce the long term complications between 40% and 75% [2]. Hence, continuous blood glucose monitoring equipped with alarm systems can help patients to take corrective action(s) such as decisions on their diet, physical exercise and when to take medication.

There are many types of glucose meters available in the market. Most of these meters rely on using a blood sample taken from fingertip, forearm or thigh. Although this method is the most popular amongst diabetic patients, it is relatively painful and requires motivation and training. The second method is the continuous glucose monitoring where a sensor is inserted under the skin and can stay in place for days before it is replaced. This technique relies on the fact that there is a good correlation between the measured glucose level of the interstitial fluid and blood with a time lag of around 5 minutes. The used sensor transmits its signal to a portable or nearby monitor using a wired or wireless transmission and is programmed to provide a measurement every 5 to 10 minutes [3]. The disadvantages of this method include: risk of infection, irritation during sweating, calibration requires the patient's own blood, measurement time delay and mechanical instability and discomfort during sleep or bathing. Currently, there are several research groups and commercial industrial establishments working on the development of in vivo implantable devices for longer term continuous monitoring using wireless systems [3][4].

The main advantages of subcutaneous implantable devices are: positive psychological implications especially with children, no infections, mechanical stability, does not cause problems during sleep, while sweating or showering, and requires less number of calibrations compared to external sensors.

#### 1.4 Challenges with Implantable Transmitters Design

Despite the many advantages of implantable wireless systems, they create a set of technical challenges such as power autonomy, signal quality, comfort,

---

---

miniaturization, number of channels, data compression, and selecting appropriate communication protocols [5]. In addition, these devices should be designed to dissipate ultra low power in the surrounding biological medium because any elevation in local temperature may damage cells under investigation.

Most of the established wireless biomedical applications or devices are custom made. To optimize power consumption and minimize dimension, different radio frequency (RF) bands and protocols have been used. The Medical Implant Communication Service (MICS) band uses UHF frequencies around 400MHz which would result in larger size antennas and integrated circuit chip area. This makes it an undesirable choice for the objectives of this research work [6][7]. Operating at higher frequencies e.g. sub-1 GHz and 2.4 GHz ISM frequencies may alleviate the problem related to size, but at the same time adds extra complications associated with increased power loss and signal absorption by the biological tissue. In addition, in order to achieve wide spread and usability these devices are required to be able to interact with their environments in two aspects. Communication wise, they are required to be able to send data to a nearby receiver, used in daily life scenarios e.g. Cellular phone rather than requiring a specific receiving unit. Power wise, they are required to be power autonomous by being able to harvest energy from their surroundings e.g. biological tissue. Moreover, chip real estate is one of the major elements in the success of the implantable device especially subcutaneous implants since they are sensitive to movement and displacement, therefore maximum level of miniaturization is required to enhance the implant reliability and durability. In conclusion, summing all the requirements mentioned previously creates a complex challenging research environment developed for low power consumption, relatively low cost and complexity applications.

## 1.5 Objective

The objective of this work is to investigate and design a low power wireless subcutaneous transmitter to be used for biotelemetry applications, specifically continuous blood glucose monitoring, capable of achieving ubiquitous medical observation. Implanted sensor design is not considered in this work.

As for any wireless transmitter choosing the appropriate frequency of operation would be the first task to investigate. To increase the system

---

---

interoperability, a selection among available wireless standards at the chosen frequency of operation will be made.

Low power system design principles will be defined, according to which the transmitter architecture will be selected that achieves both low power consumption and reduces complexity.

Since the transmitter will be subcutaneous, the electrical characteristics of the biological tissue i.e. skin will be evaluated from which the amount of power loss and absorption due to propagation through the biological tissue will be estimated.

At circuit level, the design of an efficient power amplifier will be conducted in order to compensate for the power loss mentioned previously. Since power amplifiers are known to be the major contributors to transmitters' power budget, the power amplifier in this design is required to achieve the required power gain at high level of efficiency in order to limit the power consumption.

The part that accounts for most of the transmitter chip area is the power supply unit. The power supply methodology will be investigated with aim of eliminating use of implantable batteries that not only increase the implant size but also demand periodical replacement which is infeasible in the case of implantable transmitters.

## 1.6 Thesis Contribution and Outline

The contributions of this research can be summarized in the following.

- 1) A low power, less complex transmitter architecture which incorporates the carrier generation and data modulation into a single unit has been designed.
- 2) An efficient class E PA has been designed, that achieved 76.77 % efficiency at the highest input power rating and 15.43 dB power gain at 2.4 GHz.
- 3) An inductive power unit was proposed for wirelessly powering the implantable unit consisting of a class E transmitter for which another class PA was designed with higher power gain of 17.79 dB at 72.6 % efficiency.

---

The chapters to follow are outlined as shown:

Chapter 2: The second chapter provides a comprehensive background on the fundamentals of low power transmitter design. The design constraints of implantable devices are investigated in depth in this chapter. An overview of the recent research trends in the specific application of implantable glucose monitors is presented.

Chapter 3: In this chapter the design theory and functionality of the implantable transmitter system is described. The frequency regulation that states the constraints and requirements for operating under the unlicensed frequency bands is described. System and circuit level low power design principles are derived according to which the low transmitter design is presented in chapter four.

Chapter 4: This chapter presents the design and simulation results of the wireless low power transmitter. It starts by demonstrating the RF signal and biological tissue interaction, and then moves into the design of the class E PAs for both the implantable and the external power unit. The direct modulation architecture chosen for this transmitter design is demonstrated next for which a PLL design have been conducted. Finally a system functionality scenario is presented.

Chapter 5: A discussion on the main results and findings, as well as, recommended future work is provided in this chapter.

---

## CHAPTER 2

### LITERATURE REVIEW

This chapter reviews some of the unique constraints of implanted wireless transmitters. The requirements of implantable wireless transmitters are listed along with methods for medical implants communication. The new research trends on the implementation of low power transceivers are presented.

State of the art implantable transmitters are introduced. At the end of this chapter, a review on the glucose sensors and commercially available continuous glucose monitoring systems is presented.

#### 2.1 Brief History of Medical Implants Communication

Initially, short distance magnetic coupling was utilized as the communication means with implanted medical devices. To overcome range limitations, in the mid-1990s Medtronic asked the FCC for a spectrum dedicated for medical implant communication. For this purpose The Medical Implant Communication Service (MICS) that falls in the 402-405 MHz band was allocated by the International Telecommunication Union-Radio Communication Sector (ITU-R) Recommendation SA1346 in 1998. In 1999, the FCC launched the band with similar standards followed in Europe [8][9]. The specifications of this band sustains the use of longer range (typically two meters), relatively high speed wireless links. The MICS band alleviates the drawbacks associated with inductive systems such as range limitations.

Research was conducted in the 402-405 MHz band. It is suitable for this service because of its signal propagation characteristics in the human body and reduced power loss, compatibility with the incumbent users of the band (meteorological aids such as weather balloons), and its international availability. On the other hand, higher frequencies of Industrial scientific and medical ISM band e.g. 2.4 GHz suffer from greater body attenuation, although this can be compensated for improved antenna gain. The 2.4 GHz frequency band has the advantage of a variety of available low power protocols that can be employed to the implantable device to make it interoperable with its surrounding electronics environment.

---

The available bands for medical implants communication along with the other available methods for communication are presented in more detail later in this chapter.

## 2.2 Design Constraints of Implantable Devices

The design of Implantable medical devices that communicates wirelessly with the outside world creates a set of challenges and constraints in terms of both system and circuit design. Careful analysis of these constraints is required to find the best compromise among them.

### 2.2.1 Ultra Low Power Consumption

Currently, there are two methods used to provide power to implantable devices. One is to utilize non-rechargeable batteries, usually lithium coin cell batteries. The other is to supply power by means of inductive coupling. Research and experimentation are ongoing with various methods of energy scavenging techniques. Even if this technique is employed, it will not alter the fundamental requirement of low power design constraint.

Implanted battery powered device are required to operate for long periods to eliminate the need for periodical battery replacement. This means that novel system and circuit design techniques are needed to reduce the power consumption to the lowest possible limit. One of the best ways to conserve power is to turn as much of the circuitry off when its operation is not needed. In sleep mode the domain is typically kept on to keep the state of the device. However at active device feature sizes below 130 nm, the gate leakage results in high static leakage power. This can be characterized using Equation (2.1) below [10]:

$$P_{stat} = I_0 \times 10^{-(V_T/S)} \times V_{DD} \quad (2.1)$$

Where  $V_T$  is the device threshold voltage,  $I_0$  is a constant, proportional to the total transistor width.  $S$  is the sub threshold slope. For a .35 um technology this value is typically 80mV/decade, thus, reducing the supply voltage ( $V_{DD}$ ) while increasing the threshold voltage ( $V_T$ ) results in reduced leakage power. However, higher threshold level results in increased wake up time.

---

On the other hand, for analog blocks, the faster the system can be powered up, perform its function and power down the less power will be needed. Thus a careful circuit design is needed to keep the idle mode power to minimum while still maintaining a responsive system.

### 2.2.2 Low Power Implantable Wireless Transmitter Requirements

The main functions of a wireless transmitter are to: (1) modulate the baseband data onto an RF carrier, (2) amplify the modulated signal, and (3) provide matching to the antenna for efficient power delivery to free space (to be radiated through the skin first in case of subcutaneous implanted device). In this section, the requirements of wireless transmitter are delineated along with the extra constraints of being an implantable transmitter.

Reducing the transmitter power consumption can be achieved in several different ways. The most important of which is radiated power, transmitter power efficiency and duty cycle.

#### 2.2.2.1. Radiated Power

To achieve a certain Bit Error Rate (BER) performance; a minimum power level is required to be present at the receiver. This is known as the receiver sensitivity. The minimum radiated power required for a reliable communication is governed by the link budget, given by [11]:

$$P_{rad,min} = \left(\frac{4\pi f}{c}\right)^2 \cdot \frac{d^n}{G_r G_t} \cdot R_{sens} \cdot LF \quad (2.2)$$

Where  $f$  is the operating frequency,  $d$  is the distance between two nodes,  $G_r$  and  $G_t$  are the antenna gain of the receiver's and transmitter's antennas respectively,  $R_{sens}$  is the receiver sensitivity,  $c$  is the speed of light,  $n$  is the path loss exponent and  $LF$  is the loss factor accounting for other losses (e.g. matching, cable loss, etc).

Generally in implantable transmitters applications, an isotropic antenna ( $G_r$  and  $G_t$  have unity gain) is desired since the relative orientation between transmitter and receiver is not predetermined. Also, multi-path is more severe in indoor environment

---

and the path loss exponent  $n$  is typically between 3 and 4. For a range of about 10m, a 2.4GHz communication system requires about 0 dBm (1mW) of transmit power.

#### 2.2.2.2. Power Efficiency

One of the most important performance metrics of implantable wireless transmitters is its efficiency. The major parts accounting for transmitter efficiency are power amplifier and antenna. A switching class PA is more efficient than its linear class counterpart. Ideally it behaves as a switch such that current and voltage do not attain their maximum value simultaneously which reduces power dissipation. On the other hand, switching class PAs requires the use of constant envelope modulation techniques such that the signal does not carry any amplitude information because of the aggressive amplitude compression experienced in switching PAs.

The Antenna Matching network accounts for a great part of power loss. A careful design of the matching network between PA and antenna is needed so that all the power will be delivered to the load and thus radiated to the intended receiver. One solution to reduce matching network loss is to incorporate matching network into the antenna in what is a so-called active antenna architecture [12].

#### 2.2.2.3. Data Throughput

In typical deployment scenarios, the parameters of interest (e.g. blood glucose level, blood pressure) sensor data only need to be acquired periodically at a relatively low rate (e.g. once every 10 minutes.) . In addition, the packet size is usually less than 1000 bits. With data rates of 10's to 100's kbps, this translates to a duty cycle of approximately 10% to 0.1% respectively. Thus the transmitter should operate at the lowest duty cycle possible to achieve the objective of ultra low power consumption.

#### 2.2.2.4. Single Chip Solution

To achieve a low system cost as well as a small form factor, the digital, analog and RF circuitry should be integrated onto a single die. Among currently available chip fabrication technologies, deep submicron CMOS process offers the highest integration level at the lowest cost. Deep submicron CMOS transistors possess enough speed to implement RF circuits and they offer the highest density digital circuits. However, the submicron CMOS process also has its disadvantages. These

---

disadvantages include high leakage power mentioned previously. It also gives rise to new challenges in analog/RF circuit design. Its low supply voltage limits the available voltage headroom in analog circuits and reduces the dynamic range of A/D converters. Submicron MOSFET has lower intrinsic gain, poorer matching characteristics and higher  $1/f$  and thermal noise.

In fully integrated mixed signal ICs the isolation between analog and digital circuit blocks is a key challenge. The low resistive silicon substrate in CMOS submicron process limits the isolation between the digital and analog/RF circuits resulting in coupling of digital noise to sensitive analog and RF circuits. Noise coupling also occurs through the supply, ground, package and bond wires. One solution to this problem is to employ a differential topology in order to reject common mode interference.

#### 2.2.2.5. Integration of Off Chip Components

Medical grade components are expensive and the introduction of any new component or connection adds further reliability risk. Thus it is essential to integrate as many external components as possible onto the silicon IC. Examples of such components are inductors, capacitors and TX/RX switch. However, integrating these components on chip results in poor performance. On chip inductors have low quality factor compared to their off chip counterpart which results in higher losses in matching networks and LC tanks. Insertion loss of an integrated TX/RX switch is much higher resulting in poorer noise figure and higher power dissipation.

#### 2.2.2.6. Form Factor

Gilligan et al noticed that reducing the size and mass of the sensor to prevent motion of the device reduces the time for sensor start-up by minimizing the disruption of the fragile new capillaries necessary to supply oxygen and glucose to the sensor in the case of continuous glucose monitoring. Miniaturization is also anticipated to resolve the vascular compression/postural effects. The conclusion of their work was that glucose sensor implant technology shows promise in humans but needs to be miniaturized, better sealed against water penetration, and made more robust and reliable [13].

As stated above, implantable transmitters are required to have a small size to enhance the stability and reliability of the palpable device. The smaller the implant, the faster the sensor will settle to the final value which means less time to acquire measurement i.e. less power consumption since the device will be on for shorter time. Miniaturization also provides ultra low power consumption in terms of circuits biasing, comfort, and ability of system integration. The size of a transmitter is mainly determined by (1) size of energy storage (2) antenna dimensions and (3) footprints of its components.

The size of the energy storage device depends on its energy density and the transmitter average power consumption. Although the power density of the energy sources has improved over the last few years, it is crucial to minimize the transmitter power consumption in order to achieve the goal of miniaturization.

The antenna engages a considerable area/volume of the transmitter. Dimensions in the order of  $\lambda/4$  to  $\lambda/2$  are required for efficient antenna operation, where  $\lambda$  is the operating wavelength. Hence, there exists a trade off between antenna efficiency, antenna size, power consumption and operating frequency.

### 2.2.3 The Human Body as a Medium

Transmission in the human body has its own challenges. The human body is composed of materials that are partially conductive and that have different dielectric constants. Furthermore the implemented antenna cannot be viewed in isolation of the body; the human body should be viewed as part of the antenna. This is because the radiation pattern and efficiency are influenced by the size, shape, location and composition of the body. The antenna, hence the implanted medical device, will behave differently according to the implantation site since the dielectric properties differs from one tissue layer to the other. The effective permittivity  $\epsilon_{er}$  and conductivity  $\sigma_e$  of different human tissues at 403.5MHz, relevant for Implantable Medical Devices (IMDs) are given in Table 2.1 below:

Table 2.1: Dielectric parameters of human tissue at 403.5MHz [14].

Tissue	$\epsilon_{er}$	$\sigma_e$
Muscle	57.1	0.797
Fat	5.6	0.041
Lung	23.8	0.375
Skin(dry)	46.7	0.690
Skin(wet)	49.8	0.670

Bone Cancellous	22.4	0.235
Brain gray matter	57.4	0.739
Brain white matter	42.0	0.445

Testing of antenna and system performance of an implanted antenna in the lab is done by means of tissue simulating fluids also know as phantoms.

#### 2.2.4 Communication Methods

Different methods are available for wireless communication with implanted devices. In the following section, the main methods and their functionality are described.

##### 2.2.4.1. Electromagnetic Methods

An inductive link can be used as a communication method with biomedical implants. Pacemakers utilize this communication method. A small coil is placed in a closed metal housing inside the implant. An external coil is placed on the patient’s chest on top of implanted pacemaker as seen in Figure 2.1.

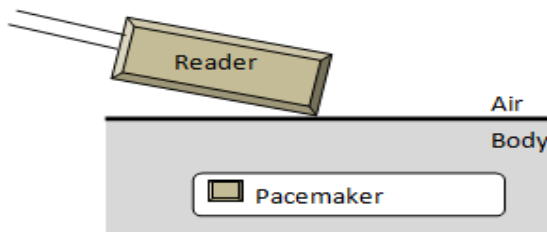


Figure 2.1: Illustration of a pacemaker which communicate by inductive coupling.

When a carrier frequency of 175 kHz was used and data rates up to 512 kbps were achieved [15]. The main drawback of the inductive link is that the low frequency used can limit the data rate. The communication is constrained to “touch” range, and coil alignment is mandatory which can complicate the communication procedure.

##### 2.2.4.2. MICS Standard

The MICS band has been allocated by the FCC for medical implants communication in the U.S and in Europe; the European telecommunication standards institute (ETSI) is responsible for frequency band allocation. The frequency band allocated is 402- 405 MHz. The maximum emission bandwidth is restricted to 300 kHz. If the implanted device is to be operated in a full duplex fashion, the bandwidth

occupied by both the down link and uplink should not exceed 300 kHz. Thus, to operate at maximum data rate, half duplex scheme should be employed. Separate uplink and downlink bands can be used, with each band having a bandwidth of 300 kHz as long as they are not used simultaneously. This frequency band is also allocated for the meteorological aids service (METAIDS), which is used by weather balloons. Therefore, MICS is recommended for indoor use only.

### 2.2.4.3. ISM Band

The ISM band is a general purpose part of the radio spectrum that can be used without a license. The only requirement for operating in this band is compliance with the rules governing operation in it. The main bodies defining these rules are the FCC and ETSI in the U.S and Europe respectively. These rules are relatively simple: the signal strength is generally restricted to less than one watt while employing one of the spread spectrum techniques [16]. Originally, applications running on this band were characterized by their low data rates, but recently data rates in this band are experiencing a noticeable enhancement.

- Wireless Standards in the ISM Band

Different wireless standards operate in the ISM band. These standards differ from each other by their data rate, output power, communication range, and modulation techniques. Table 2.2 compares the four standards available in the ISM band.

Table 2.2: Wireless standards in ISM band

	Bluetooth	Wi-Fi	ZigBee	Bluetooth low energy
IEEE Spec	802.15.1	802.11a/b/g	802.15.4	Bluetooth forum
Frequency Band	2.4GHz	2.4GHz	2.4GHz	2.4GHz
Max Data Rate	1Mb/s	54Mb/s	250kb/s	1Mb/s
Distance Range	1-100m	100m	10-100m	10m
Transmitted power	0-20dBm	15-20dBm	(-25)-0dBm	(-20)-10 dBm
RF Channels	79	14	16	40
Channel Bandwidth	1MHz	22MHz	5MHz	1MHz
Modulation	GFSK	(CCK-QPSK), (OFDM-BPSK,QPSK,QAM)	OQPSK	GFSK
Spread spectrum Technique	FHSS	FHSS,DSSS	DSSS	FHSS

- 
- Bluetooth: It is based on IEEE 802.15.1 standard. It operates in 2.4-2.4835 GHz band. It allows wireless devices such as cellular phones, Personal Digital Assistants (PDAs) etc. to communicate within a range up to 100m when operating at the maximum power rating. It uses Gaussian Frequency Shift Keying (GFSK) modulation with FHSS [17].
  - Wi-Fi: It is the most widely used wireless technology for connecting to the internet. It integrates most personal computers, PDAs and other wireless devices. It is based on IEEE 802.11 standard and the majority of Wi-Fi standards operate in 2.4 GHz band. It utilizes a variety of modulation schemes and supports both spread spectrum techniques.

ZigBee: It is based on IEEE 802.15.4 standard and operates in 24-2.4835 GHz band. It has been developed by a consortium of companies know as ZigBee Alliance [18]. It is suitable for mesh networking since it has the ability to support a large number of nodes at low cost. It uses Offset Quadrature Phase Shift Keying (OQPSK) modulation with DSSS.

- Bluetooth low energy: According to Bluetooth Special Interest Group (SIG), it is up to 17 times more efficient than the class Bluetooth technology. A significant amount of intelligence is placed on the Bluetooth low energy controller that allows the host device to spend most of the time in sleep mode. The low power consumption is mostly achieved by using lower frequency set in the advertising state with sniff sub-rating technique [17].

#### 2.2.4.4. Acoustic Link

Acoustic links can be used for communication with biomedical implants. The implant is energized by the incoming ultrasound signal. This method has been used in pacemakers to communicate the state of the device e.g. low voltage level, using an audible alarm buzzer [14].

#### 2.2.4.5. Optical Link

Communication with biomedical implants is possible since biological tissues have a low, but non zero, transmission of visible light. The downlink transmission

---

from an external device to the implant is most likely to be restricted to the touch range while the uplink transmission might be prohibitive in terms of power [14].

From the constraints associated with the design of communicating implantable devices stated previously we conclude that the mission of designing such a device is quit challenging. The design specifications and requirements need to be clearly defined in order to meet the intended design goals. This includes the intended application, data rate, technology used, etc. Design tradeoffs will have to be made for the operating frequency, output power and achievable range.

In the following section, an overview of low power transmitters' architectures is presented along with a feasibility analysis on employing them in this low power implantable transmitter design.

### 2.3 Low Power Transmitters System Architecture Trends

Different radio architectures have been proposed for low power transceiver design. These include Ultra Wide Band (UWB) transceivers, RFIDs, Sub-sampling, Super-Regenerative transceivers, and spread spectrum transceivers. To achieve the goal of low power consumption these architectures employ different techniques. An outline of the basic features and functionality of these architectures is presented below.

#### 2.3.1 Ultra Wideband Transceivers

FCC rules defines UWB technology as any wireless transmission scheme that occupies more than 500 MHz of absolute bandwidth. Shannon theorem defines the relation between the data rate, bandwidth, and signal- to-noise ratio (SNR) as given by Equation (2.3) below [19]:

$$C = BW \times \text{Log}_2 \left( 1 + \frac{P_S}{P_N} \right) \quad (2.3)$$

Where  $P_S$  is the average signal power at the receiver,  $P_N$  is the average noise power at the receiver and  $BW$  is the channel bandwidth. For low data rates applications, the utilization of a wide bandwidth allows the use of low SNR and hence low signal power levels. The basic architecture of UWB transceivers is shown in Figure 3.2.

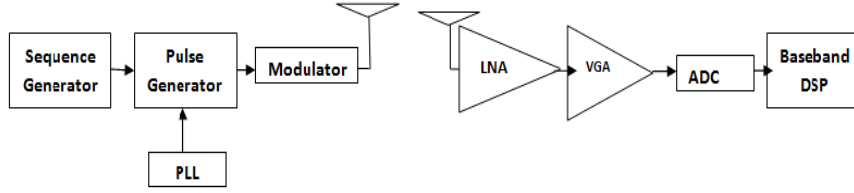


Figure 2.2: The building blocks of an impulse based UWB transceiver

UWB transceiver’s design imposes a set of challenges. The main challenge is in terms of Analog to Digital Converter (ADC) design. The ADC is required to have a wide dynamic range to obtain the weak desired signal from the strong interferers. Due to the wide bandwidth used, sampling has to be in the order of several Giga samples per second. Even for a 1-bit ADC at 2 G samples/s, the power consumption is anticipated to be around 5 mW [20]. The LNA design can be quiet challenging as well due to the wide bandwidth used.

### 2.3.2 RFID, Subsampling and Super-Regenerative Architectures

In RFIDs, an external reader known as the interrogator sends a wake up signal to the transmitter which transmits the required data back to the reader. The most widely used modulation scheme in RFID transmitters is On Off Keying (OOK). Usually the transmitters are characterized by the limited amount of intelligence placed on them rendering them inflexible for applications that require some level of interaction in the transmitter side. RFIDs are usually characterized by their short communication range.

Subsampling transceivers exploit Nyquist theorem to reduce the overall power consumption. They rely on the principle that reducing the operating frequency of the analog blocks aids in reducing their power consumption. However, the VCO phase noise requirements of sampling oscillator can get quite demanding. Due to noise aliasing, the noise degradation can be found by [21]:

$$D = 10 \text{ Log}_{10} \left( 1 + \frac{2MN_p}{N_0} \right) \quad (2.4)$$

Where M is the ratio between the carrier frequency and the sampling frequency,  $N_0$  is the white noise spectral density and  $N_p$  is the Band Pass filtered (BPF) version of  $N_0$ . Thus, the choice of the sampling frequency as well as the BPF bandwidth is quite critical in determining the overall noise performance. In the presence of interferers, the poor VCO noise characteristics can degrade the BER through reciprocal mixing.

---

For this reason, this architecture has been used mainly in interferer free scenarios i.e. space applications.

Super regenerative architectures had been proposed for low power transceivers implementation. In the transmit mode, the oscillator is directly modulated by the baseband data, with the most widely used modulation scheme being On Off Keying (OOK). The receiver consists of an oscillator, a tuned circuit and an envelope detector. Even though this architecture achieves reduced complexity and a power consumption of 1.6 mW has been reported [22], the performance can be heavily spoiled in the presence of interferers with high power levels compared to the desired signal. For this reason super regenerative transceivers rely on the use of non-standard components such as Bulk Acoustic Wave (BAW) resonators to achieve better selectivity.

### 2.3.3 Spread Spectrum Systems

Spread Spectrum systems utilize modulation techniques such that the bandwidth of the transmitted signal is much larger than bandwidth of the original message. The ratio between the bandwidth of the original message and the transmitted data is known as spreading ratio [23].

The spreading can be applied in two aspects: the carrier frequency of the modulated signal which forms Frequency Hopping Spread Spectrum (FHSS) and the spreading code can be applied directly to the original message to form Direct Sequence Spread Spectrum (DSSS).

Lopelli et al. developed a frequency pre-distortion-based FH transmitter as shown in Figure 2.3. The Frequency Locked Loop (FLL) in the baseband measures the VCO signal, and calibrates the output frequency via the coarse tune input of the front-end (FE), to ensure that the complete TX band falls within the ISM band. The TX operate at 900 MHz and has a chip area of 3.6 mm<sup>2</sup>. The overall TX power consumption is 4.4 mW at -5 dBm radiated power. To reduce the pre-PA circuitry current consumption, the PA and the VCO have been merged in a power-VCO. A dedicated digital algorithm on the receiver side reduces the center frequency offset from a maximum value of 8.2 MHz to less than 8 ppm avoiding the use of any crystal on the transmitter side. The FHSS synthesizer is implemented based on digital

predistortion technique. The synthesizer draws a total of 2 mA current from a 2 V power supply [24].

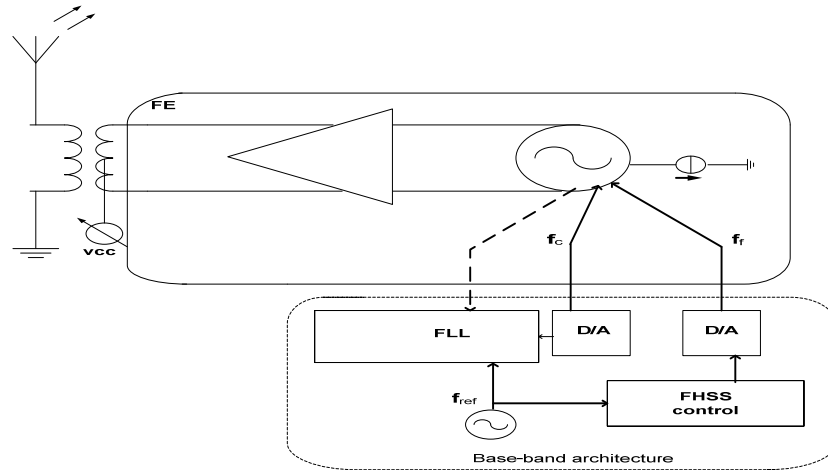


Figure 2.3: Frequency pre-distortion-based FH transmitter [24]

## 2.4 State of The Art of Implantable transmitters

Several research development institutes and centers have attempted to address the challenges incorporated with low power implantable transmitter design. Most of the published wireless biomedical applications or devices are custom made i.e. to optimize device power consumption and minimize its dimensions, different frequency bands and wireless protocols have been used.

Zarlink Inc. developed a low power radio chip ZL70101 transceiver with 5mA transmitter current consumption operating at 2.1-3.5 volts despite using a 0.18 $\mu$ m CMOS low voltage technology [7]. It was designed to operate at the MICS band making it less transportable to standard protocols discussed previously. The base transmits a 2.45 GHz wake-up signal to the implantable unit. The implantable unit consists of a whole transceiver system that employs a superhetrodyne architecture which demands use of power hungry circuits such as mixers increasing the complexity, power consumption and size of the implant. It also uses three external components: a crystal, two decoupling capacitors and a matching network which results in a larger implant size.

Toumazu Inc. developed a 1 V wireless transceiver for low power system on chip for biotelemetry applications [6]. It is part of an ultra low power SoC, the Sensium™. The transceiver utilizes FSK/GFSK modulation at a data rate of 50 kbit/s

---

to provide wireless connectivity between target sensor nodes and a central base station node in a single hop star network topology operating in the 862–870 MHz European (SRD) and the 902–928 MHz North American (ISM) frequency bands. Controlled by a proprietary media access controller which is hardware implemented on chip, the transceiver operates half-duplex, achieving -102 dBm receiver input sensitivity (for  $10^{-3}$  raw bit error rate) and up to -7 dBm transmitter output power through a single antenna port. It consumes 2.1 mA during reception and up to 2.6 mA during transmission from a 0.9 to 1.5 V supply. It was fabricated in a 0.13  $\mu\text{m}$  CMOS technology and occupies 7  $\text{mm}^2$  in a SoC die size of  $4 \times 4 \text{ mm}^2$ .

Beach et al developed an implantable system where he used a lithium battery and 303MHz On Off Keying (OOK) modulation [25]. Remotely configurable features included in the in vivo implanted unit include: sensor excitation changes; filter frequency cutoff values, amplifier gain; and transmission intervals utilizing 303.825-MHz UHF RF telemetry for end-to-end remote data monitoring. The developed mP/Gstat printed circuit board measures about  $51 \times 22 \times 1 \text{ mm}^3$  thick, and is suitable for bench top or encapsulated use. The implant consumes a maximum of 15 mA while being powered by 3V lithium coin cell battery.

M. Ahmadi developed an integrated circuit chip for continuous monitoring of glucose [3]. The microsystem comprises a microfabricated glucose biosensor flip chip bonded to a transponder chip. The transponder chip is inductively powered by an external reader with a 13.56-MHz carrier. The measured glucose signal is transmitted back to the external reader using load-shift keying (LSK). The transponder chip has been fabricated with the TSMC 0.18 $\mu\text{m}$  CMOS process and has a total area of  $1.3 \times 1.3 \text{ mm}^2$  with a total current consumption of about 110  $\mu\text{A}$ .

Before presenting the commercially available glucose meters, we provide a summary on the types of glucose sensors. This overview is mainly based on the literature provided previously.

#### 2.4.1 Glucose Sensors

A biosensor can be defined as the analytical device that outputs an electrical signal in response to a biological reaction. A successful biosensor must have the following qualities [26]:

- 
- It must be highly specific for the purpose of the analysis and maintains good stability under normal conditions. The sensor reaction must be accurate, precise and reproducible over the diagnostic range.
  - The response should be independent of physical factors such as temperature, pH level, etc.
  - The sensor materials need to be biocompatible since it is intended for implantation in this case.
  - Miniaturization is a major requirement for a successful sensor. This will reduce the overall implant size and make the sensor less vulnerable to patient's movement, thus more accurate measurements can be obtained.

The biological reaction of the biosensor is determined by the biocatalytic membrane which accomplishes the transformation of reactant to product. Immobilised enzymes have a number of valuable characteristics; they may be re-used, which guarantees that the same catalytic activity is present for a series of analyses.

Most of the available glucose sensors are electrochemical sensors, where the sensor's output current is proportional to the glucose concentration. Oxygen-based and Hydrogen peroxide-based are the most common electrochemical sensors for glucose sensing. The enzyme used in these sensors is Glucose oxidase (GOD). However, these sensors are limited by the availability of Oxygen in the biological tissue, short life-time, and interference from other chemical materials such as urate [26].

As an example of glucose sensors' functionality, the amperometric glucose sensor used is described [3]. The sensor used is an amperometric sensor i.e. the current produced is proportional to the potential between the applied electrodes. The sensor used consists of three electrodes, working electrode, reference electrode and counter electrode [3]. The reaction between the glucose and the GOD enzyme takes place on the reference electrode surface. The potential of the biological solution under investigation, which is the interstitial fluid in the case of a subcutaneous implanted device or blood, is measured through the reference electrode. The chemical reaction takes place at the working electrode. The sensor output current ranges between 1nA to 1 $\mu$ A, with the ability to detect glucose levels from 0 to 40 mM. A Data rate of 8 kbps

---

was reported for a glucose sensor with a periodical measurement every 5 minutes [27].

Currently there are few available glucose meters. They provide continuous glucose monitoring but they cannot be considered as implantable devices since the wireless transmitter is externally snapped to the sensor that provides glucose measurement taken from interstitial fluid. The sensor duration and achievable range of those devices are still far away from a miniaturized, autonomous implant.

#### 2.4.2 Commercially Available Continuous Glucose Monitoring Systems

Commercially, DexCom, USA, has developed an implantable glucose monitor to provide continuous glucose monitoring known as Seven<sup>®</sup> Plus [27]. The monitoring system contains a battery, circuit board, microprocessor, radio transmitter, and biosensor covered with a membrane. An analog to digital converter translates the data to digital form, and a radio transmitter sends the glucose signal data to the receiver. The sensor determines glucose levels every 30s in subcutaneous tissue and radio transmits glucose data to the receiver every 5 minutes. The implant operates in MICS band at a frequency of 402.142 MHz. It uses OOK modulation with a data rate of 8192bps. The transmit duty cycle is 9.28 ms every 5 minutes while the data detection range is only 1.5 m. The sensor needs to be replaced every 7 days. The sensor is implanted in the subcutaneous tissue of the abdomen. The receiver is an externally worn pager sized device.

Free Style Navigator<sup>®</sup> Continuous Glucose Monitoring System has been developed in Abbot Laboratories, USA [28]. The Navigator consists of three main parts, the sensor which has a lifetime of 5 days and it is implanted 5mm under the skin. The second part is the transmitter, which is snapped into the sensor mount on the skin's surface. It is powered by a coin cell battery. The total transmitter weight is 13.6 grams including batteries which can last up to 30 days. The transmitter transmits information wirelessly to a receiver which is about the size of a pager, and its total weight is 99 grams. It receives information from the sensor / transmitter every minute. The transmitter needs to be placed within 3m from the receiver to be able to detect transmitted data.

Minilink is the transmitter part of the Guardian<sup>®</sup> Real-Time Continuous Glucose Monitoring System presented early this year by Medtronic, USA. The

---

transmitter operates at 868.35 MHz worldwide and 916.5 MHz in US. The duration of the transmitter AAA battery is 14 days. The receiver, defined here as the monitor, performs the same function stated in previously mentioned glucose monitoring systems [29]. Medtronic has another glucose monitor system known as Paradigm<sup>®</sup>. It is similar to the Guardian<sup>®</sup> expect for the fact that it has an insulin infusion pump to adjust the blood insulin level. Also, it does not have a separate receiver; the glucose level is displayed on the insulin pump.

A summary of the features of commercial glucose monitoring systems is provided in Table 2.3 . As stated in Table 2.3 all glucose monitoring systems require regular calibration. The calibration procedure can be performed by means of conventional capillary blood glucose measurements in order to transform the sensor signals obtained from the specific compartment into blood glucose values [30].

Table 2.3: Features of the real-time continuous glucose monitoring systems [31]

	Abbott Free Style Navigator	DexCom Seven Plus	Medtronic Guardian Real Time System	Medtronic Paradigm Real Time system
Range of glucose values	20-500 mg/dL	40-400 mg/dL	40-400 mg/dL	
Update of glucose values	Every minute	Every 5 minutes	Every 5 minutes	Every 5 minutes
Sensor duration	5 days	7 days	3 days	3 days
Sensor length, angle, and gauge	6 mm, 90°, 21 gauge	13 mm, 45°, 26 gauge	12 mm, 45°-60°, 23 gauge	12 mm, 45°-60°, 23 gauge
Transmitter size	2.05" × 1.23" × 0.43"	1.5" × 0.9" × 0.4"	1.4" × 1.1" × 0.3"	1.4" × 1.1" × 0.3"
Transmitter battery duration	No charging needs to be replaced.	Non replaceable.	3 days on 20 mins charge	3 days on 20 mins charge
Distance between TX& RX	< 1.5 m	< 3 m	< 1.8 m	< 1.8
Required frequency of calibration	4 times at about 10, 12, 24 , and 72 after sensor insertion	2 times a day	2 times a day	2 times a day
Glucose display graph	2,4,6,12, and 24 hours	1,3,6,12, and 24 hours	3,6,12, and 24 hours	3,6,12, and 24 hours
Food & Drug Association (FDA)	Age 18 and above	Age 18 and above	Age 7 and above	Age 7 and above

---

## CHAPTER 3

### SYSTEM ARCHITECTURE

Low power wireless transmitter design presents a set of challenges and constraints. These constraints are further enhanced when this transmitter is intended for Implantable medical applications.

Considering the unique requirements and operating environment of an implantable low power transmitter, the main design principles required to achieve the desired high performance transmitter can be summarized in the following points [11]:

- Minimizing the overhead power, which is defined as the power dissipated when the transmitter is active but not sending data. This can be considered as the time required to turn on the circuitry at the onset of communication.
- Maximizing circuit efficiency.
- Minimizing active time, which the transmitter spends on the “ON” state. The transmitter should have very low duty cycle; it should be sent to sleep and turned on only when needed.
- Radiating the minimum power needed for communication.

Based on these principles, low power design techniques at system, circuit and technology levels are investigated. Adhering to these design principles and techniques result in a high efficiency, low power, low cost and small form factor transmitter. As discussed in chapter two, several tradeoffs are needed to achieve the optimum transmitter design. For example the decision on the operating frequency will affect many other design factors such as power consumption, achievable range, size, etc. All that being set, the physical transmitter architecture needs to be selected by employing low power system and circuit techniques to achieve the desired performance at minimum possible power consumption. Moreover miniaturization and high level of integration is a major requirement especially for implantable transmitters achieve the desired performance at minimum possible power consumption. Moreover miniaturization and high level of integration is a major requirement especially for implantable transmitters. Interoperability is also a desired feature in wireless

---

transmitters where the operating frequency is applicable worldwide and ability to communicate with wireless devices available in the environment is possible. Interoperability can be defined as the ability of systems to provide services to and accept services from other systems. Among communication-electronics interoperability is composed of three dimensions: compatible communications paths (compatible frequencies, equipment and signalling), radio system coverage or adequate signal strength, and scalable capacity [32].

In this chapter the architecture design theory and functionality of the implantable transmitter system is described starting with frequency regulation and requirements for operating in the unlicensed frequency bands. Available wireless protocols in selected operating frequency were investigated to enhance the transmitter interoperability. For the system architecture, direct modulation architecture was chosen which results in reduced system components and ability to integrate carrier generation and modulation circuitries into a single unit. For this purpose a Phase Locked Loop (PLL) design has been conducted. The power attenuation and RF power safety limits for the implantable device were calculated. To counter the effect of this power attenuation; an efficient class E PA has been designed. Finally we describe a design for the external powering unit that supplies power inductively to the implantable transmitter.

### 3.1 Frequency Regulation

A summary of the investigation on available communication methods for implantable devices presented in chapter three is described next.

In the past, inductive links were used for communication between the implanted unit and an external reader. The frequencies used were in the order of 10's to 100's of kHz's. The range of communication is constrained to "touch" range. The main drawback of inductive links is that the low frequency limits the available bandwidth which results in low data rates. The coils alignment is a major requirement in order to get a reliable link. This adds to the complexity of the communication procedure.

To overcome range limitations, a dedicated frequency band has been allocated for medical implantable devices communication i.e. MICS, which uses the frequency

---

band of 402-405 MHz with a channel bandwidth of 300 kHz. The MICS solves the range limitations associated with inductive links. They also hold good signal propagation characteristics in the human body, congruent with the current users of the band (meteorological aids such as weather balloons), and its worldwide availability. On the other hand, from device form factor point of view, it might not be the best solution. In order to achieve acceptable radiation efficiency and minimize reflections, the antenna dimensions need to be approximately in the order of quarter the wave length ( $\lambda$ ) given by:

$$\lambda = \frac{c}{f} = \frac{3 \times 10^8}{400 \times 10^6} = 75 \quad (3.1)$$

Where  $c$  is the speed of light. At 400 MHz,  $\lambda = 75$  cm. This dimension results in an impractically large implant size.

The ISM has different frequency bands, with the most used being the 2.4 GHz and sub 1GHz band. The 2.4 GHz band is known for its high speed. This due to the wider channels used which allow for higher data rates that can be attained by the lower frequency bands. Many wireless technologies operate in this band as given. Therefore, components for this frequency band are more readily available and hence cost much lower than the other bands.

From an implantable device point of view, the 2.4 GHz band suffers from greater body attenuation, although this can be compensated by improved PA and antenna gains. Thus a careful design is needed to compensate for the increased skin and tissue attenuation at this band.

Also interference at this band is much higher than other presented bands. This can be compacted by applying one of the spread spectrum techniques.

For all the formerly listed advantages of the 2.4 GHz band, it will be selected as the operating frequency for this implantable transmitter design application.

The FCC defines a set of rules when operating a transmitter in the ISM band. Radiators operating on this band should employ one of the spread techniques. These define the spread spectrum techniques to be used, peak transmitter output power, etc.

### 3.1.1 FCC requirements for ISM bands

Operation under the ISM band is restricted to frequency hopping and direct sequence spread spectrum intentional radiators that meet the specifications illustrated in Table 3.1.

Table 3.1: FCC requirements for ISM bands

FCC DSSS rules	FCC FHSS rules
The minimum 6 dB bandwidth shall be at least 500 kHz.	The maximum 20 dB bandwidth of the hopping channel is 1 MHz.
The maximum peak output power shall not exceed 1 Watt.	The maximum peak output power shall not exceed 1 Watt.
If transmitting antennas has directional gain greater than 6 dBi, the peak TX output power must be reduced accordingly.	At least 75 hopping frequencies.
The peak power spectral density shall not be greater than 8 dBm any 3 kHz band.	The average time of occupancy on any frequency shall not be greater than 0.4 seconds within a 30 second period.

The spreading code in a DSSS system is applied to the modulated data, unlike in a FHSS system where the spreading is applied to the modulated data carrier frequency. To compare the performance of the two spread spectrum systems, the average acquisition time for a spread spectrum system is given by Equation (3.2) [33].

$$T_s = (C - 1)T_{da} \left( \frac{2 - P_d}{2P_d} \right) + \frac{T_i}{P_d} \quad (3.2)$$

Where  $T_i$  is the integration time for the evaluation of each cell in the time frequency plane,  $P_d$  is the probability of detection when the correct cell is being evaluated,  $T_{da}$  is the average dwell time at an incorrect phase cell, and  $C$  is the total number of cells. DSSS systems are synchronized with within  $\pm T_c/2$  where  $T_c$  is the chip duration, while FHSS systems are synchronized with  $\pm T_{\text{symb}}/2$ , where  $T_{\text{symb}}$  is the symbol period. Since, the processing gain in DSSS systems is related to the ratio between the symbol and chip rates, the chip rate is always less than the symbol rate by at least an order of magnitude. Therefore, the number of cells that have to be evaluated in a DSSS system is larger than in a FHSS system.

---

#### 3.1.1.1. Spread Spectrum And Modulation Schemes

Binary phase shift keying (BPSK) is usually used in DSSS systems. It achieves good performance and it is relatively simple to employ. However, a PLL is needed at the receiver side to recover the phase. The PLL is required to be fast enough to match the high chip rates in DSSS systems.

In FHSS systems, frequency shift keying (FSK) is usually employed. The signal reception can be coherent or non-coherent.

PSK modulation requires the use of a linear PA since the information is carried in phase transitions. While the modulated signal using FSK modulation has a constant envelope which allows the use of an efficient nonlinear PA.

#### 3.1.1.2. Interference

One of the key features of spread spectrum systems is their ability to reject interference. DSSS and FHSS systems react definitely to mitigate the effect of interference.

Usually interferences are not correlated with the spreading code. Thus, in the presence of interference only part of the transmitted data will be affected. Increasing the chip rate, i.e. spreading more, increases the interference rejection capability.

Unlike DSSS, FHSS avoids interference. It periodically hops from one frequency to another, which means that it stays for a short period of time in each frequency band. This will limit its exposure to interference present in a particular band. Further interference avoidance can be achieved by increasing the hop set [34].

#### 3.1.1.3. Near-Far Problem

Spread spectrum systems are generally affected by the so called near-far problem. It is a situation where a strong interferer captures the receiver rendering it unable to detect the weak desired signal. The performance of DSSS systems can be heavily spoiled in the presence of this problem. For this reason a proper power control scheme needs to be used. Usually Automatic gain control is used in DSSS systems. In FHSS, this can be avoided reducing the complexity and power consumption of the system.

Table 3.2: DSSS versus FHSS summary

	DSSS	FHSS
Modulation	PSK	FSK
Demodulation	Coherent	Non-coherent
Interference resistance	Weak (Wideband)	Higher
Near-Far problem	Very sensitive	Slightly sensible
Multipath and fading	Medium sensitivity	Low sensitivity
Multiple access	High compactness	Low compactness
Synchronization And timing	Slow	Fast
Amplification method	Linear (lower efficiency)	Non-linear (higher efficiency)

A summary of DSSS and FHSS features discussed previously is shown in Table 3.2 above. With regards to low power transmitters, FHSS offers an attractive solution in terms of hardware complexity, system performance and power consumption. FHSS also enables the simplicity of using FSK modulation, which allows the possibility of employing direct modulation transmitter architecture. In this way, a greater integration level and lower power consumption can be achieved. Furthermore, FSK modulation can easily be superimposed on the hopping carrier by simple digital techniques. Finally, the modulated output has a constant envelope, and is amenable to the highly efficient non linear power amplification. From the above discussion it can be concluded that FHSS is the most suitable technique for low power transmitter design.

### 3.1.2 Wireless Protocols in 2.4 GHz ISM Band

The frequency of operation of 2.4 GHz and FHSS were chosen for this low power transmitter design. In order to increase the system interoperability a wireless protocol that acts in accordance with the previously chosen frequency band and spread spectrum technique can be employed.

As discussed in chapter two, among the available wireless protocols in the 2.4 GHz ISM band, Wi-Fi, Bluetooth, and Bluetooth low energy use FHSS. Wi-Fi has an output power as high as 100 mW, and has range coverage up to 100 m with a data rate of 54 Mbps; this makes it an undesirable choice for this transmitter design. Bluetooth Low energy appears to be the most suitable choice, since it complies with design specifications of low power consumption and low complexity. Bluetooth low energy meets all of these requirements and has the added advantage of ability to communicate with the Bluetooth chips likely to be fitted to the next generation of mobile phones. That means patient data could be transmitted to a medical facility via

---

the cellular network eliminating the need to build expensive specialized communication links.

### 3.1.3 Bluetooth Low Energy Protocol

Bluetooth low energy is the low power edition of the classic Bluetooth technology that is specified in the Bluetooth core specification v4.0. It consumes a small portion of the power of classic Bluetooth radios. This technology expands the deployment of Bluetooth wireless technology to devices that are powered by small, coin-cell batteries. Under many circumstances, it makes it conceivable to manage these devices for years without recharging. Using energy harvesting techniques or inductive links is also possible as will be described later in this chapter.

The range of Bluetooth radios can be optimized according to the application. The typical range used by the majority of Bluetooth radio is the 10 meters range but there is no limit imposed by the specifications. Bluetooth low energy possesses the following features [35]:

- Ultra-low peak, average and idle mode power consumption.
- Ability to run for years on standard coin-cell batteries.
- Low cost.
- Multi-vendor interoperability.
- Enhanced range

The complete technical details of the Bluetooth low energy technology are provided in Appendix A.

#### 3.1.3.1. Bluetooth Low Energy Technology And Medical Applications

Wireless technology is highly developed and has encompassed almost all applications with the remarkable exception of medical applications. This is expected given the rigorous requirements of the medical community. These requirements are motivated by the necessity to ensure that a selected technology does not threaten user's health and is completely reliable.

In order for a wireless technology to meet the challenge of medical monitoring it must fulfil certain requirements. These requirements incorporate interoperability,

---

where a global standard is crucial so that products from different manufacturers can communicate with each other. Ultra low power consumption is a critical requirement; a low power RF radio with an efficient protocol that can run for years without the need for battery replacement is required. Materials used for wireless device need to be biocompatible, sensors used need to be reliable and accurate. Since medical data is confidential; data transmission must be kept safe and secure. In order to relay acquired medical information to remote health specialists; a firm distribution network is needed where wireless devices can communicate through services such as the Internet and the cellular network [36].

Bluetooth low energy technology satisfies all of these requirements. Due to reduced protocol complexity, radios consume ultra low currents during transmit and receive modes and consume currents as low as few nanoamperes in sleep mode. Regarding security concerns, Bluetooth low energy technology supports Advanced Encryption Standard (AES) encrypted wireless communication. In addition, Bluetooth low energy technology is an open standard ensuring that devices from different vendors can still communicate with each other. Since it builds on the inheritance of Bluetooth wireless technology, it will be easy to form a Personal Area Network (PAN) involving several devices.

From the characteristics of Bluetooth low energy technology described previously, it can facilitate well integrated and compact devices, with a reduced protocol stack providing ultra low power sleep mode operation, secure and reliable communication at the lowest possible cost.

After setting the frequency of operation and further enhancing the system interoperability by employing a low power wireless protocol, the transmitter system architecture needs to be designed such that it will achieve the target of low power consumption, compactness, and high level of integration.

### 3.2 Transmitter Design Principles

The basic building block of a wireless transmitter can be simplified into three units, a power amplifier (PA) power amplification, a matching network that matches the antenna to the PA, and a pre-PA stages that performs carrier generation and modulation functions as shown in Figure 3.1 [11].

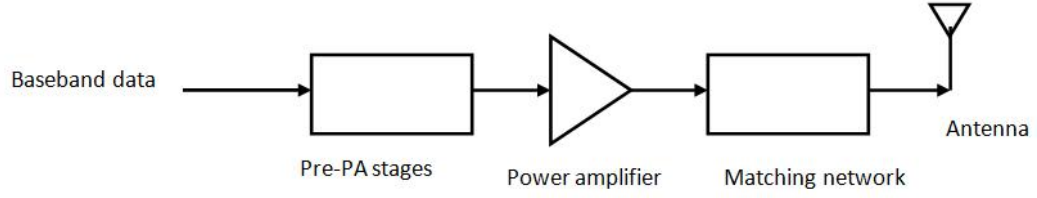


Figure 3.1: Wireless transmitter model [11]

The average power consumption of the transmitter  $P_{TX,avg}$  is given as:

$$P_{TX,avg} = \frac{T_{setup} \cdot [P_{pre-PA} + P_{PA, inactive}] + T_{transmit} \cdot \left[ P_{pre-PA} + \frac{P_{rad}}{\eta_d \cdot \eta_{MN}} \right]}{T_{data}} \quad (3.3)$$

Where  $T_{setup}$  is the transmitter setup time,  $T_{transmit}$  is the data transmission time,  $T_{data}$  is the duration between data packets,  $P_{PA, inactive}$  is the PA power consumption when it is not transmitting,  $P_{pre-PA}$  is the power consumption of the pre-PA stages,  $P_{rad}$  is the radiated power,  $\eta_d$  is the PA drain efficiency and  $\eta_{MN}$  is the matching network efficiency. Minimizing the transmitter energy consumption requires [11]:

1. Minimizing the overhead power:  $P_{pre-PA}$  and  $P_{PA, inactive}$ .
2. Minimizing losses in the power amplifier's device and matching network.
3. Minimizing the duration in which the transmitter is active:  $T_{setup}$  and  $T_{transmit}$
4. Radiating the minimum power required for the communication link:  $P_{rad}$

### 3.2.1 Design Methodology

When  $P_{rad}$  is large compared to  $P_{pre-PA}$  as in cellular and WLAN applications, PA efficiency dictates the overall transmitter efficiency. For this reason, the research focuses on enhancing the PA efficiency in order to boost the transmitter efficiency. However, in implantable medical transmitters applications,  $P_{rad}$  should be much smaller ( $\sim 1\text{mW}$ ) due to the shorter communication distance and to reduce power dissipation in the biological tissues.

$P_{pre-PA}$  is independent of the communication range, thus for low radiated power levels it becomes comparable or larger than  $P_{rad}$ . When  $P_{pre-PA}$  dominates, Equation (3.3) becomes  $P_{TX,ave} = DC_{TX} \cdot P_{pre-PA}$ , where  $DC_{TX} = (T_{setup} + T_{transmit})/T_{data}$  is the transmitter duty cycle. Consequently, reducing  $P_{rad}$  or increasing the PA efficiency

does not achieve considerable power savings. Therefore it is important for a low power transmitter to first achieve low power consumption in pre-PA stages.

Thus, reducing  $P_{\text{Pre-PA}}$  to less than  $P_{\text{rad}}$ , while improving the PA efficiency is useful in reducing the average transmitter power consumption. Conversely, an efficient PA regularly requires higher drive requirements, which translates into higher  $P_{\text{Pre-PA}}$ . This makes it challenging to design an efficient transmitter at low radiated power. This demands enhancing the whole transmitter simultaneously to accomplish the objective of low power consumption.

### 3.2.2 Transmitter Architectures

Low efficiency transmitters usually acquire high pre-PA power. Pre-PA stages comprise carrier generation and modulation circuitries. Thus an effective procedure for reducing pre-PA power is to make use of techniques that reduce the complexity and power consumption of pre-PA stages.

Among the different transmitter architecture, direct conversion and direct modulation architectures are the most commonly used architectures. In the following section, these architectures are presented in terms of their relevance to low power transmitter design.

#### 3.2.2.1. Direct Conversion Architecture

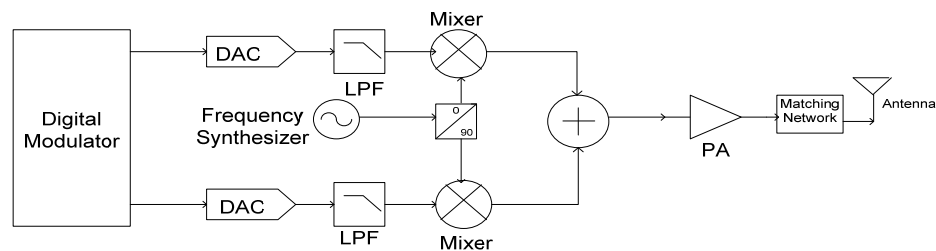


Figure 3.2: Direct conversion transmitter architecture [11]

The direct conversion transmitter shown in Figure 3.2 employs two mixers to convert the baseband signal to the RF band with a pair of quadrature Local Oscillator (LO) signals. This architecture is very flexible because it can maintain a variety of modulation schemes at very high data rates. On the other hand, it entails multi stage circuitry with some stages such as the frequency synthesizer and mixers being very power hungry. This causes high pre-PA power which leads to poor transmitter

---

efficiency as evident in the transmitters reported in [37] and [38] whose efficiencies are roughly 3.3%.

### 3.2.2.2. Direct Modulation Architecture

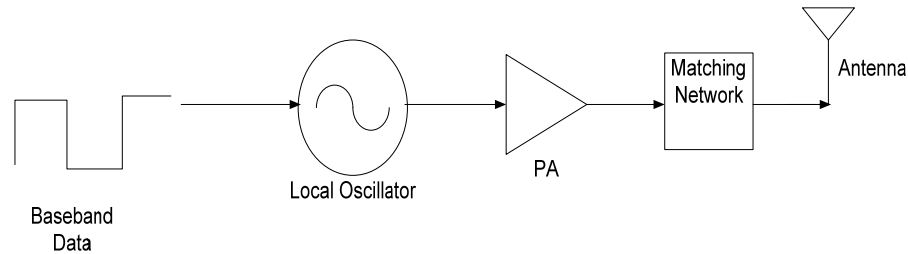


Figure 3.3: Direct modulation transmitter architecture [11]

In implantable transmitter applications, high data rate is not needed due to the low data throughput. With lower data rates, less complex modulation schemes such as On-Off Keying (OOK) and Frequency Shift Keying (FSK) can be used. The use of this simple modulation schemes allow the implementation of the simple direct modulation transmitter as shown in Figure 3.3.

In the direct modulation transmitter, the LO is directly modulated by the baseband data. This removes the need for the power hungry pre-PA blocks such as Digital to Analog Convertors (DACs), I/Q mixers, and I/Q generation circuitry leading to lower pre-PA power which enhances the transmitter efficiency. FSK is attained by modulating the frequency of the LO, while OOK is achieved by power cycling the transmitter. Also, both OOK and FSK relax the PA linearity requirement and allow the use of more efficient PA.

After comparing the features of both transmitter architectures, the direct modulation architecture offers the most suitable solution because of the reduced circuitry and ease of implementation. Moreover, since FHSS is to be employed with FSK which is one of the modulation schemes that this architecture supports, the low power transmitter can be realized on direct modulation architecture.

### 3.2.3 Direct Modulation Implementation

For further reduction in transmitter power consumption the clock generation and carrier modulation can be integrated. The transmitter's modulator consists of PLL whose voltage controlled oscillator (VCO) is modulated directly via the VCO's control line or indirectly through the PLL's frequency divider ratio. When the former

approach was used it implemented energy efficient 6.5 GHz BFSK modulator [39]. The VCO was directly modulated in a closed loop fashion. The variable loop bandwidth scheme employed in this system achieves faster lock time of 20  $\mu$ s compared to fix loop bandwidth schemes. One of the drawbacks of this design is that in the closed loop VCO modulation the achievable data rate is limited by the PLL loop bandwidth.

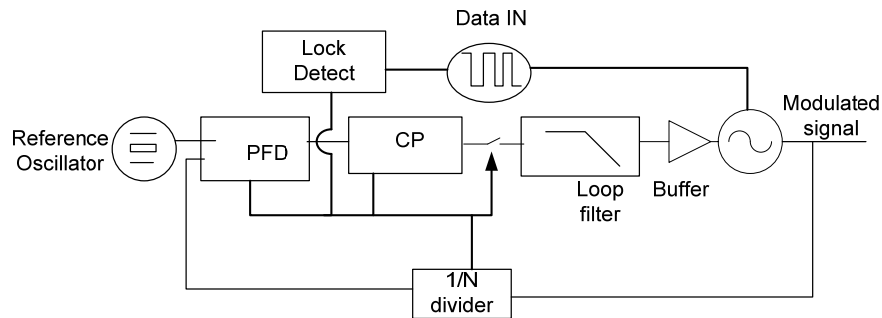


Figure 3.4: FSK direct modulation transmitter topology [40]

To show the feasibility of the direct modulation principle, the topology in Figure 3.4 is proposed to serve as carrier generation and modulation circuit in the low power transmitter.

The PLL can be used as a low power modulator where the VCO is indirectly or directly modulated. In indirect modulation, the modulation is done through the PLL divider. The disadvantage of this scheme is that the data rate is limited by the low pass filtering of the loop. Whereas in direct modulation, the baseband data directly modulates the VCO through its control line, hence there is no upper bound on the data rate. Since the PLL behaves as a high pass filter from the VCO's point of view, low frequency components of the modulated data will be corrupted. One solution to this problem is to open the PLL and then directly modulate the VCO. However, without PLL feedback, the VCO's output frequency is susceptible to being pulled by noise. Still, the frequency drift can be reduced up to 2.5 Hz/ $\mu$ s [41].

The direct modulation architecture shown in Figure 3.4 uses open loop direct VCO modulation. At the beginning of operation, the TX is powered up and the PLL locks the VCO to the desired carrier frequency. Once the VCO is locked, the lock detect will be enabled which will then power off the Phase frequency Detector (PFD), Charge Pump (CP), and 1/N divider to further reduce power consumption, while the carrier is being modulated by the input data through the VCO control line. This design was implemented in [40].

In order to implement the direct modulation architecture described above; a PLL system has been designed. The following section describes the functionality of the PLL system.

### 3.2.4 Phase Locked Loop (PLL)

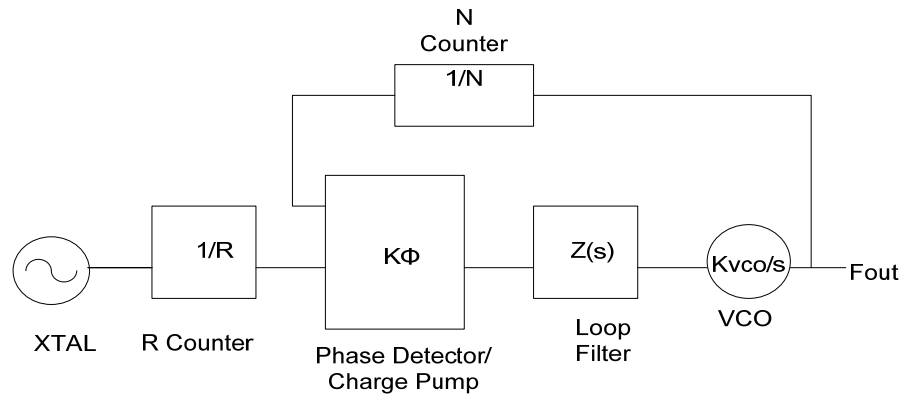


Figure 3.5: Basic PLL topology [42]

The basic architecture of the PLL system is shown in Figure 3.5 above. The reference frequency of the crystal oscillator is compared to the output frequency of the VCO through the PFD. It is optional to employ the R counter where the reference is converted to a lower value for the purpose of comparison. The output current of the PFD represents the phase/frequency difference between the reference frequency and the output frequency. The constant of proportionality is called  $K_{\Phi}$ , which is the amount of current the charge pump circuit can source or sink. The VCO output frequency is controlled by the voltage resulting from the multiplication of the PFD current with loop filter impedance ( $Z(s)$ ). The loop filter bandwidth has the highest impact in many of the performance criteria of the PLL system [42].

#### 3.2.4.1. PLL Performance Characteristics

Phase noise, spurs, and lock time are the most important performance characteristics of PLL system. Phase noise can be defined as phase fluctuations due to the random frequency fluctuations of a signal. Phase noise can be caused by a number of conditions, but is mostly affected by oscillator frequency stability. The parameter that has the largest impact on phase noise is the N counter value and the loop bandwidth. The smaller these value are, the better the phase noise performance because the N counter value multiplies the noise while the wider the loop width the more noise accumulates inside the loop.

---

Another parameter is spurs level which is the noise energy that is focused at discrete offset frequencies from the carrier. The loop bandwidth has the biggest impact on the spurs level, the wider the loop bandwidth the higher the spurs level.

Lock time is the total time the PLL takes to change frequencies when the N counter value is changed. The wider the loop bandwidth the shorter the lock time.

Now we have introduced the basic PLL functionality and performance characteristics, in the next chapter we will present the design of a PLL system the will be used to implement the concept of the direct modulation transmitter.

### 3.3 System Architecture

The transmitter system specifications obtained so far can be summarized as follows. The operating frequency is 2.4 GHz, FHSS as a part of Bluetooth low energy wireless protocol, an inductive link will be used as transmitter power supply, and direct modulation transmitter architecture will be employed. From this a system level architecture of the low power transmitter can be sketched. In the following each block of the system architecture will be analyzed.

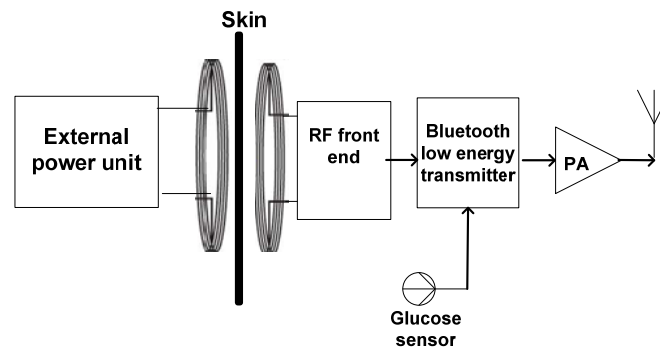


Figure 3.6: System level architecture

This section gives an overview of the system functionality. It addresses the issues associated with the major system units: implantable unit, telemetry power unit and the receiving unit.

A simplified diagram of the system is shown in Figure 3.6 above. The power will be supplied inductively to the implantable unit. The external powering unit produces a high frequency magnetic field in an external coil, through which the power is inductively conveyed to an internal coil that is associated with the implantable

---

system. The frequency at which the inductive link operates as well as the rest of external power unit circuitry is investigated and presented later in this section.

At sensor level, in order to define any waveform, sampling must be done at a frequency that will represent the full dimensions of the waveform. For the specific application of continuous glucose monitoring, the glucose sensor provides time series data, including amount, direction, rate of change and rate of acceleration. This enables use of derivative information to predict the waveform of glucose which allows the user to act proactively and take appropriate treatment decisions. High fidelity monitoring sufficient to follow the intrinsic blood glucose dynamics of all diabetic subjects requires a Nyquist sampling period of almost 10 minute [43]. The sensor needs to be left on for some time to settle for its final value before taking the measurement. This period of time depends on type of sensor used and as stated earlier the smaller the implant size the shorter this time would be.

In the system architecture in Figure 3.6, the measured glucose data is then supplied to the Bluetooth low energy transmitter unit which contains the protocol stack, frequency synthesizer, and data modulation circuitry. The modulated carrier is passed to the power amplifier to boost the signal power up to the level required for reliable communication. The power amplifier is required to be highly efficient in order to minimize the power dissipation so that the low power consumption goal is achieved. The power amplifier class and mode of operation was investigated in depth and is presented later in this section.

The amplified signal will then be radiated through the skin to the intended receiver. The patient's mobile phone or PDA which most likely supports Bluetooth can be exploited as the target receiver. The Bluetooth in the receiver has to be operated in dual mode operation i.e. supporting both Bluetooth Enhanced Data Rate (EDR), which is used in most mobile phone applications, plus Bluetooth low energy in order to be able to communicate with the single mode Bluetooth low energy module embedded in the implantable transmitter.

### 3.3.1 Bluetooth Low Energy Transmitter

In this section we introduce carrier generation and modulation procedure. We start by introducing the concept of FHSS and then present the Bluetooth Low energy

---

transmitter architecture. Implementing low power techniques discussed earlier to carrier generation and modulation will be presented as well.

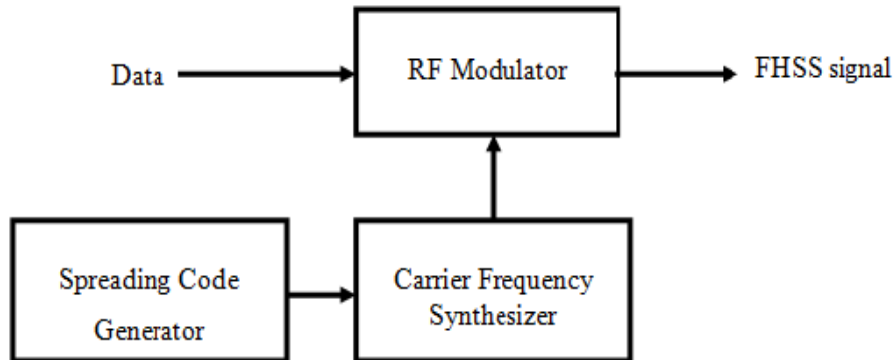


Figure 3.7: General FHSS transmitter

The architecture of a general FHSS transmitter is shown in Figure 3.7. The frequency of the carrier is modified periodically (hopped) according to a specific sequence of frequencies provided by the spreading code generator. In FHSS systems, the spreading code is the list of frequencies to be used for the carrier signal, the “hopping sequence”. For operation in 2.4 GHz band the FCC requires that 75 or more frequencies to be used with a maximum dwell time of 400 milliseconds.

The message modulates the (hopping) carrier through FSK modulation, thus generating a narrow band signal for the duration of each dwell.

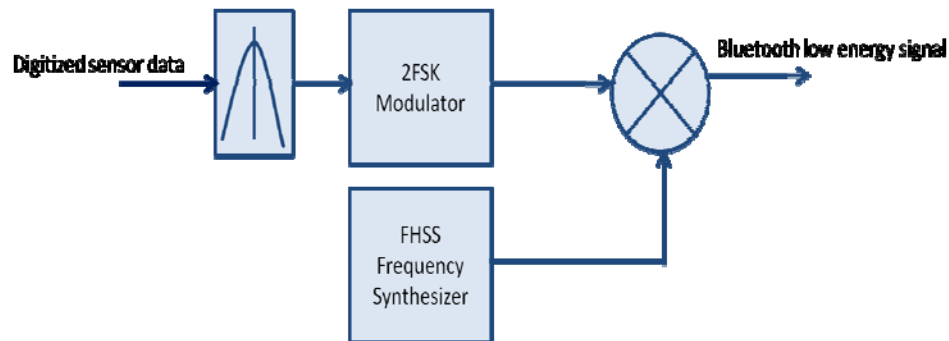


Figure 3.8: Bluetooth low energy transmitter

The BLE transmitters in Figure 3.8 implements the same principles of the general FHSS transmitter introduced previously with slight modifications. The basic system blocks in the Bluetooth low energy transmitter are discussed below.

### 3.3.1.1. GFSK Modulation

A Bluetooth low energy transmitter employs Gaussian Frequency Shift Keying (GFSK). This binary bit stream is passed through a Gaussian low pass filter that has a

---

pulse shaping coefficient (BT) of 0.5. Accordingly, for a binary data rate of 1.0 Mbps the filter's -3.0 dB Bandwidth is 500 kHz.

$$\begin{aligned} \text{Filter's } -3 \text{ dB cutoff} &= BT \times \text{Bit rate} \\ &= 0.5 \times 10^6 = 500 \text{ kHz} \end{aligned} \quad (3.4)$$

The modulation index ( $\mu$ ) is the frequency deviation divided by bit rate. Bluetooth low energy utilizes a modulation index of 0.5, while the classic Bluetooth technology uses 0.35. An index of 0.5 is close to the Gaussian Minimum Shift Keying (GMSK) scheme which lowers the radio power requirements.

The only difference between a GFSK and an FSK modulator is that in GFSK modulation the baseband data is passed through a Gaussian filter. This makes the pulses smoother and helps reduce the transmitter spectral width.

#### 3.3.1.2. Frequency Hopping Mechanism

There are two major differences between the frequency hopping scheme used in classic Bluetooth technology and that used in Bluetooth low energy. Bluetooth low energy uses fewer channels compared to the classic Bluetooth technology. The reason for this can be concluded from the previous discussion on modulation index. Since Bluetooth low energy employs higher modulation index the requirements for how steep the channel filters need to be are relaxed, therefore its signal takes up more bandwidth. Consequently, Bluetooth low energy channels are spaced 2 MHz apart, rather than 1 MHz apart as in classic Bluetooth technology.

In addition, the frequency hopping scheme in Bluetooth low energy is less complex compared to that applied in classic Bluetooth technology. The hopping sequence is defined by pseudo-random sequences in classic Bluetooth, as opposed to that utilized in Bluetooth low energy where the radio simply hops in channels every time it hops, wrapping around when it comes to the end of the possible values. Moreover, Bluetooth low energy supports adaptive frequency hopping, which implies identifying channels utilized by other devices (particularly Wi-Fi) and avoiding using those, this allows better coexistence with other 2.4 GHz radio devices [44].

All of these relaxed frequency hopping requirements were made in order to make it possible for Bluetooth low energy radios to achieve the target of lower power consumption.

---

### 3.3.2 Power Amplifier Design

Linearity and efficiency are two major requirements needed from an RF PA. Linearity is the capability of amplifying a signal without distorting it while efficiency is the ability to translate DC to RF energy with minimum power dissipation and heat generation. Both these requirements are significant for contemporary wireless communication systems but incompatible in nature. Amplifiers are rated at a maximum power output for use in different applications. The most efficient output for an amplifier typically occurs when operating at the highest rated output. In contrast to Class A, B and C amplifiers where operation in the triode region should be avoided, class D, E, and F amplifiers rely on operation in the triode region for optimum efficiency and output power. These amplifiers are often called 'switching mode' amplifiers and are typically used in ISM band transmitters and transceivers because of their inherent high efficiency operation at low voltage levels [45].

Compared to the conventional linear class operation of PAs, the amplifiers with displacement of peak drain/collector voltage and current can attain much higher efficiency. This incident only occurs when the transistor act as an ideal switch which only permits either current or voltage peak to take place at one time. In such switching mode, power dissipation in the transistor can be completely eliminated, and consequently can achieve 100% efficiency, theoretically. In contrast linear PAs, switching mode operation requires the output voltage and current of the amplifier to be the transient response of a specifically designed output matching network to the time variant switch and a constant DC power supply. In addition, switching implies that the output current and voltage are discontinuous so that they have many higher order harmonic components. Thus, a proper filtering scheme must be used to suppress the harmonics in order to obtain high efficiency since they also dissipate power [46].

Class E, which is a switching mode PA has been chosen for this design. The most important advantage of class E power amplifiers over linear mode classes is their ability to provide high efficiency. The benefits of using a class E PA for this design over other switching mode PAs can be summarized in two points: it only needs a single transistor with no baluns (balanced to unbalanced) and it is a circuit that converts a differential signal to a single-ended signal. Contrary to the class E topology, the class D topology utilizes two transistors and involves input and output

---

baluns [47]. Whereas class F PA requires harmonic termination, an open circuit at third harmonic and short circuit at the second one.

Subsequently, class E PAs are relatively easy to design with a small size, light weight and relative intolerance to circuit variation, which fulfils the requirement for system integration and miniaturization. Furthermore, class E power amplifiers can be designed to operate either at a specific frequency, i.e., narrow-band operation, or at a wide frequency band, depending on the demand.

Before moving into the PA circuit design it is extremely important to discuss the transistor bias conditions. Since PA will be used for RF frequencies, it is necessary to assess the effect of this on the bias region for the transistor and also the implications of the choice of a specific bias region on the transistor frequency response at relatively high frequencies i.e. GHz range.

### 3.3.3 Low Power Circuit Techniques

Low power consumption is a desired feature in wireless transceivers. In certain applications such as implantable devices, low power consumption is mandatory to allow the device to run in a battery less regime or for long durations without the need of battery replacement.

#### 3.3.3.1. MOSFET Regions of Operation

CMOS technology persists to be a viable candidate for the implementation of low power ICs. Biasing the transistor in the weak inversion region not only reduces the power consumption but also achieves the highest transconductance efficiency ( $gm/ID$ ). However, for RFIC design, the transistor frequency response needs to be considered. This is usually given in terms of the unit gain frequency ( $f_T$ ). A weakly inverted transistor exhibits a poor frequency response. For this reason, a new figure of merit needs to be defined to characterize the transistor performance under high frequency of operation.

The performance criteria is defined as ( $gmf_T/ID$ ), which is expressed as a function of the normalized drain current [48] as given in Equation (3.5) below:

$$\frac{gmf_T}{I_D} = \frac{4\mu_0}{\pi L^2} \cdot \frac{I_N[n-1+P(I_N)]^{-1}}{(1+\theta\sqrt{I_N})(1+\sqrt{4I_N+1})^2} \quad (3.5)$$

Where  $\mu_0$  is the low field mobility,  $L$  is the channel length of the transistor,  $\theta$  is process dependent parameter. The drain current is normalized in order to decide on the transistor's region of operation irrespective to aspect ratio. The normalized current is given by:

$$I_N = \frac{I_D}{I_Z} \quad (3.6)$$

Where

$$I_Z = 2nU_T^2 \frac{W}{L} \mu_0 C_{ox} \quad (3.7)$$

Equation (3.5) was used to find the optimum value for  $I_N$  that yields the maximum value for  $gm_f/I_D$ . The optimum value for  $I_N$  range between [48]:

Table 3.3: Bounds for transition from weak to moderate and from moderate to strong inversion [48]

	Transition from weak to moderate inversion	Transition from moderate to strong inversion
$V_{GS}-V_T$	0	$4.6nU_T$
$I_N = I_D/I_Z$	0.48	5.75

### 3.3.3.2. $gm_f$ -to-Current Ratio ( $gm_f/I_D$ )

Power consumption is becoming as important as performance requirements including reliability and speed in contemporary wireless communication systems. To identify both performance and DC power consumption of a MOS transistor in any region of operation, a new figure of merit is defined, the  $gm_f$ -to-current ratio ( $gm_f/I_D$ ). By considering both  $gm$  and  $f_t$ , maximizing the  $gm_f/I_D$  for a set bias current results in maximum achievable Gain Bandwidth Product (GBW). This distinctive aspect makes the  $gm_f/I_D$  an appropriate goal function for the optimization of the ultra low power RF/analog circuits. The  $gm_f/I_D$  can be expressed as a function of the normalized current  $I_N$ . This will permit to show that to maximize the  $gm_f/I_D$ , the MOS transistor must operate in moderate inversion region. The  $gm_f$ -to-current ratio is given by:

$$\frac{gm_f t}{I_D} = \frac{4\mu_0}{\pi L^2} \cdot \frac{I_N [n-1+P(I_N)]^{-1}}{(1+\theta\sqrt{I_N})(1+\sqrt{4I_N+1})^2} \quad (3.8)$$

Equation (3.8) is utilized to find the optimum value of the normalized current at which the  $gm_f/I_D$  reaches its maximum value. The optimum value of  $I_N$  varies from 0.5 to 2.5 for different values of  $n$  and  $\theta$  [48]. As seen in Table 3.3, the transistor stays

---

in moderate inversion region for  $0.48 < I_N < 5.75$ , and therefore, the maximum  $gm_f/I_D$  occurs in moderate inversion region.

### 3.3.4 Power Supply Methodology

Supplying power to implantable devices for long term operation is a challenging task. Conventionally, implantable batteries and percutaneous link power supply systems are used. Nevertheless, the batteries have limited life time after which they require charging or replacement, and the percutaneous links across the skin entail infection risks.

Wireless systems have been utilized to supply power to implantable biomedical devices [49]. This greatly reduces the implant size since the energy storage device takes a considerable space of the implant size.

Some experimentation has been conducted on using energy scavenging techniques to supply power to implantable devices; however the output voltages are still not stable to be used as power supply for implantable devices [50].

An inductive link between two magnetically coupled coils can be utilized to wirelessly power implantable devices. These devices can either be battery-less or need to be constantly powered from an external battery, or have miniature rechargeable batteries that should be periodically charged. In both cases, the inductive power transmission should be very efficient to minimize the size of the external battery, and eliminate overheating the surrounding tissue as a result of exceeding the exposure limit to an electromagnetic field [51].

Miniaturization is another major requirement for implantable devices, so little room is left for antennas. This increases the operating frequency of any wireless link within a given space, which therefore increases the frequency of a power transmitter used to supply power inductively to the implantable device. However, the transfer of energy becomes less efficient as the frequency of transmission increases presenting a dilemma that size restrictions increase the possible frequency of operation, yet transmission efficiency is reduced as the frequency increases.

#### 3.3.4.1. Electromagnetic Fields

When electromagnetic fields are intentionally created, it is generally the case that the external unit antenna is primarily intended to create either an electric field (E)

---

---

or a magnetic field (H). However, when either of these is created, the laws of electrodynamics automatically imply that the other field is also created.

In this interaction, two regions of operation can be identified. Whether the power receiving unit i.e. implantable unit is in the near or far field depends on how close it is to the external antenna and the operating frequency or wavelength. This boundary is commonly referred to as the radian sphere, inside which the device is said to be in the near field otherwise it is in the far field. The radius of this is a sphere which has a value of  $\lambda/2\pi$  and sets the border between near and far field regions [52].

With this we conclude the concepts behind low power transmitter system architecture. A direct application of these concepts is presented in the next chapter where low power circuit and system techniques are used in the design of the transmitter system. The design calculations and simulation results are shown for each system unit described previously.

---

## CHAPTER 4

### TRANSMITTER DESIGN AND SIMULATION RESULTS

The low power transmitter is intended for use in biomedical applications, specifically continuous glucose sensing. Thus characterizing the signal interaction with biological tissue is of paramount importance to this system design. This can be summarized in two ways: Firstly, the maximum limit of energy absorption by a living tissue should not be exceeded. Secondly, RF signals propagating through biological tissue would necessarily encounter attenuation; the amount of this attenuation depends on the RF frequency itself, tissue electrical properties as well as tissue thickness. Thus it is mandatory to identify the amount of this attenuation in order to design appropriate circuitry to compensate for it. The limits for maximum allowed power absorption as well as the amount of RF power attenuation at the transmitter operating frequency i.e. 2.4 GHz were presented first in this chapter.

Adhering to the low power system and circuit techniques established in the previous chapter, and safe operation guidelines to be presented in this chapter, the low power transmitter design has been realized.

According to the power gain needed to combat the attenuation encountered from the propagation through the biological tissue, the implantable transmitter class E PA has been designed. The design of the external power unit that will be used to supply power inductively to the implantable transmitter is described. It also incorporates a class E PA.

The implementation of direct modulation architecture is demonstrated for which a PLL has been designed. The results for PLL design as well as the principle of direct VCO modulation are illustrated.

Bluetooth low energy protocol defines certain standards for transmitter operation. To verify that the operation of low power transmitter complies with these rules; the complete transmitter design has been integrated and tested against these requirements.

---

Finally a system functionality scenario is illustrated in which the transmitter functionality time line, duty cycle, and proposed wake up procedure, and detection range are demonstrated.

#### 4.1 RF Signal –Biological Tissue Interaction

Signal propagation and attenuation in biological tissues is an important factor to be considered when designing implantable devices. The factors which determine the RF signal power attenuation in a biomedical implant are frequency, permittivity, conductivity and permeability [53][54]. Therefore, it is desirable to keep the transmitted power as low as possible while ensuring that the detected signals are able to faithfully reproduce the required information. These two important issues are discussed in the next two sections covering the maximum local electric field, power density, specific absorption rate and signal attenuation. In short we are determining what is the maximum energy allowed to be absorbed by a biological tissue without causing damage for cells under investigation, and under this limit what is the gain required by the power amplifier necessary to compensate for the power attenuation due to tissue absorption.

##### 4.1.1 Energy Absorption

The RF safety of implantable devices is of paramount importance because they expose patients, their families and medical professionals to RF radiations. This is due to the heating effects that might be caused by internal electric fields. Since biological tissues are primarily nonmagnetic, energy absorption due to magnetic field is negligible. The implantable device under consideration will be subcutaneous which means it will be directly beneath the skin.

The guidelines for Electromagnetic Field exposure (EMF) are in terms of Specific Absorption Rate (SAR) and the equivalent plane wave power density (S W/m<sup>2</sup>). SAR is a measure of the rate of energy absorption per unit mass due to exposure to an RF source. SAR is normalized to mass and is defined as:

$$SAR = \frac{\sigma_{eff} E_{rms}^2}{\rho} (W / kg) \quad (4.1)$$

Where  $\rho$  is the mass density which is approximately  $1000 \text{ kg/m}^3$  for most biological tissues,  $E_{rms}$  is the root mean square value of the electric field  $E$  at the measurement point,  $\sigma_{eff}$  is the effective conductivity of the biological material such as skin and is proportional to the frequency of the applied field. Figure 4.1 below depicts measurements in-vivo of the permittivity and conductivity of skin [55][57].

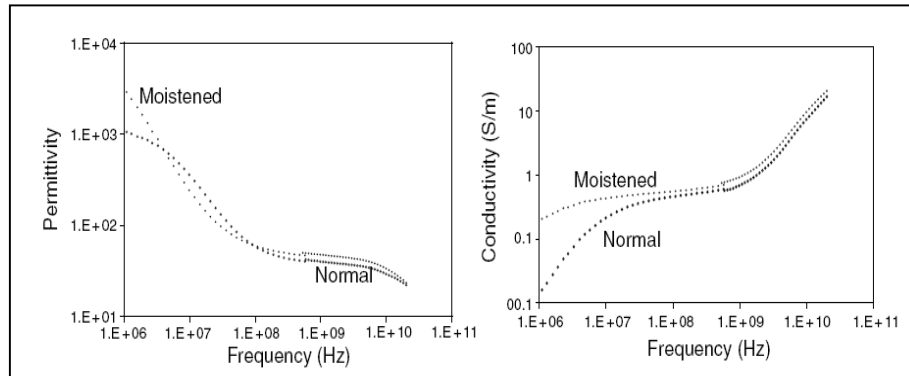


Figure 4.1: Dielectric properties of skin tissues between 1M and 10GHz [55][57]

There has been much research in the area of health effects of EMF exposure of human populations. There are now published guidelines to establish a safe SAR for all frequency bands. Examples of these published guidelines and restrictions are shown in Table 4.1 and Table 4.2 which are extracted from a document published by the International Commission on Non Ionizing Radiation Protection (ICNIRP) [58]. Other more recent guidelines and standards are published by the IEEE [59]. Occupational exposure applies to adults aware of the risk of radiations and exposed to controlled amounts of radiations. The general public are people of all ages and health status who are unaware that they are being exposed to radiations. Table I below shows the guidelines for safe SAR. If the implantable device under consideration is operated at 2.4GHz, implanted under the skin and in one of the limbs, then the local SAR limit is 4 W/kg.

The guidelines in [58] also specify the maximum electric field  $E$  (V/m) and equivalent plane power dissipation  $S$  ( $\text{W/m}^2$ ).

Table 4.1: Basic restrictions for time varying electric and magnetic fields for frequencies up to 10 GHz [58]

Exposure characteristics	Frequency range	Current density for head and trunk (mA m <sup>-2</sup> ) (rms)	Whole-body average SAR (W kg <sup>-1</sup> )	Localized SAR (head and trunk) (W kg <sup>-1</sup> )	Localized SAR (limbs) (W kg <sup>-1</sup> )
Occupational exposure	up to 1 Hz	40	—	—	—
	1–4 Hz	40/ <i>f</i>	—	—	—
	4 Hz–1 kHz	10	—	—	—
	1–100 kHz	<i>f</i> /100	—	—	—
	100 kHz–10 MHz	<i>f</i> /100	0.4	10	20
General public exposure	10 MHz–10 GHz	—	0.4	10	20
	up to 1 Hz	8	—	—	—
	1–4 Hz	8/ <i>f</i>	—	—	—
	4 Hz–1 kHz	2	—	—	—
	1–100 kHz	<i>f</i> /500	—	—	—
	100 kHz–10 MHz	<i>f</i> /500	0.08	2	4
	10 MHz–10 GHz	—	0.08	2	4

<sup>a</sup>Note:

1. *f* is the frequency in hertz.
2. Because of electrical inhomogeneity of the body, current densities should be averaged over a cross-section of 1 cm<sup>2</sup> perpendicular to the current direction.
3. For frequencies up to 100 kHz, peak current density values can be obtained by multiplying the rms value by  $\sqrt{2}$  (~1.414). For pulses of duration  $t_p$ , the equivalent frequency to apply in the basic restrictions should be calculated as  $f = 1/(2t_p)$ .
4. For frequencies up to 100 kHz and for pulsed magnetic fields, the maximum current density associated with the pulses can be calculated from the rise/fall times and the maximum rate of change of magnetic flux density. The induced current density can then be compared with the appropriate basic restriction.
5. All SAR values are to be averaged over any 6-min period.
6. Localized SAR averaging mass is any 10 g of contiguous tissue; the maximum SAR so obtained should be the value used for the estimation of exposure.
7. For pulses of duration  $t_p$ , the equivalent frequency to apply in the basic restrictions should be calculated as  $f = 1/(2t_p)$ . Additionally, for pulsed exposures in the frequency range 0.3 to 10 GHz and for localized exposure of the head, in order to limit or avoid auditory effects caused by thermoelastic expansion, an additional basic restriction is recommended. This is that the SA should not exceed 10 mJ kg<sup>-1</sup> for workers and 2mJ kg<sup>-1</sup> for the general public, averaged over 10 g tissue.

Table 4.2: Reference levels for general public exposure to time-varying electric and magnetic fields (unperturbed rms values) [58]

Frequency range	E-field strength (V m <sup>-1</sup> )	H-field strength (A m <sup>-1</sup> )	B-field (μT)	Equivalent plane wave power density $S_{eq}$ (W m <sup>-2</sup> )
up to 1 Hz	—	$3.2 \times 10^4$	$4 \times 10^4$	—
1–8 Hz	10,000	$3.2 \times 10^4/f^2$	$4 \times 10^4/f^2$	—
8–25 Hz	10,000	4,000/ <i>f</i>	5,000/ <i>f</i>	—
0.025–0.8 kHz	250/ <i>f</i>	4/ <i>f</i>	5/ <i>f</i>	—
0.8–3 kHz	250/ <i>f</i>	5	6.25	—
3–150 kHz	87	5	6.25	—
0.15–1 MHz	87	0.73/ <i>f</i>	0.92/ <i>f</i>	—
1–10 MHz	87/ <i>f</i> <sup>1/2</sup>	0.73/ <i>f</i>	0.92/ <i>f</i>	—
10–400 MHz	28	0.073	0.092	2
400–2,000 MHz	1.375/ <i>f</i> <sup>1/2</sup>	0.0037/ <i>f</i> <sup>1/2</sup>	0.0046/ <i>f</i> <sup>1/2</sup>	<i>f</i> /200
2–300 GHz	61	0.16	0.20	10

<sup>a</sup>Note:

1. *f* as indicated in the frequency range column.
2. Provided that basic restrictions are met and adverse indirect effects can be excluded, field strength values can be exceeded.
3. For frequencies between 100 kHz and 10 GHz,  $S_{eq}$ , E<sup>2</sup>, H<sup>2</sup>, and B<sup>2</sup> are to be averaged over any 6-min period.
4. For peak values at frequencies up to 100 kHz see Table 4, note 3.
5. For peak values at frequencies exceeding 100 kHz see Figs. 1 and 2. Between 100 kHz and 10 MHz, peak values for the field strengths are obtained by interpolation from the 1.5-fold peak at 100 kHz to the 32-fold peak at 10 MHz. For frequencies exceeding 10 MHz it is suggested that the peak equivalent plane wave power density, as averaged over the pulse width does not exceed 1,000 times the  $S_{eq}$  restrictions, or that the field strength does not exceed 32 times the field strength exposure levels given in the table.
6. For frequencies exceeding 10 GHz,  $S_{eq}$ , E<sup>2</sup>, H<sup>2</sup>, and B<sup>2</sup> are to be averaged over any 68/*f*<sup>1.05</sup>-min period (*f* in GHz).
7. No E-field value is provided for frequencies <1 Hz, which are effectively static electric fields. perception of surface electric charges will not occur at field strengths less than 25 kVm<sup>-1</sup>. Spark discharges causing stress or annoyance should be avoided.

From Table 4.2, it is concluded that for this application, the maximum E and S are 61 V/m and 10 W/m<sup>2</sup> respectively. The magnitude of the power density stored in a sinusoidal electric field E in a biological material can be calculated using Equation (4.2):

$$P = \frac{E_{rms}}{\sqrt{2}} \sqrt{\frac{\epsilon}{\mu_0}} \sqrt{1 + \sqrt{1 + \left(\frac{\sigma_{eff}}{\omega\epsilon}\right)^2}} \quad (4.2)$$

#### 4.1.2 Signal Propagation and Attenuation

In lossy biological materials, the RF signal can be attenuated before being detected by the neighbouring receiver. The magnitude of the sinusoidal RF signal propagating in a biological material decreases exponentially and can be calculated at distance  $z$  from the source according to:

$$E(z, t) = E_0 e^{-\alpha z} \sin(\omega t - \beta z - \phi) \quad (4.3)$$

Where,  $\alpha$  is the attenuation coefficient in (Np/m), Np is dimensionless and therefore  $\alpha$  represents the signal loss per m.  $\beta$  is the phase constant in (radians/m), and  $\phi$  represents an arbitrary phase shift. To calculate the amount of attenuation only  $\alpha$  is required which is defined as [54]:

$$\alpha = \omega \sqrt{\frac{\mu_0 \epsilon}{2} \left( \sqrt{1 + \left(\frac{\sigma_{eff}}{\omega\epsilon}\right)^2} - 1 \right)} \quad (4.4)$$

The dielectric properties for the skin at 2.4 GHz are given in Table 4.3 below:

Table 4.3: Dielectric properties of skin tissue at 2.4 GHz

Property	Value
Effective conductivity ( $\sigma_{eff}$ )	0.7 S/m
permittivity ( $\epsilon$ )	$50 \times 8.85 \times 10^{-12}$ F/m
Permeability ( $\mu$ )	$4\pi \times 10^{-7}$ H/m
Attenuation constant ( $\alpha$ )	13.3 Np/m

As mentioned earlier, the implantable transmitter will be placed in the subcutaneous tissue directly underneath the skin. Thus the biological tissue would be modelled by a single layer i.e. skin. The average skin thickness of a human ranges between 0.5 mm up to 4 mm in palms and soles [60]. The implantable unit could be placed in patient's thigh, which is quit an appropriate place for implantation since it is less exposed than other limbs like hands and arms, therefore, less interaction is likely to occur with the surrounding environment that might lead to implantable device displacement or damage. The skin thickness at thigh of an average human is typically in the range of 1.55 mm [61].

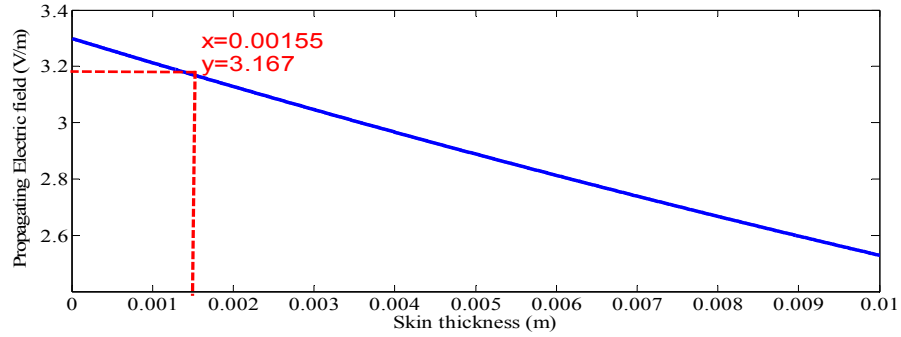


Figure 4.2: Electric field (V/m) versus skin thickness (m) at 2.4 GHz

The attenuation encountered by the RF signal electric field as it propagates through the skin is depicted in Figure 4.2. Starting from a maximum electric field value of 3.3 V/m, at 1.55 mm the electric field decreased to a value of 3.167 V/m. This means that the electric field has been attenuated approximately by 4%. The electric field attenuates further as it propagates through the skin. In deeply implantable devices where the biological tissue is characterized by several layers such as fat, muscle, organ tissue, etc the attenuation would be more severe. Further signal loss would be encountered due to reflection between different body layers.

In order to compensate for this attenuation; the PA needs to be designed for a specific power gain. Therefore, it is more useful to present the RF signal attenuation in terms of power units. The power density is computed using Equation (4.2) and the result is shown in Figure 4.3.

At 1.55 mm, the RF signal power is attenuated by 16.7 dB as shown in Figure 4.3. The PA needs to have a power gain large enough to cancel this attenuation or at least compensate for most of it. The minimum power gain needed depends on the receiver sensitivity communication range. This will be explained later in this chapter.

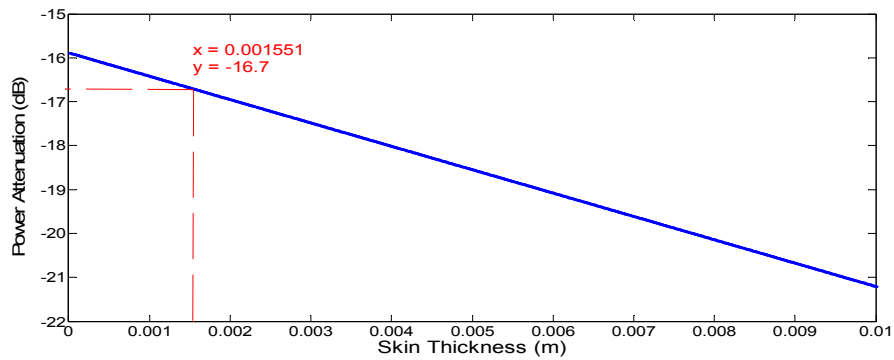


Figure 4.3: Power attenuation at 2.4 GHz

## 4.2 Class E PA Circuit Design

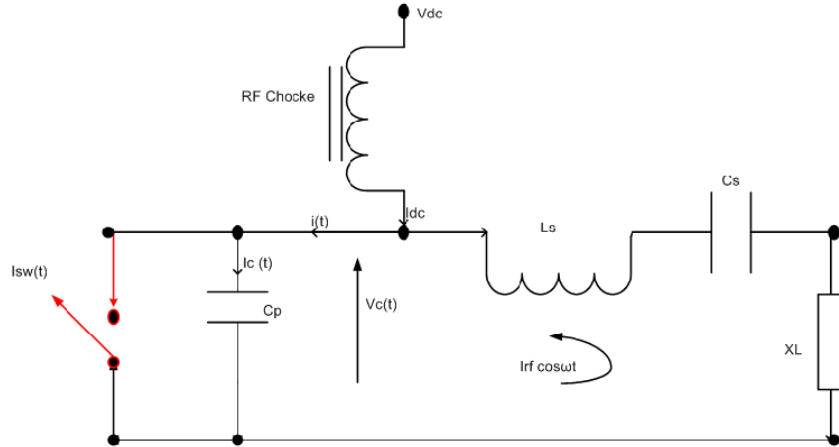


Figure 4.4: Basic class E PA schematic

The class E PA design was based on the analysis provided in [46]. A summary of this analysis is provided below. Figure 4.4 shows the basic class E PA schematic that has been used in this analysis:

- An ideal switch is assumed to simplify the analysis.
- RF choke: to block alternating currents.
- $C_p$ : neither small enough to be a parasitic nor large enough to be a harmonic short.
- $L_s$  and  $C_s$ : series resonant circuit at the operating frequency which in this design is 2.4 GHz.

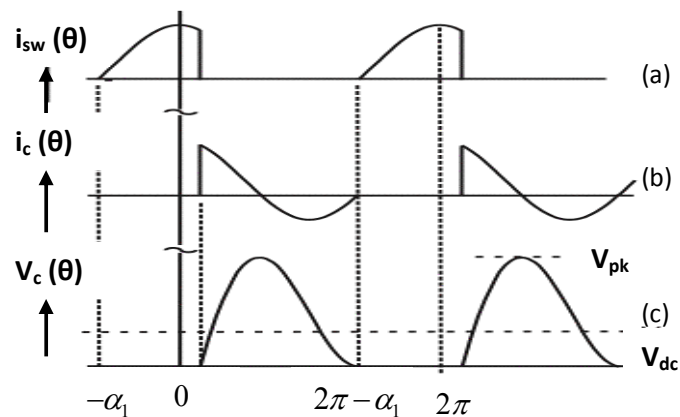


Figure 4.5: Class E RF waveforms (a) switching current, (b) shunt capacitor current, and (c) switch/shut capacitor voltage [46]

- Conduction angle ( $\phi$ ): The Conduction is the portion of the input signal cycle during which the amplifying device conducts,  $\phi = \alpha_1 + \alpha_2$ . The  $\alpha$  parameter characterizes the sharpness of the switch-off characteristics, which becomes instantaneous when  $\alpha = \pi$ . The transistor switching characteristics are illustrated in Figure 4.5 above.
- When the switch is open, the voltage across  $C_p$  rises up and reaches its peak when the capacitor current crosses zero.
- As a direct consequence of assuming an ideal switch, voltage and current do not coexist resulting in a high efficient circuit.
- The efficiency of an ideal class E amplifier will always be 100% in spite of the conduction angle.

#### 4.2.1 Design Parameters

The first parameter to be selected is an appropriate value for the maximum device current  $I_{max}$ . Since the device is to be forced into the role of a switch it is necessary to lower the value of  $I_{max}$  to be a suitable value for the device peak current  $I_{pk}$ . From previous designs of class A and B PAs [46], the device working value was 2.5 A, for class E application a value of  $I_{pk} = 0.1$  A will be taken. This value of current might seem large for low power design but we need to consider the PA components values. Pushing for very low peak currents results in unrealistic values for amplifier component values, especially capacitors. They would be small enough to be waived by circuit parasitic. Pushing for rail-to-rail voltage swings to obtain higher efficiencies certainly results in much reduced peak RF currents, even for standard reduced conduction angle modes.

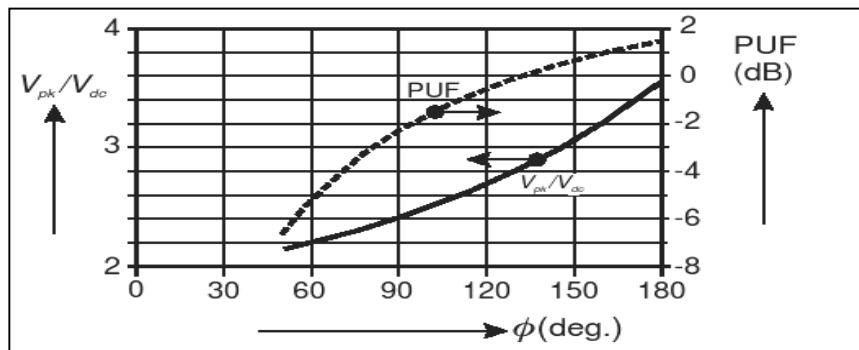


Figure 4.6: Class E design chart for conduction angle ( $\phi$ ) [46]

Using Figure 4.6, a value of  $125^\circ$  is chosen for the conduction angle ( $\phi$ ). This value seeks to attain the highest Power Utilization factor (PUF) (just below 0 dB). PUF is the ratio of the RF power delivered by a device in a specific mode under consideration to the power it would deliver as a simple class E PA. This value was chosen such that the peak voltage is kept below 3:1 factor of the DC supply.

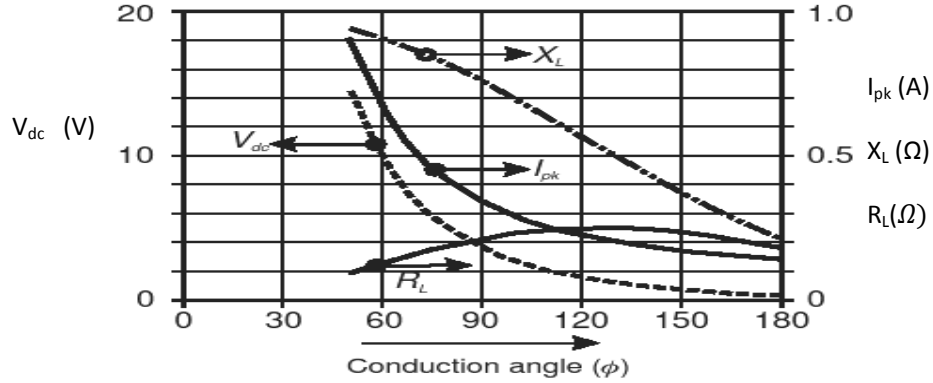


Figure 4.7: Design parameters for class E PA, as a function of the conduction angle[46]

The values for the four normalized circuit parameters are given in Figure 4.7, as follows,  $V_{dc} = 1.36 \text{ V}$ ,  $I_{pk} = 4.8 \text{ A}$ ,  $R_L = 0.252 \Omega$ ,  $X_L = 0.533 \Omega$ .  $V_{dc}$  and  $I_{pk}$  were rescaled for the desired design values. 3.3V and 0.1A were chosen for  $V_{dc}$  and  $I_{pk}$  respectively. Through simulations those values achieved a good performance in terms of switching capabilities and low current and voltage supply requirements. This means that all the impedance elements have to be rescaled by a factor of:

$$K = \frac{3.3}{1.36} \div \frac{0.1}{4.28} = 103.8 \quad (4.5)$$

The values of the circuit components values  $C_p$ ,  $L_S$  and  $C_S$  can be calculated as follows :

$$C_p = \frac{1}{\omega K} \quad (4.6)$$

$X_L$  and  $R_L$  which are the load series reactance and resistance respectively need to be rescaled by the factor K. A resonator at 2.4GHz needs to be placed in series with the series  $R_L/X_L$  combination.

$$\begin{aligned} X_L^* &= 0.533 * K = 55.35\Omega \\ R_L^* &= 0.252 * K = 26.17\Omega \\ L_l &= X_L^* / 2\pi f = 3.67nH \end{aligned} \quad (4.7)$$

Resonant elements are not uniquely determined and it is necessary to select only a reasonable value for the quality factor of the inductor.  $Q=10$  was chosen, it gives an acceptable degree of selectivity,

$$\omega X_s = 40 \quad (4.8)$$

$L_s$  and  $C_s$  were then calculated. The last step is to transform the rescaled  $26.17\Omega$  load resistor to a  $50\Omega$  load. The series R-C part of the resonator can be transformed to parallel R-C, where the shunt resistor is specified to be  $50\Omega$ . The required transformation ratio is:

$$m = \frac{R_o}{R_T} = \frac{50}{26.17} = 1.91 \quad (4.9)$$

Where  $R_o$  is the output ( $50\Omega$ ) and  $R_T$  is the resistance to be transformed =  $26.17\Omega$ . This value of  $m$  did not achieve the optimum performance. The maximum gain value was achieved at  $2.4\text{GHz}$ . Tuning simulation parameters to a value of  $m=0.955$ , achieved an acceptable performance in terms of component values and circuit efficiency. The value of shunt capacitance is given by

$$X_{p1} = \frac{50}{\sqrt{m-1}} = 236.38\Omega$$

$$\Rightarrow C_{p1} = 0.281\text{pF} \text{ , at } 2.4\text{GHz} \quad (4.10)$$

The series resonating inductance will now have a different value given by:

$$X_s = 4\sqrt{m-1} = 0.85\Omega$$

$$\Rightarrow L_s = 0.056\text{nH} \quad (4.11)$$

The DC blocking capacitor blocks low frequency currents and allows maximum output current to flow at working frequency

$$X_c = \frac{1}{2\pi f_c} \Omega \quad (4.12)$$

Usually  $X_c$  is less than 2 ohms at working frequency ( $f_c$ ). RF choke presents high impedance to RF energy while offering minimal resistance to direct current reactance

$$X_{L(choccke)} = 2\pi f l \Omega \quad (4.13)$$

$X_{L(choccke)}$  is usually greater than 500 ohms at working frequency ( $f_i$ ).

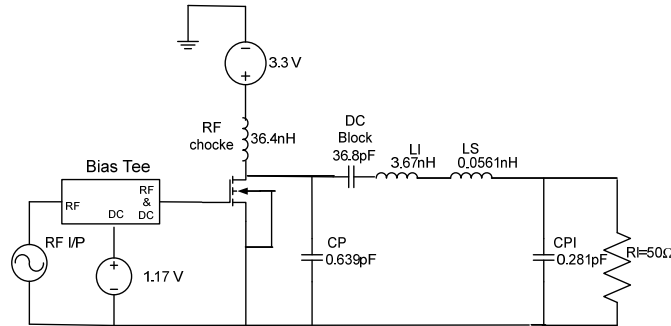


Figure 4.8: 2.4 GHz class E power amplifier schematic

The class E PA designed for the implantable transmitter operating at 2.4 GHz is shown in Figure 4.8 above, indicating the capacitances and inductors values are labelled after performing impedance matching. The bias Tee allows a DC current to bias an active device. The DC bias current and the AC/RF signal are added together and come out of the AC+DC output port.

After designing the circuit parameters for the class E PA in order to verify the PA design introduced previously; circuit simulation were performed on Analog Office (AO) of the Advanced Wave Research (AWR) simulation software.

#### 4.2.2 Circuit Simulation and Results

In the previous design procedure, the PA transistor assumed to have a perfect switch-like behaviour as can be seen in Figure 5.4, where the transistor is modelled as a switch. However, in real scenarios this might not be true.

The transistor model used in the class E PA design was 3.3V NMOS transistor for AMS s35 library.

In order to decide on the transistor gate bias voltage, the IV curves for the transistor were obtained using the setup in Figure 4.9

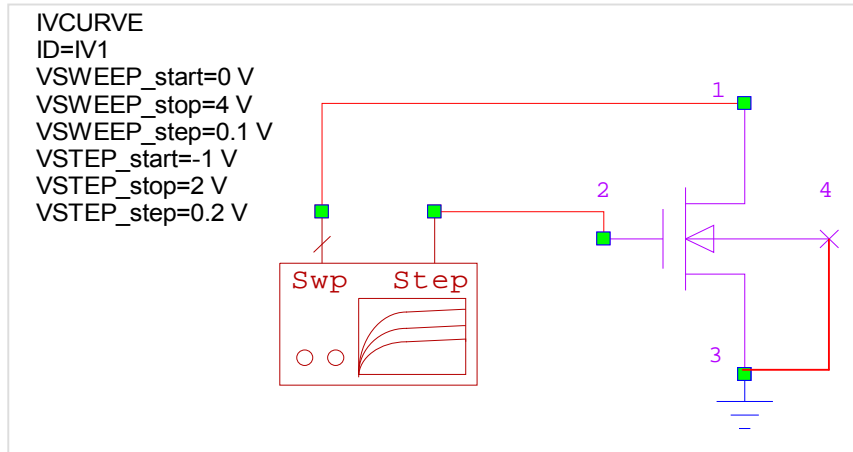


Figure 4.9: IV curve measurement setup

The transistor drain voltage was swept from 0 to 4 volts against transistor drain current for different gate bias voltages; the transistor IV curves appears as in Figure 4.10 below

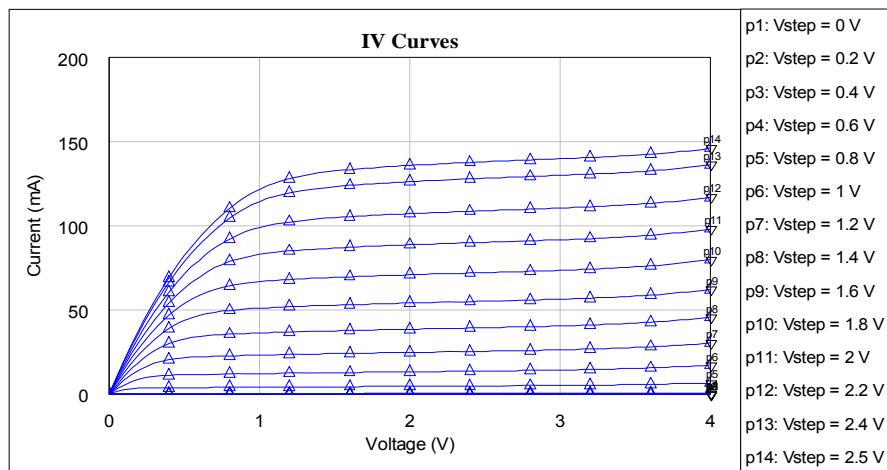


Figure 4.10: Transistor IV curve

The gate voltage was stepped between 0 and 2 volts. This range was selected according to the discussion in the previous chapter on transistor bias range. Since moderate inversion was selected as the optimum range of operation for transistors operating in the RF frequency band, the lower boundary for the moderate inversion region is zero volts, while the upper limit is bounded by the thermal voltage and sub threshold slope factor.

In Figure 4.10, there are three parameters to optimize, namely transistor drain voltage, drain current, and gate bias voltage. Since we are bounded by using a drain voltage of 3.3 V due to the transistor model used, the interplay reduces to drain current and gate bias voltage only. To limit the power consumption, one can design

for the lowest drain current value but this will result in reduced power gain. The power attenuation encounter due to signal propagation through skin was found to be 16.7 dB as seen in Figure 4.3. If we choose to design for a power gain of 14dB, by different iterations the bias voltage needed to achieve this power gain was found to be 1.17 V at which the circuit drain current is 18.93 mA. The transistor's channel width to length ratio  $\left(\frac{W}{L}\right)$  was chosen such that the bias point is kept in the moderate inversion region while still achieving the gain requirements at a reasonable drain current. The circuit schematic used in the class E PA simulation is shown in Figure 4.11 below:

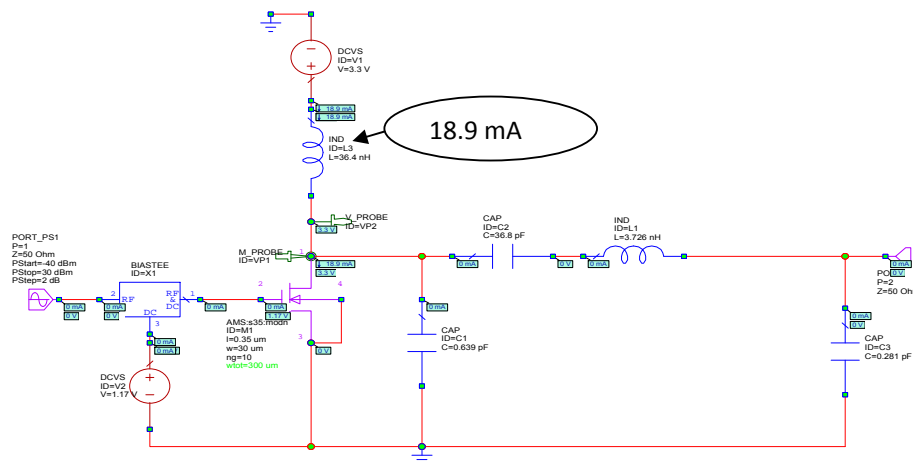


Figure 4.11: Class E PA simulation schematic

This value is relatively high for low power transmitters, but since we are constrained with the given transistor designing for a lower current will result in reduced power gain which is mandatory to combat skin power attenuation effect.

#### 4.2.2.1. Basic PA Test

After setting the adequate transistor bias voltage, the first step to validate the class E PA functionality is to verify its switching pattern.

The voltage and current waveforms at the transistor drain terminal are shown in Figure 4.12. PAs with displacement in drain voltage and current can achieve high efficiency. This phenomenon only happens when the transistor behaves as an ideal switch which only allows either current or voltage peak to occur at a time. In such a scenario, power dissipation can be totally eliminated and hence, theoretically, achieve 100% efficiency.

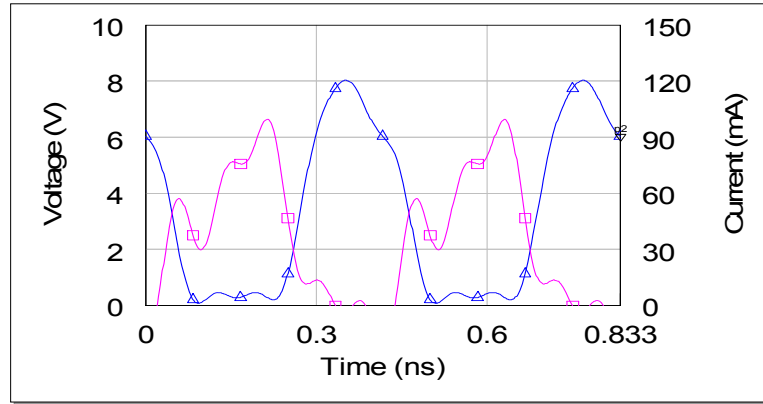


Figure 4.12: Output voltage ( $V_o$ ) ( $\Delta$ ) versus output current ( $I_o$ ) ( $\square$ )

As noticed in Figure 4.12, the voltage and current waveforms experience partial elapse thus perfect switching is not achieved. This is the resultant of imperfect switching capabilities of the active device used. Consequently the PA efficiency will be less than 100%, which is shown in Figure 4.13 below:

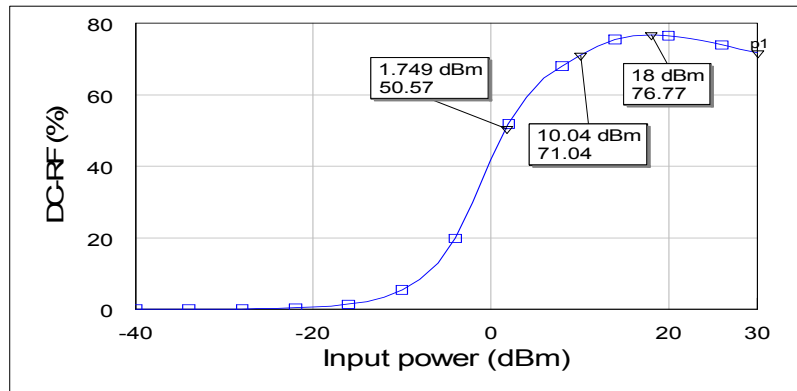


Figure 4.13: DC to RF efficiency at 2.4 GHz

The maximum DC to RF efficiency achieved was 76.77%, at maximum allowed input drive power of 18 dBm, when accounting for all the losses encountered including skin attenuation, matching network and antenna losses as well as the PA power gain. If the PA was rated to work at 10 dBm input power it achieves an efficiency of 71.04 %.

The DC to RF efficiency measures the ratio of output RF power to input DC power as given by Equation (4.17) below [62]:

$$\eta = 100 * \frac{[P_{out}]_{RF}}{[P_{in}]_{DC}} \quad (4.17)$$

An alternative measure of PA efficiency is Power added efficiency (PAE). It takes into account the effect of amplifier gain. It is calculated as:

$$PAE = 100 * \frac{\{[P_{out}]_{RF} - [P_{in}]_{RF}\}}{[P_{DC}]_{Total}} \quad (4.18)$$

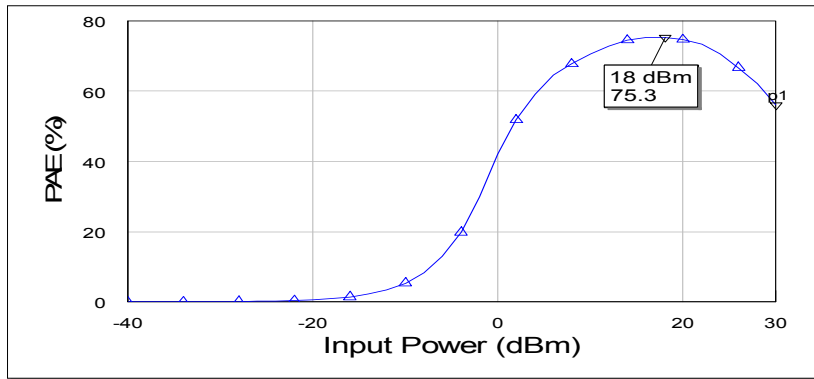


Figure 4.14: Power Added Efficiency at 2.4 GHz

The PAE for this class E PA design appears as shown in Figure 4.14 above. There is a slight difference, in the order of 1%, between the two efficiency measurements. Since the PAE takes into account the input RF power, the value of efficiency is reduced accordingly. From the slight reduction seen in the PAE compared to the conventional efficiency measurement, it is concluded that the input power is much less than the output power. In conclusion the difference between these two efficiency measurements diminishes if the PA gain is sufficiently high.

The second corner in the PA performance is the power gain. We designed for a maximum power gain of 15 dB in order to combat the power attenuation due to propagation through the skin. The gain versus input power is shown in Figure 4.15 below:

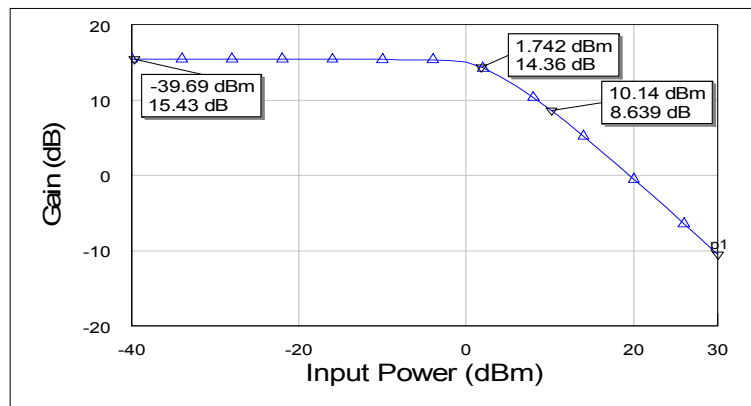


Figure 4.15: Power gain

The gain is constant over a certain range of input power after which it starts to decrease according to a phenomenon known as gain compression. The input power level at which the output power level is 1 dB less than it would be in an absolutely linear device is known as the 1-dB compression point. This point can be measured directly from the gain graph and it is found to be approximately at 1.75 dBm input power. Thus, if the device is to be operated at 10 dBm input power to maintain an efficiency level of 71%, the power gain will be reduced to 8.6 dB.

As mentioned earlier in Section 4.3.3, operating the transmitter in the sub threshold regime i.e. weak inversion achieves the highest possible (gm/Id). However, for RF frequencies, the PA frequency response needs to be considered. This value decreases as the channel moves from strong inversion to weak inversion. A good compromise between both requirements was to operate the transistor in the moderate inversion region. As given in Table 3.3, the boundary between weak and moderate inversion occurs where  $V_{GS} - V_T > 0$ . The typical threshold voltage for the NMOS transistor model given by the AMS\_s35 library is 0.69 V, so to operate the transistor at moderate inversion  $V_{GS}$  should be higher than 0.69 V. Figure 4.16 below illustrates this phenomenon, when the transistor is biased in the weak inversion i.e.  $V_{GS}$  is below 0.69, it attains the highest DC-RF efficiency, given that the channel has entered the weak inversion region. The power gain on the other hand, is at its minimum value when the transistor in the weak inversion and starts increasing as the bias voltage rises from weak inversion to moderate inversion and then to strong inversion. The gain continues to rise in the strong inversion until the maximum bias voltage ( $V_{GS \text{ max}}$ ) after which both gain and efficiency decrease gradually.

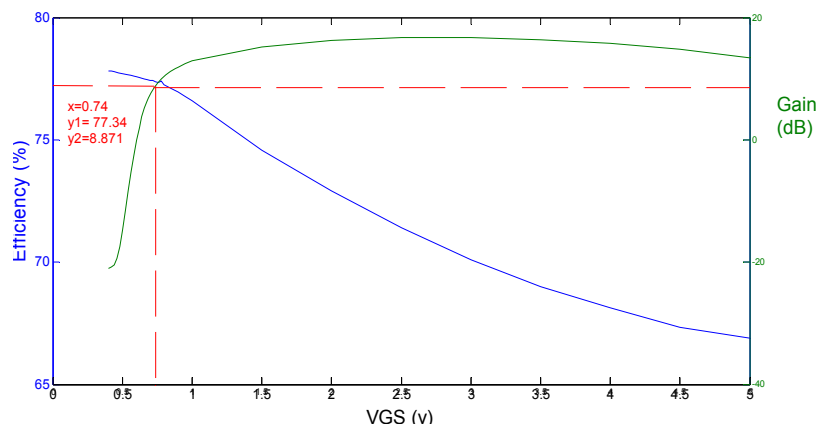


Figure 4.16: Gain and efficiency versus gate bias voltage

The optimum region of operation occurs in moderate inversion at 0.74 V as seen in Figure 4.16 where  $V_{GS} = 0.74$  V. The strong boundary between moderate and strong inversion was calculated using Table 3.3 and it was found to be approximately at 0.9157.

The power gain needed to compensate for the skin attenuation was found to be 16 dB approximately. By operating the transistor at a  $V_{GS}$  of 1.17 V, approximately in on the onset of strong inversion, the gain achieved is 15.43 dB with reduction of 3% in efficiency. On the other hand, in the external power unit PA, the transistor was pushed into the strong inversion region to achieve the maximum power gain at an acceptable efficiency level.

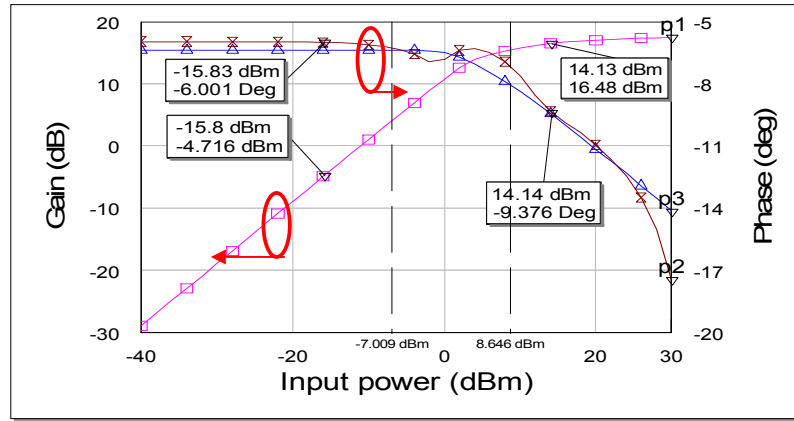


Figure 4.17: AM-AM ( $\square$ ), AM-PM ( $\boxtimes$ ) and gain ( $\Delta$ )

Any amplifier, when driven into a strongly nonlinear state, will reveal phase as well as amplitude distortion. This is usually described in terms of “AM to PM” conversion, and represents a change in the phase of the transfer characteristic as the drive level is increased towards and beyond the compression point [46]. Whereas AM to AM is related to the gain compression behaviour stated previously. When the transistor is driven into saturation any amplitude variation in this region will result in gain compression. As can be seen in Figure 4.17, the gain is constant until the point where to cross with the AM to AM curve after which gain compression takes place. The AM to PM can be calculated using Equation (4.19) and referring to Figure 4.17 as given below:

$$AM\ to\ PM\ (degrees/dB) = \frac{\Delta(Phase)}{\Delta(amplitude)}$$

$$\frac{-6.-9.37}{-4.71-16.48} = -0.16^\circ/dB \quad (4.19)$$

---

It is desirable to keep this value as low as possible, ideally 0°/dB, where amplitude compression does not result in any phase alteration i.e. linear behaviour.

#### 4.2.2.2. Tow-Tone Test

In an ideal system, the output is linearly related to the input. Amplifier linearity describes the ability of the amplifier to correctly reproduce the amplitude and phase of the input signal at the amplifier output. With non linear devices like PAs the output consist of a fundamental output signal plus other undesired output. A mathematical formulation of this non linear behaviour is carried out in short. The output from a non linear device for which an input ( $v_{in}$ ) is applied, can be given by the power series expansion as [62]:

$$v_{out} = k_o + k_1 v_{in} + k_2 v_{in}^2 + k_3 v_{in}^3 + \dots \quad (4.20)$$

To completely characterize nonlinearity, an infinite number of terms is required. Nevertheless, in many practical systems the first three terms are enough to describe the system behaviour with an acceptable degree of accuracy.

A known way of describing the linearity of a circuit is the two-tone test. In this, an input composing of two sine waves is applied to the circuit. If we have an input signal given by:  $v_{in} = v_1 \cos \omega_1 t + v_2 \cos \omega_2 t$ , when this signal is applied to the system having the transfer function shown in Equation (4.20), the outcome will be:

$$v_{out} = +k_1(v_1 \cos \omega_1 t + v_2 \cos \omega_2 t) + k_2(v_1 \cos \omega_1 t + v_2 \cos \omega_2 t)^2 + k_3(v_1 \cos \omega_1 t + v_2 \cos \omega_2 t)^3 \quad (4.21)$$

In the case of an amplifier, only the terms at the input frequency are desired. Across all the terms in Equation (4.21), the terms at frequencies  $(2\omega_1 - \omega_2)$  and frequencies  $(2\omega_2 - \omega_1)$  are the most troublesome, since they can fall in the band of the desired outputs and therefore cannot be easily filtered out. These two tones are generally referred to as third-order intermodulation terms (IM3 products).

A common way to verify the linearity of a circuit is to apply two signals at the input, having equal amplitude and offset by some frequency, and plot fundamental output and intermodulation output power as a function of input power. For the purpose of the two tone test the conventional termination port was replaced by a two tone port supplying a power signal of two tones, separated by frequency  $F_{\Delta}$ , swept

---

from PStart to PStop and also swept across the frequency range specified for the schematic containing the port. A close view of the two tone port is shown in Figure 4.18 below:

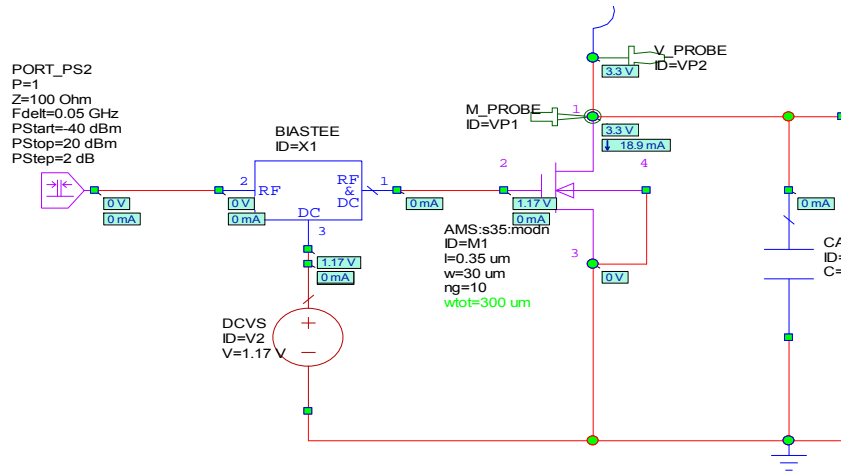


Figure 4.18: two tone port used in two tone test

The principle of two-tone test is illustrated in Figure 4.19. The first tone applied was at the fundamental frequency ( $f_1 = 2.4 \text{ GHz}$ ), the second one is given by:  $f_1 + f_{\text{delta}} = 2.4 + 0.5 = 2.45 \text{ GHz}$ . The intermodulation products are located at ( $2 * 2.4 - 2.45 = 2.35 \text{ GHz}$ ) and ( $2 * 2.45 - 2.4 = 2.5 \text{ GHz}$ ). The difference between the fundamental and IM3 power levels is approximately 73.69 dBc.

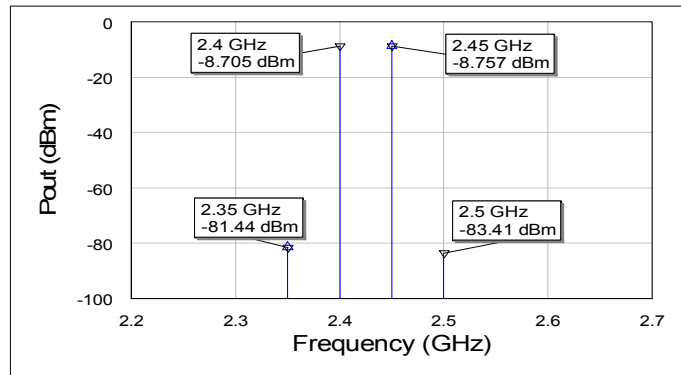


Figure 4.19: Intermodulation distortion

The fundamental power component at 2.4 GHz and IM3 component at 2.35 GHz are shown as function of the swept input power in Figure 4.20 below.

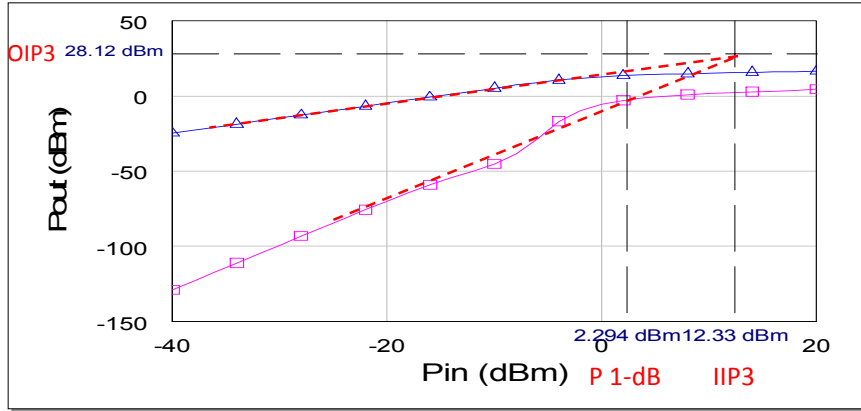


Figure 4.20: Output power of fundamental and IM3 versus input power

The third-order intercept point (IP3) is determined from Figure 4.20 above. The third-order intercept point is a theoretical point where the amplitudes of the intermodulation and the fundamental tones are equal. The Input IP3 (IIP3) and Output IP3 (OIP3) were found to be 12.33 and 28.12 dBm respectively. Ideally those values should be infinity to reach linear device behaviour. The 1-dB point is approximately at 2.294 from Figure 4.20 above. This agrees with the relationship given in [62] that relates the 1-dB point to the IIP3 as follows:

$$IIP3(dBm) = 1 - dB(dBm) + 9.6 dB \quad (4.22)$$

The IIP3 can be calculated from the intermodulation distortion graph shown in Figure 4.19 using Equation (4.23) below [62]:

$$IIP3(dBm) = P_{in}(dBm) + \frac{(P_{outFund.} - P_{outIM3})}{2} \quad (4.23)$$

From Figure 4.19,  $P_{in}$  is -24 dBm, while fundemntal-IM3 difference is 73.69 dBc. Direct application in the Equation (4.23) gives a value of 12.84 dBm for IIP3, which agrees with results found from Figure 4.15.

It is worth mentioning that linearity is not a requirement for this class E PA design, the signal to be amplified through this PA is frequency modulated, hence no data is contained in the signal amplitude or phase. Consequently gain compression and AM to PM conversion do not spoil the information signal. This test was performed for reference, if the PA is to be used for linear non constant envelope modulation schemes.

The SAR was calculated for the class E PA using Equation (4.1), the maximum voltage level at the amplifier can be deduced from Figure 4.12, where the

---

switching property takes place. The maximum switching voltage was found to be 8.027 V for which the corresponding SAR value is 45.1 mW/Kg.

The external power unit design is introduced next which includes a class E PA as well. In addition a comparison between the performance characteristics of the two class E PA designs will be conducted.

### 4.3 External Power Unit

As mentioned earlier the limit of inductive power transfer without implications of parasitic and reduced efficiency is set to below 20 MHz region. The choice of frequency in kHz region can actually elevate both of those problems but it is actually not an option for IMDs application due to the large required antenna sizes. A frequency of 13.56 MHz which falls in the upper limit of recommended frequency band for inductive power links was chosen to be the operating frequency for the external powering unit in this design. It is relatively high which results in smaller antenna size. It also has the advantage of being a worldwide ISM frequency, and it has an excellent immunity to environmental noise and interference.

#### 4.3.1 Distinction between Near and Far Fields

At the 13.56 MHz operating frequency, the wavelength is about 22 m which is several times greater than the standard distance between the implantable unit and the external power unit, thus inductive coupling takes place in the antenna near field region. Consequently, power transfer to the implantable is achieved by coupling of reactive near-field energy in the instant surrounding area of the antenna. The boundary between the near and far field region is approximated at  $\lambda/2\pi$ . At 13.56 MHz, this places the near field-far field boundary at 3.5 m. If the external power unit is placed right outside the implantation side, this ensures that inductive coupling occurs in the near field region.

In the near field, the magnetic field strength attenuates according to the relationship  $(1/d^3)$  i.e. the magnetic field intensity decays as rapidly as the inverse cube of the distance between the external powering unit antenna and the implantable transmitter. In power terms, this equates to a dramatic  $(1/d^6)$  reduction with the distance of the available power to energize the implant, not forgetting that skin attenuation needs to be accounted for as well. The magnetic field strength is thus high

---

in the immediate vicinity of the transmitting coil, but a very low level exists in the distant far field; hence a spatially, well-confined localized powering zone is created.

This rapid attenuation of the energizing field with increasing distance is the fundamental reason why we propose to fix the external powering unit on top of the implantable transmitter right outside the implantation side. This also provides flexibility for coils alignment. Through the principle of antenna reciprocity and the minimization of stray E-field susceptibility, it is also the reason why well designed near field powering systems such as RFIDs have good immunity to environmental noise and electrical interference [52].

With the increasing demand to transmit power at higher frequencies, efficiency is an escalating concern, and in the field of high frequency transmission, switched-mode amplifiers are quite popular.

Class E power transmitter has demonstrated a good performance in the area of power transfer at high frequencies up to 20 MHz. However, as the frequency of operation increases, the size of capacitors and inductors decreases, and at frequencies above 100 MHz typical capacitor sizes are in the low pF region. This will give rise to parasitic capacitance to appear in the class E transmitter [63]. Thus the frequency chosen for the inductive link i.e. 13.56 MHz gives rise to acceptable class power transmitter performance as well.

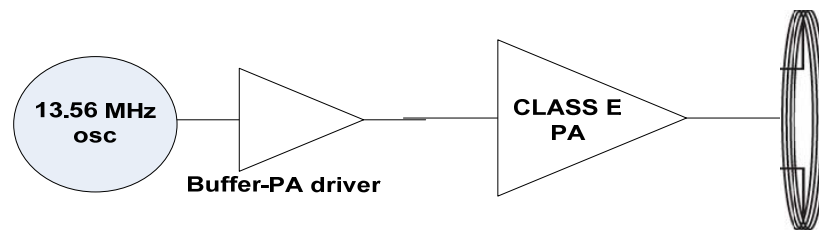


Figure 4.21: External power unit

The structure of the proposed external power unit is shown in Figure 4.21 above. The buffer was introduced to prevent loading the oscillator by the high drive power required by the class E PA.

The same procedure used in designing the implantable transmitter class E PA was followed. The first step was to calculate the power attenuation encountered when transferring power inductively to the implantable unit at 13.56 MHz. The dielectric properties of the skin at this frequency are given in Table 4.4.

Table 4.4: Dielectric properties of skin tissue at 13.56 MHz

Property	Value
Effective conductivity ( $\sigma_{eff}$ )	0.23802 S/m
Permittivity ( $\epsilon$ )	$285.25 \times 8.85 \times 10^{-12}$ F/m
Permeability	$4\pi \times 10^{-7}$ H/m
Attenuation constant ( $\alpha$ )	1.3225 Np/m

Using Equations (4.2) and (4.3) the propagating electric field and power attenuation through the skin were calculated respectively.

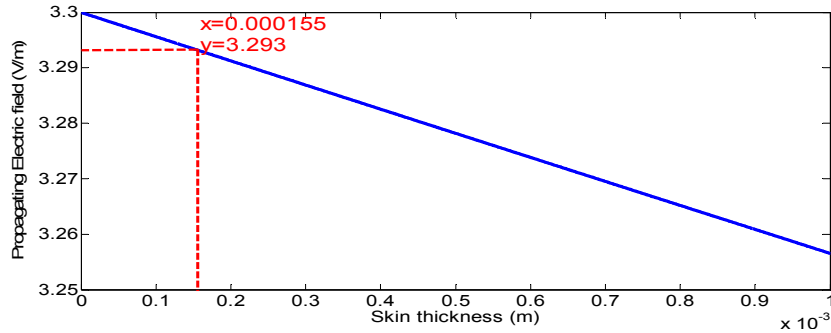


Figure 4.22: Electric field (V/m) versus skin thickness (m) at 13.56

The propagating electric field at 13.56 MHz is shown in Figure 4.22. At a distance of 1.55 mm through the skin the electric field has a value of 3.293 which corresponds to an attenuation of less than 0.2% compared to 4% at 2.4 GHz. This was expected since signal attenuation decreases as the frequency of operation is reduced.

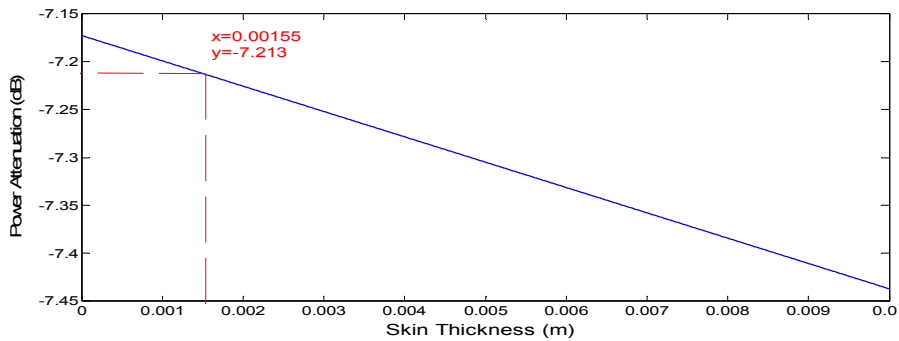


Figure 4.23: Power attenuation at 13.56 MHz

The power attenuation at 13.56 MHz at a distance 1.55m through the skin was found to be 7.213 dB. In order to design for class E transmitter PA gain, this value needs to be considered as well as the amount of power to be supplied to the implantable unit. The coupling coefficient between the two inductive link components needs to be considered when deciding on the amount of power needed from an inductive link. The coupling coefficient is usually between 0 and 1 and is used to specify the orientation of an inductor with respect to another one. The efficiency of

RF front end unit shown in Figure 3.6 needs to be considered as well. This unit consist mainly of a rectifier and a voltage regulator to provide steady power supply to the implantable transmitter. High efficiency levels for the rectifier and voltage regulator units have been reported in [64] and [49] respectively. Assuming high efficiency for those units e.g. 96% the power needed by the inductive power unit can be calculated as below:

$$\begin{aligned} \text{Required Inductive Power} &= \frac{\text{Implanatable TX power+Attenuation}}{\text{Efficiency of transmission and reception units}} \quad (4.24) \\ &= \frac{10 \text{ dBm} + 7.213}{96\%} = 17.9 \text{ dB} \end{aligned}$$

Thus, in order to supply the implantable unit by 10 dBm i.e. 10 mW of power the class E power transmitter, specifically saying class E PA needs to have a power of approximately 18 dB.

A similar procedure for the class E PA designed for the implantable unit at 2.4 GHz was followed for designing the external powering unit PA at 13.56 MHz. The complete calculations can be found in [65]. The circuit schematic for which is shown in Figure 4.24.

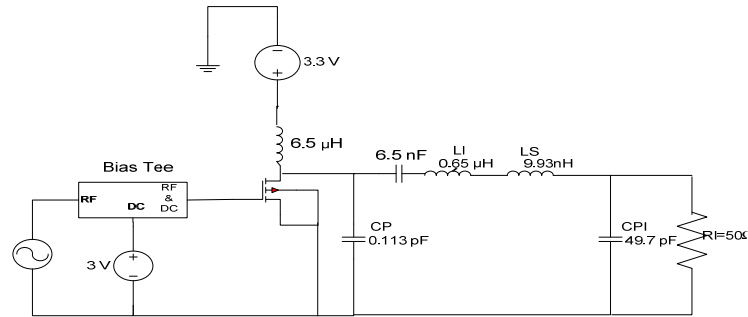


Figure 4.24: External powering unit class E PA

### 4.3.2 Simulation Results

Compared to Figure 4.12, the output voltage and current in this PA encounters more elapsed periods than in the previous class E design. Consequently, we can predict that the efficiency would be lower. In fact, the first version of this class E PA design achieved efficiency of approximately 80% but at a power gain of only 9 dB at a gate bias voltage of .75 volts.

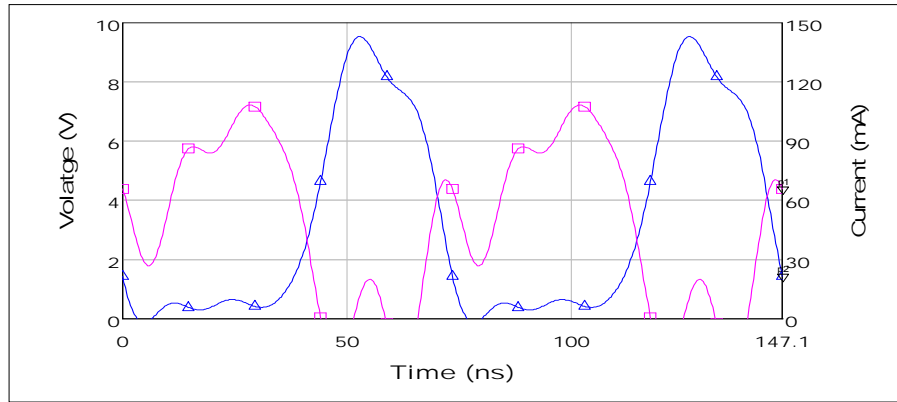


Figure 4.25: Output Voltage (  $\Delta$  ) Vs Output Current (  $\square$  )

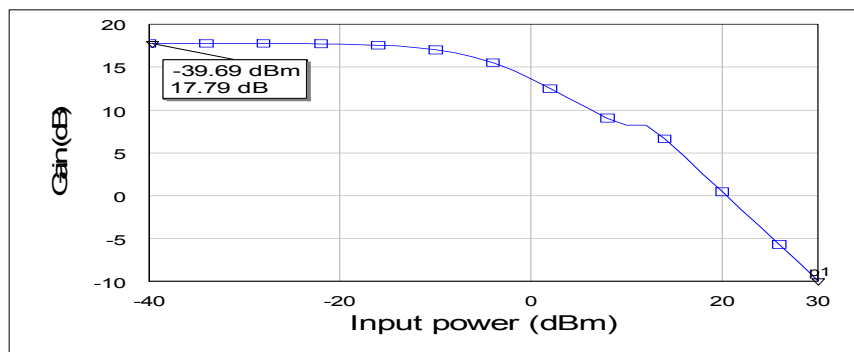


Figure 4.26: Power gain at 13.56 MHz

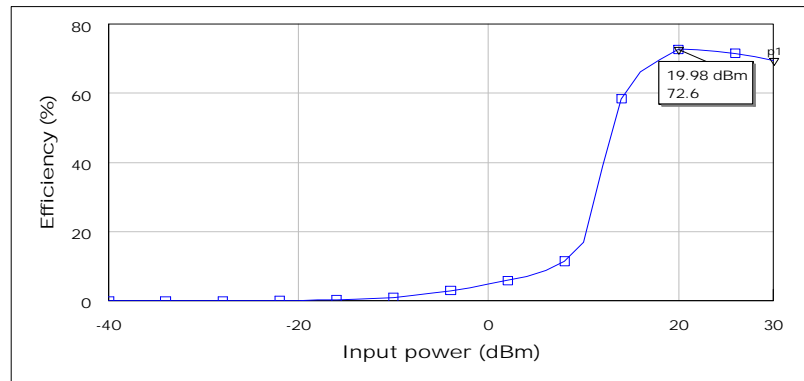


Figure 4.27: Efficiency at 13.56 MHz

Since higher power gain is needed, the gate bias voltage was increased in order to achieve higher power gain. The gate bias voltage was increased to 3 volts this boosted the gain level to almost 17.8 dB but with reduced efficiency of 72.6 % as shown in Figure 4.26 and Figure 4.27, respectively.

The overall current consumption of the PA was 143 mA which is tolerable since this unit is external and power consumption is not as critical compared to the implantable one.

As previously done for the implantable unit, the SAR from the external powering unit needs to be considered as well. Since the external power unit will be operated in the near-field with almost purely magnetic radiation, from Table 4.2, the maximum value for magnetic field (H) at 13.56 MHz is 0.073 A/m or 73  $\mu$ A/mm. The SAR for this PA was calculated using the same procedure described for the implantable PA. The 13.56 MHz PA has a SAR value of 54 mW/Kg.

Table 4.5: Class E PAs performance characteristics

Parameter	Implantable PA	External PA
Frequency (MHz)	2400	13.56
VDD (V)	3.3	3.3
Gate bias voltage (V)	1.17	3
Current consumption (mA)	18.9	143
Maximum DC to RF efficiency (%)	76.77	72.6
Power gain (dB)	15.43	17.79
AM-PM (deg/dB)	-0.16	-0.737
P-1dB (dBm)	1.75	-8.55
$\Delta$ IM3 (dBc)	73.69	47.9
IIP3 (dBm)	12.84	2.59
OIP3 (dBm)	28.12	24

A comparison between performance characteristics of the two class E PA designs is given in Table 4.5. It can be noticed that the external power unit PA is more nonlinear than the implantable PA because it is driven by higher voltage, thus it is further pushed into the compressed mode. This can be seen from the linearity tests provided in Table 4.5. The AM to PM ratio is 80% higher for the 13.56 MHz PA which reflects the aggressive amplitude compression behaviour. The P-1 dB and IIP3 points occur at lower input power levels of only -8.5 and 2.59 dBm, respectively. This again indicates that amplitude compression occurs at lower input power levels than that for the 2.4 GHz PA.

#### 4.4 Direct Modulation Architecture

For the purpose of implementing the direct modulation architecture chosen for the design of this transmitter, a PLL system has been designed. The VCO needs to be locked to the intended carrier frequency, which comes from the frequency hopping sequence in the case of Bluetooth low energy transmitter, before applying the data through the VCO modulation line.

---

#### 4.4.1 PLL Design

As mentioned in the previous chapter, the purpose of the VCO is to lock the frequency of a free running oscillator like the VCO to a reference oscillator e.g. crystal oscillator. It does so by comparing the frequency coming from the VCO to the reference frequency through a PFD/CP which incorporates the charge pump circuitry that outputs a current proportional to the difference in phase/ frequency. This current needs to be converted to voltage in order to adjust the output VCO frequency. This is done through the PLL loop filter. Many of the PLL performance characteristics stated earlier such as lock time, phase noise, spurs levels depend on the loop filter bandwidth.

Since there are no stated requirements for these performance characteristics, the PLL is designed for the criteria of faster lock time along with enhanced loop stability. Adhering to low power transmitter design principles in Section 4.2, relatively fast lock time is essential to minimize the transmitter setup time. The second requirement is important for the purpose of direct VCO modulation where the PLL is kept at the locked state while the data is being applied through the VCO modulation line. This will be done through the optimization of the loop bandwidth, lock time and phase margin. It is desired to have reasonable component values provided that the system other performance characteristics such as phase noise and spur levels are not spoiled to the extent that affect the overall system performance.

##### 4.4.1.1. Loop Filter Design

Probably the design of the PLL loop filter is the most critical part in PLL design. Many performance requirements depend on the choice of the loop filter bandwidth, order and component values as mentioned earlier.

Loop filter design entails selecting the proper loop filter topology, loop bandwidth, type, order, phase margin, and pole ratios.

##### 4.4.1.2. Determining and Adjusting Loop Gain

The loop filter is designed for a VCO gain, charge pump gain, and N counter value. However, the loop gain  $K$  is the most important factor. The loop gain is given by:

$$K = \frac{K_{\phi} \cdot K_{VCO}}{N} \quad (4.25)$$

If the loop gain is kept constant, then it is not critical from the loop filter design perspective if the VCO gain, charge pump gain, or N counter value vary.

#### 4.4.1.3. Determining Loop Filter Topology and Order

There are two types of loop filters, passive and active. Passive loop filters are generally preferred over active loop filters, since adding active devices adds phase noise, complexity and cost. However, there are cases where an active filter is necessary. The most common case occurs when the maximum PLL charge pump voltage is lower than the VCO tuning voltage requirements.

Higher filter order is beneficial in terms of reduced spurs level, but it has drawbacks because more passive components are added to the loop, increased resistor noise and the VCO input capacitance might cause distortion because it will be added in series to the filter capacitance. Thus we need to make sure that the filter capacitance has a much higher value than the VCO input capacitance, such that it would not be affected by the VCO input capacitance. A third order loop filter has been chosen for this design. The simulation results show that this choice achieves both faster lock time and lower spurs gain.

#### 4.4.1.4. Third Order Passive Loop Filter Design

The topology of a third order loop filter is shown in Figure 4.28. The loop filter transfer function is described as the variation in voltage at the port of the VCO divided by the current at the charge pump that caused it. The transfer function of a third order PLL loop filter is given by:

$$Z(s) = \frac{1 + s \cdot T_2}{s \cdot A_0 (1 + sT_1)(1 + sT_3)} \quad (4.26)$$

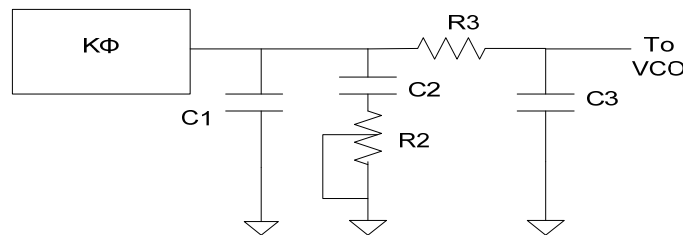


Figure 4.28: Third order loop filter topology

---

Where  $T_1$ ,  $T_2$  and  $T_3$  are the loop filter poles. These poles must have negative real parts in order to ensure loop stability. Equation (4.26) can be written as:

$$Z(s) = \frac{1 + s \cdot C_2 \cdot R_2}{s(A_2 \cdot s^2 + A_1 \cdot s + A_0)} \quad (4.27)$$

$A_0$ ,  $A_1$ , and  $A_2$  are the filter coefficients. In the case of a passive loop filter,  $A_0$  is defined as the sum of the capacitor values in the loop filter. The relationship between loop filter poles and coefficients is given as by:

$$\begin{aligned} A_2 &= A_0 \cdot T_1 \cdot T_3 = C_1 \cdot C_2 \cdot R_2 \cdot C_3 \cdot R_3 \\ A_1 &= A_0 \cdot (T_1 + T_3) = C_2 \cdot C_3 \cdot R_2 + C_1 \cdot C_2 \cdot R_2 + C_1 \cdot C_3 \cdot R_3 + C_2 \cdot C_3 \cdot R_3 \\ A_0 &= C_1 + C_2 + C_3 \end{aligned} \quad (4.28)$$

#### 4.4.1.5. Choosing The Phase Margin, Loop Bandwidth, and Pole Ratios

The phase margin( $\phi$ ) relates to the stability of the system. This factor is usually chosen between 40 and 50 degrees. Within this range the phase margin has an inverse relationship with lock time.

The most important parameter of the loop filter is its bandwidth ( $F_c$ ). The choice of the loop bandwidth typically involves a trade-off between spur levels and lock time. If the lock time and spurs are not a major consideration, then the filter component values have to be considered, especially the capacitors. A very narrow loop bandwidth results in impractically large capacitors, whereas with a very wide one, they may turn out to be too small and be waived by parasitic capacitance and the input capacitance of the VCO.

The pole ratio ( $T_{31}$ ) has less effect on the PLL design than the loop bandwidth, but it is still important in terms of spurs level performance. It is the ratio of the third pole ( $T_3$ ) to the first pole ( $T_1$ ).

$$T_{31} = \frac{T_3}{T_1} \quad (4.29)$$

Theoretically choosing the poles ratio to be one results in the lowest spurs level, although it is physically impossible for passive filters. In general, the VCO input capacitance is in the order of 10 to 100 pF and it is required to have the

capacitor in the loop filter next to the VCO to be at least three times the input capacitance of the VCO. The cause of this is that the input capacitance of the VCO tends to vary with frequency and is usually not specified within limits [42].

Once the impedance ( $Z(s)$ ), charge pump gain  $K_{\phi}$ , and VCO gain  $K_{vco}$  are known, then the open loop gain ( $G(s)$ ) is given by:

$$G(s) = \frac{K_{\phi} \cdot K_{vco}}{s} \cdot Z(s) \quad (4.30)$$

#### 4.4.1.6. PLL Design Methodology

As a summary of the steps mentioned previously, the PLL design procedure is illustrated in Figure 4.29 below. To begin with, the system specifications such as frequency range, channel spacing, and N counter value has to be set.

The loop filter parameters which include loop bandwidth, filter order, phase margin, and pole ratios will be chosen using a rule of thumb selection. Those rules can get a close approximation but not an optimal design.

After selecting filter parameters, the other loop gain components of the PLL system i.e. VCO gain and charge pump gain are selected, as well.

From this we can get the filter components and then simulate the PLL system to obtain the performance characteristics: lock time, phase noise, and spurs level.

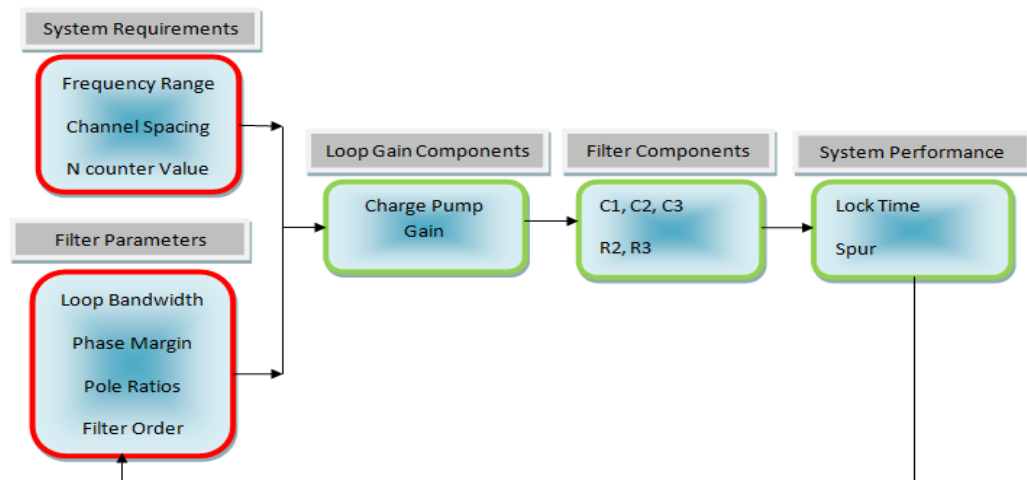


Figure 4.29: PLL design procedure [66]

This is an iterative process if the performance characteristics did not match the requirements; the parameters mentioned above have to be tuned to obtain the desired

performance. Since there are many of those parameters, this iterative design process can be time and computationally consuming. Thus for this iterative process we used the EasyPLL<sup>®</sup> software provided by National Semiconductor for the calculation of the loop filter components under the specified system requirements and for different loop bandwidths. These components values were then fed into Matlab simulation to estimate the PLL lock time and loop stability.

The highest charge pump gain usually gives the best performance in terms of phase noise. On the other hand the highest charge pump gain gives rise to unrealistically large capacitor values which would also reduce the lock time. A value of 0.8 mA was chosen for this design. From previous PLL designs a value of 30 MHz/V appears to be reasonable for the VCO gain. The pole ratio was chosen to be 80% to achieve good spurs performance while keeping the loop invulnerable to the VCO input capacitance. A phase margin of 50% appears to be a good compromise between loop stability and lock time performance. A crystal oscillator of 16 MHz was chosen for this design. Table 4.6 below shows the system parameters used in this PLL design.

Table 4.6: PLL system parameters

Symbol	Description	Value	Units
$K_{\phi}$	Charge Pump Gain	0.8	mA
$K_{vco}$	VCO Gain	30	MHz
Fout max.	Maximum Output Frequency	2483	MHz
Fout min.	Minimum Output Frequency	2400	MHz
Fosc	Oscillator Frequency	16	MHz
N	N counter	150-155.1875	Unit less

#### 4.4.1.7. Simulation And Results

To determine the loop filter parameters, the specification in Table 4.6 were fed to the EasyPLL<sup>®</sup>. As mentioned earlier in Section 4.4.1.2, the loop filter will be designed for a certain output frequency and N counter value but the overall loop gain (K) needs to be kept constant when the output frequency changes. An arbitrary value was chosen for the output frequency from the output frequencies range (2.4-2.483) GHz, typically 2.432 GHz. Consequently the N counter value is  $\frac{2432}{16} = 152$ .

Several iterations have been made for different loop filter bandwidths (7.5, 10, 12, 15, 20) kHz. The loop filter components values for each loop bandwidths are shown in Table 4.7 below.

Table 4.7: Loop filter component values

	7.5 kHz	10 kHz	12 kHz	15 kHz	20 kHz
C1	14.804 nF	8.327 nF	5.783 nF	3.701 nF	2.082 nF
C2	186.397 nF	104.82 nF	72.79 nF	46.587 nF	26.25 nF
C3	1.48 nF	832.73 pF	578.285 pF	370.102 pF	208.103 pF
R2	312.875 $\Omega$	417.166 $\Omega$	500.599 $\Omega$	625.749 $\Omega$	834.332 $\Omega$
R3	2.319 k $\Omega$	3.092 k $\Omega$	3.17 k $\Omega$	4.638 k $\Omega$	6.183 k $\Omega$

It is observed from Table 4.7 above that as the loop bandwidth increases the capacitors value decreases while the resistors value increases. This range of loop bandwidths was considered after several iterations starting from 10 kHz going above and below. A bandwidth of less than 7.5 kHz resulted in unreasonably large capacitor values especially for C2, while loop bandwidths higher than 20 kHz resulted in low C3 values that might make it susceptible to VCO input capacitance variation. As stated earlier, the criteria to be considered are lock time along with loop stability under reasonable components values and overall system performance.

The simulations were implemented in Matlab, where the loop filter coefficients were calculated from which the filter transfer function ( $Z(s)$ ) was obtained using Equations (4.28) and (4.27) respectively. The open loop transfer function can be written as:

$$GH = G(S) * N \tag{4.31}$$

Where GH is the open loop transfer function, G(s) is the open loop gain given in Equation (4.30) and N is  $\frac{F_{comp}}{F_{out}}$ . The closed loop is then implemented as the feedback of the open loop transfer function. The step response and Bode plots were carried out for both open loop and closed loop systems from which the lock time, open loop and closed loop stability margins were obtained.

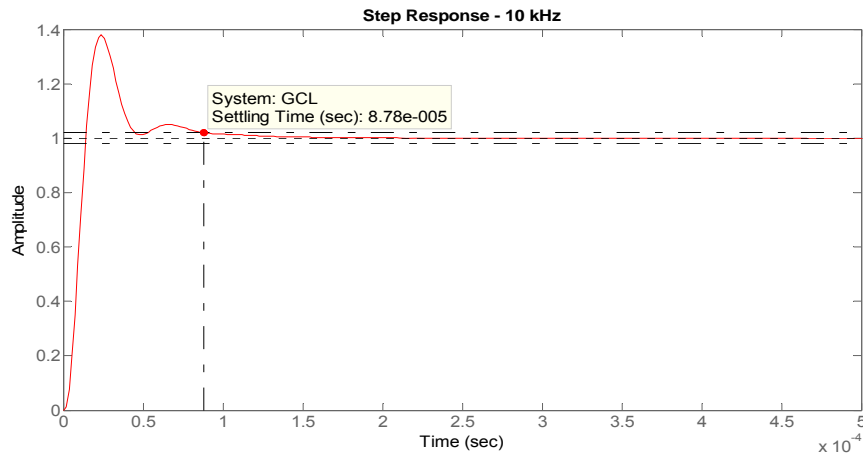


Figure 4.30: PLL lock time for 10 kHz loop filter

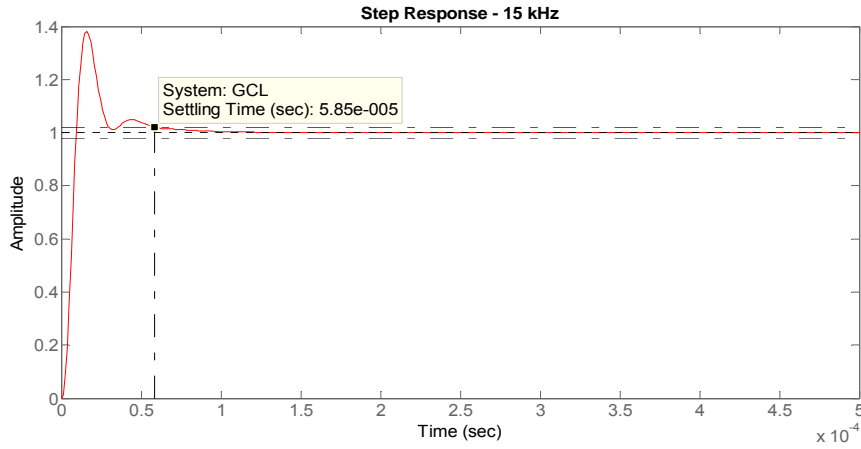


Figure 4.31: PLL lock time for 15 kHz loop filter

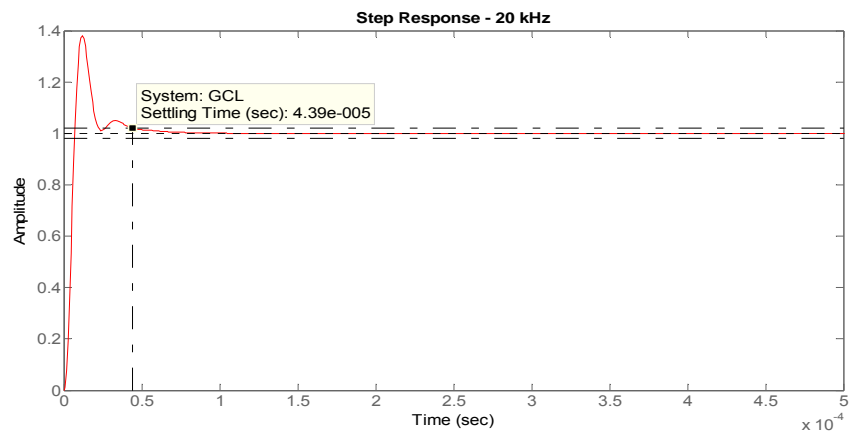


Figure 4.32: PLL lock time for 20 kHz loop filter

The 7.5 kHz loop filter was excluded from this design since it achieved the highest lock time in the order of 117  $\mu$ s and has relatively large capacitor values in the order of 100's nF.

The step response for the 10 kHz loop filter is shown in Figure 4.30. It achieved a lock time of 87.8  $\mu$ s. The 12 kHz loop filter achieved a close enough performance to the 10 kHz loop filter with a lock time of 74  $\mu$ s. Thus there is no substantial benefit of the additional 2 kHz. However, there is about 34% reduction in lock time when emerging from 10 kHz to 15 kHz, where, the lock time for the 15 kHz loop filter closed loop system has reduced to 58.5  $\mu$ s as illustrated in Figure 4.31.

Adding extra 5 kHz i.e. 20 kHz bandwidth, did not result in considerable reduction in the lock time as with the previous case. The lock time reduction percentage was 25% compared to 34% in the case of 15 kHz bandwidth as seen in Figure 4.32.

From the above, the 15 kHz loop filter offers a good compromise between the lock time and loop bandwidth, but as stated earlier there is another factor to be considered which is loop stability. It is essential for any closed loop system to be stable otherwise oscillation will build inside the loop and settling state will not be achieved. Thus all the closed loop systems presented previously for the 7.5, 10, 12, 15 and 20 kHz are stable systems.

However, among the shortlisted loop bandwidths if a choice demonstrates remarkable stability performance with no significant increase in lock time, it would be the most appropriate candidate for this design. The open and closed loop stability margins are shown in the following figures:

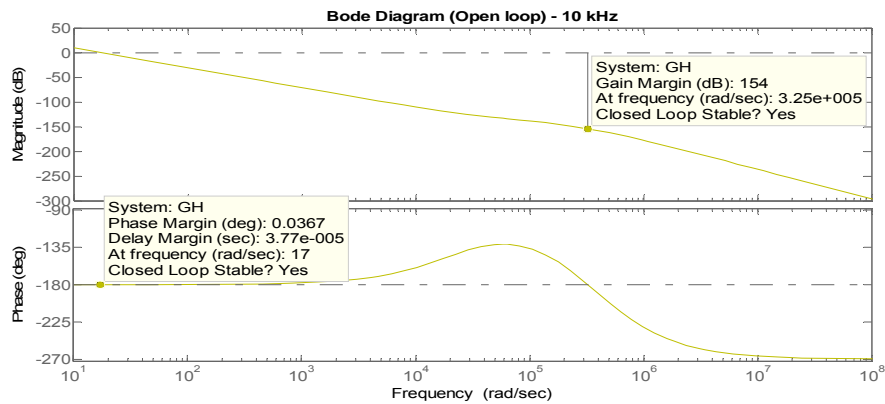


Figure 4.33: Open loop frequency response for 10 kHz loop filter

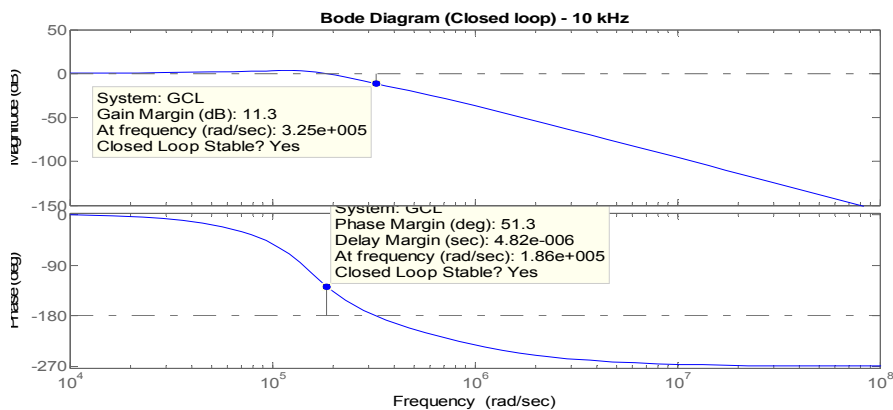


Figure 4.34: Closed loop frequency response for 10 kHz loop filter

Both open loop and closed loop systems are stable for the 10 kHz loop filter. It achieved a higher phase margin than what it was designed for i.e.  $50^\circ$ . With an increase of  $1.3^\circ$ , the phase margin attained was  $51.3^\circ$ .

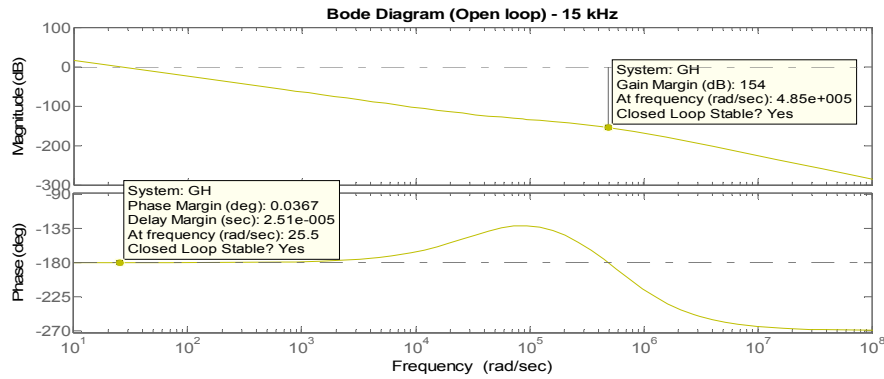


Figure 4.35: Open loop frequency response for 15 loop filter

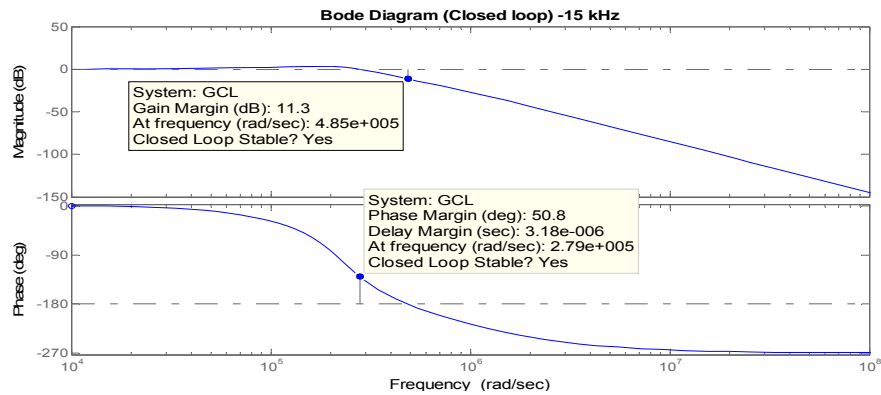


Figure 4.36: Closed loop frequency response for 15 kHz loop filter

The stability margins of the open loop and closed loop systems for the 15 kHz loop filter are shown in Figure 4.35 and Figure 4.36 kHz above. The phase margin for the closed loop system is 50.8°. The difference in phase margin between the 10 kHz and 15 kHz loop filters is less than 1°. Whereas for the 20 kHz loop filter, the phase margin is 50.9° which is 0.1° higher than that for 15 kHz loop filter as shown in

Figure 4.37 and Figure 4.38 below. There is a 25 % increase in loop bandwidth between 15 kHz loop filter with a 21% reduction in lock time for the 20 kHz loop filter and 0.2% increase in phase margin compared to the 15 kHz loop filter.

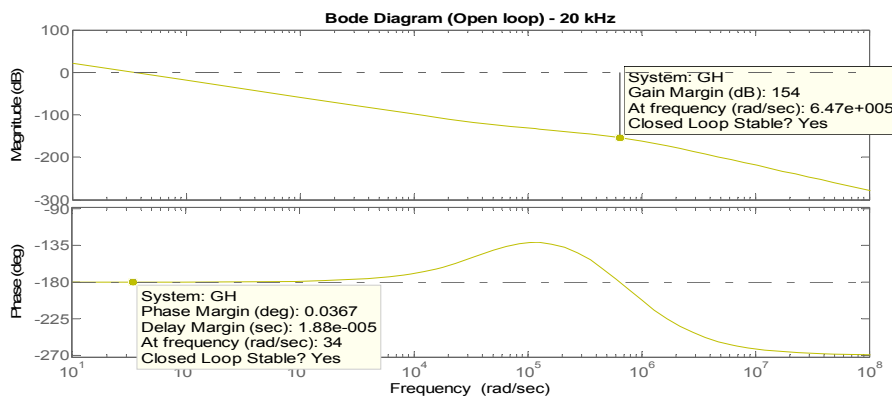


Figure 4.37: Open loop frequency response for 20 kHz loop filter

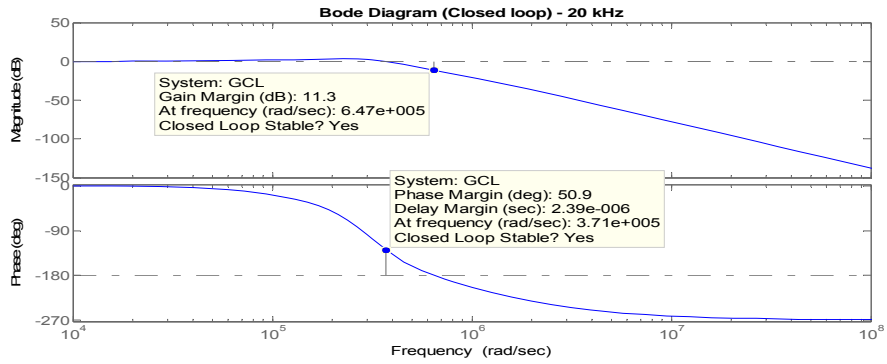


Figure 4.38: Closed loop frequency response for 20 kHz loop filter

From the discussion provided above, it is concluded that the 15 kHz loop filter offers the optimal performance in terms of lock time and loop stability thus it will be used for this PLL system design.

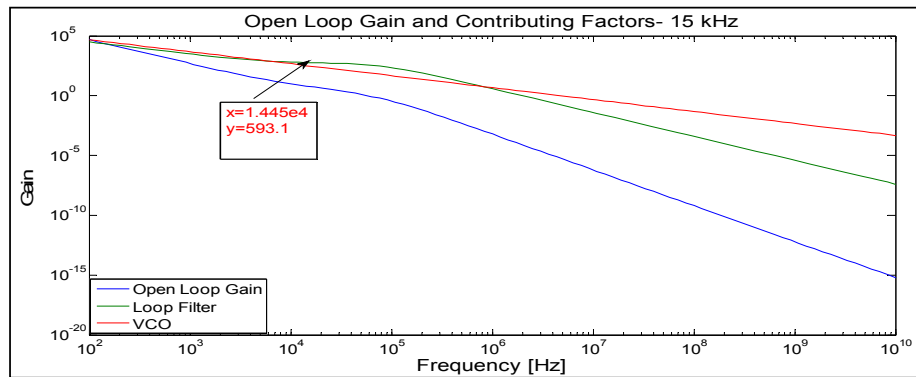


Figure 4.39: Open loop gain at 15 kHz

To get a closer insight on the loop dynamics at this loop bandwidth, the open gain components at this loop bandwidth are shown in Figure 4.39. Up to the loop bandwidth, the loop filter is the major contributor to loop gain after which the loop gain starts falling rapidly. The VCO gain starts falling after the cut-off frequency of the loop filter but at a slower rate.

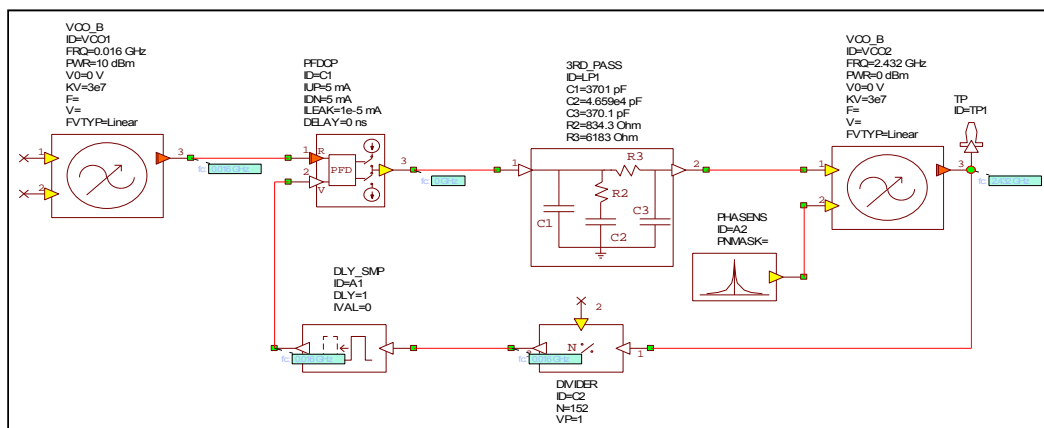


Figure 4.40: system diagram used in PLL simulations

The PLL system simulations were then performed in AWR incorporating all the system specifications stated earlier in Table 4.6 in addition to the recently designed loop filter. The system diagram used in PLL simulations is shown in Figure 4.40.

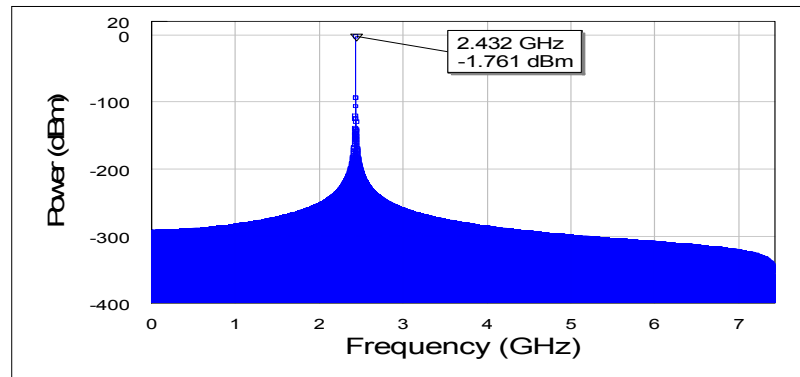


Figure 4.41: PLL output spectrum

The output spectrum of the PLL is shown in Figure 4.41. A single carrier at 2.432 GHz was obtained but surrounded by noise. The main source of the PLL noise is the VCO, the VCO phase noise was estimated. It has a noise floor  $-133\text{dBc/Hz}$  and a close-in phase noise of  $-90\text{ dB}$  at  $150\text{ Hz}$  offset. After locking the VCO to the intended carrier using the PLL through the VCO control line, the data will be applied to the VCO through the VCO modulation line. The simulator did not support VCO with two control lines thus we assumed that the lock state has been detected and then applied the data separately to the VCO as shown in Figure 4.42.

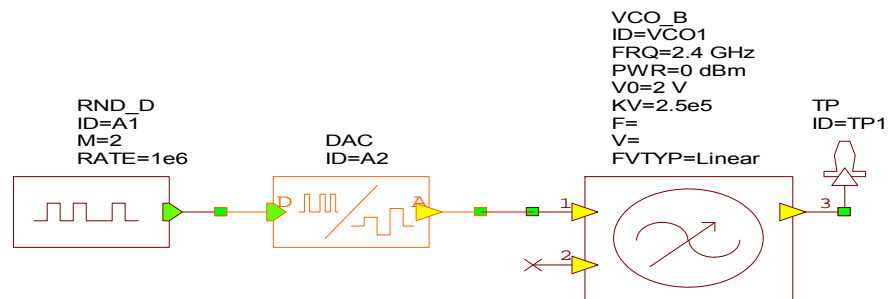


Figure 4.42: Direct VCO modulation

The modulating signal which is assumed to be the output of the sensor in the case of implantable transmitter is applied directly to the VCO control line. In order to test for the requirements of the adopted communication protocol, the maximum data rate was used in the modulating signal i.e.  $1\text{ Mbps}$ . A VCO frequency sensitivity of

0.25 MHz/V was sufficient to reflect the dynamics of the modulating data signal. The modulated signal at the output of the VCO appears as shown in Figure 4.43:

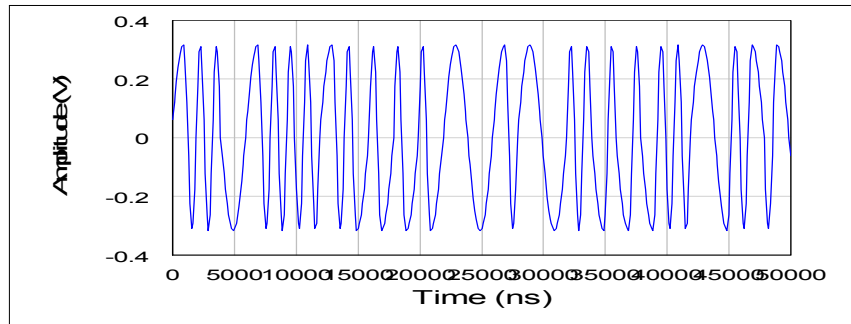


Figure 4.43: Frequency modulated data at the output of the VCO

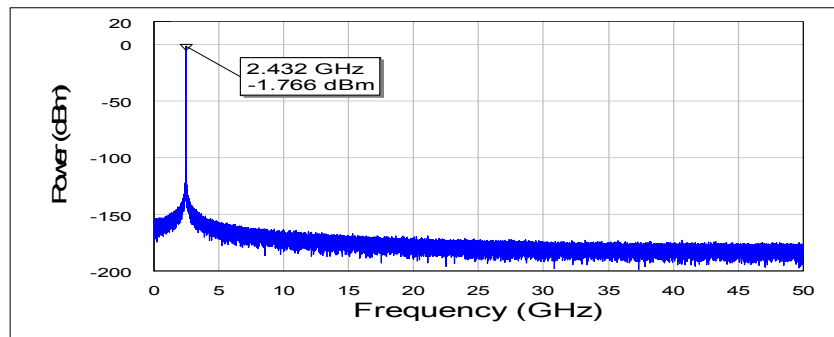


Figure 4.44: Power spectrum of VCO modulated output

In conclusion, the direct modulation principle has been demonstrated through the design of PLL that was used for locking the VCO to the intended frequency before applying the modulating data to the VCO modulation line. The modulated output signal of the VCO was a frequency modulated sinusoidal wave as shown in Figure 4.43. The output spectrum of the frequency modulated carrier located at 2.432 GHz is shown in Figure 4.44.

## 4.5 Low Power Transmitter Simulation and Results

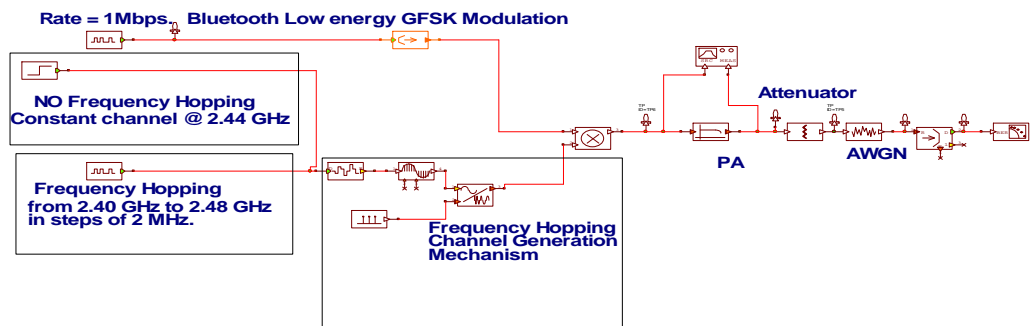


Figure 4.45: Transmitter test bench

For the purpose of simulating the complete implantable transmitter in one system unit, incorporating the PA and Bluetooth low energy transmitter and reflecting skin attenuation effect as well the environment conditions such as Additive White Gaussian Noise (AWGN) channel between the implantable transmitter and receiver unit, the transmitter test bench in Figure 4.45 above was implemented. The random real source generate real data at the maximum data rate of 1 Mbps which required for testing of Bluetooth low energy transmitters specified in [67].

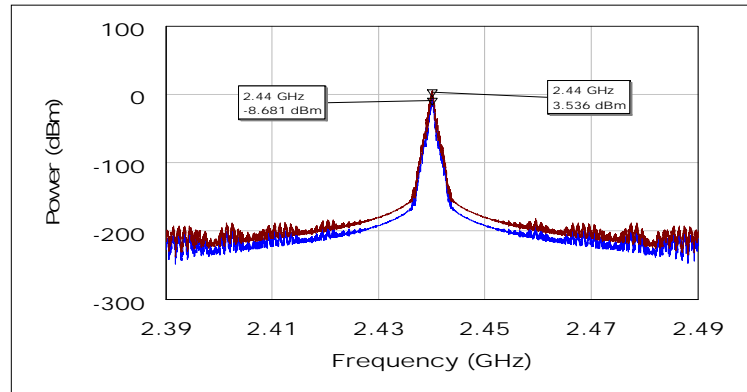


Figure 4.46: Output spectrum before (-) and after PA (-)

The signal power spectrum before and after the PA is shown in Figure 4.46. The difference between the two power levels resembles the PA power gain. As indicated earlier Bluetooth low energy channels are each 1 MHz wide. The frequency hopping occurs over the 40 channels, unlike the classic Bluetooth which hops frequency over 79 different channels. Figure 4.47 depicts the Bluetooth low energy frequency hopping characteristic, where at one instant the carrier frequency was at 2.402 GHz, in a consecutive interval the carrier was located at 2.408 GHz. This measurement was implemented by measuring the carrier signal at the output of the Bluetooth low energy GFSK modulation block in Figure 4.45 and the signal resulting from multiplying the GFSK modulated signal with FHSS signal.

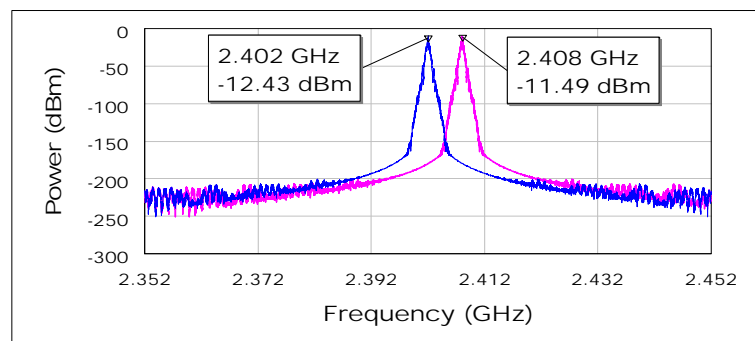


Figure 4.47: Frequency hopping of Bluetooth low energy

---

The attenuator block in Figure 4.45 resembles the skin attenuation effect. The signal at its output is attenuated by 16 dB much like the skin attenuation. It is illustrated in Figure 4.3. The RF communication channel between the transmitter and the receiver was modelled by a simple Additive White Gaussian Noise (AWGN) channel. This channel is not appropriate for typical indoor environments where multipath and fading need to be considered. This model simplifies the calculation of transmitter performance such as the Bit Error rate (BER) as will be shown shortly.

Bluetooth low energy signal is a pure frequency modulated signal, so non linear power amplification does not affect the modulated signal characteristics since no information is contained in the signal amplitude. Thus, the signal constellation is not altered by the amplitude compression in the class E PA as shown in Figure 4.48. However, after being the transmitted through AWGN channel, the constellation diagram is drastically spoiled as shown in Figure 4.49.

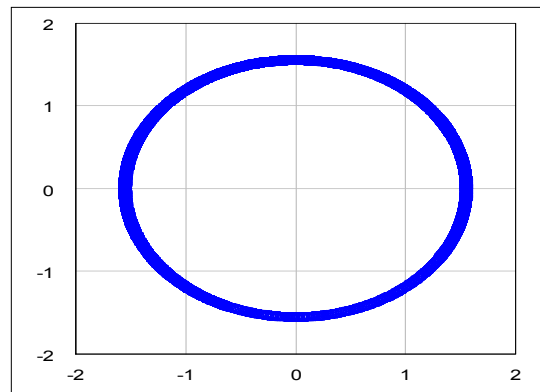


Figure 4.48: Signal constellation after the PA

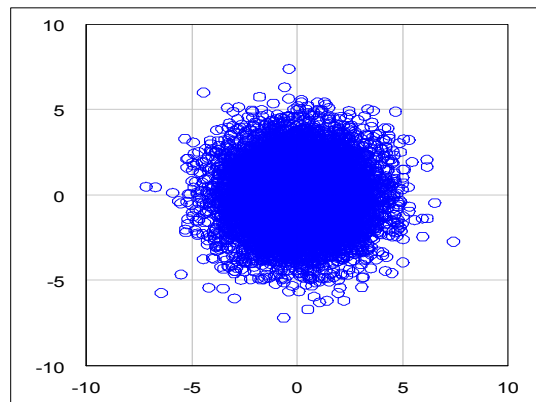


Figure 4.49: Signal constellation after AWGN channel

The recovered constellation at the receiver is shown in Figure 4.50, which fairly resembles the 2-GFSK transmitted signal.

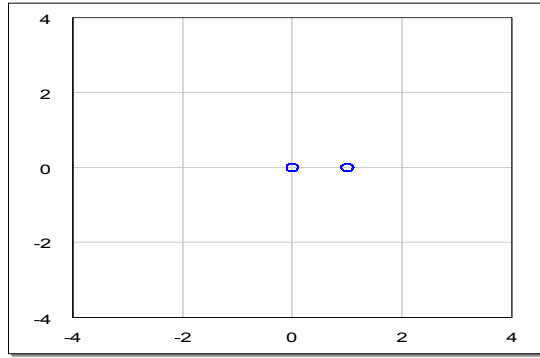


Figure 4.50: Recovered signal

The eye diagram interprets many performance characteristics of the received signal in a noisy channel. For instant, distortion of the signal waveform due to Intersymbol Interference (ISI) and noise appears as a closure of the eye pattern. The eye width reflects timing synchronization and jitter effects. The eye diagram of signal at PA output is shown in Figure 4.51. The eye is not completely open which indicates the presence of Intersymbol interference (ISI), due to signal filtering and non linear amplification.

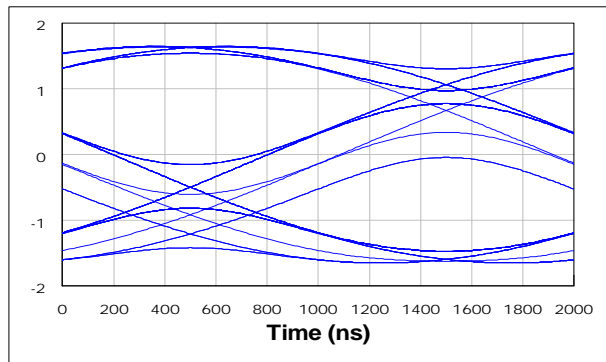


Figure 4.51: Eye diagram of signal at PA output

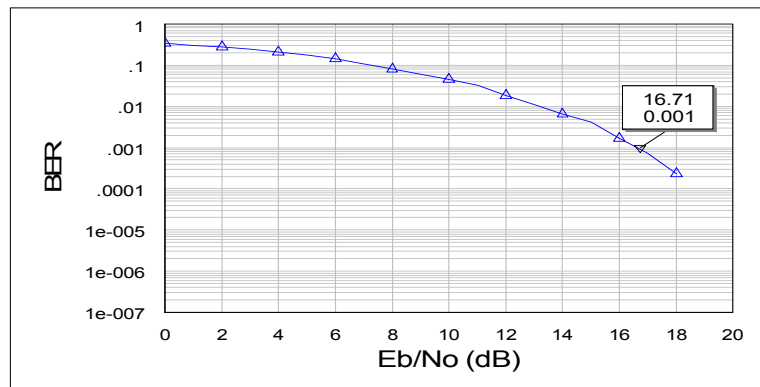


Figure 4.52: Bit Error Rate (BER)

The BER measurement is shown in Figure 4.52. The BER performance of the system is relatively poor since the receiver sensitivity BER of 0.1% is achieved at SNR value of 16.7 dB.

#### 4.5.1 Spectrum Mask Test

Within the ISM band the transmitter must pass a spectrum mask. The spectrum shall comply with 20 dB bandwidth definition in the Federal Communication Commission (FCC). In addition, an adjacent channel power on adjacent channels with a difference in RF channel number of two or greater is defined.

Table 4.8: Bluetooth low energy transmitter spectrum mask

Frequency offset	Bluetooth low energy specs.	This Transmitter design
$\pm 500$ kHz	-20 dBc	-22dBc
2MHz ( $ M - N  = 2$ )	-20 dBm	-66 dBm
3MHz or greater ( $ M - N  \geq 3$ )	-30 dBm	-87 dBm

The transmitted power was measured in a 100 kHz bandwidth. This measurement requires the transmitter to transmit pseudo random data pattern throughout the test while the frequency hopping is switched off. Table 4.8 shows the specified Bluetooth low energy transmitter power requirements and the results obtained in this design. All the three power requirements were met.

With this we conclude the part on low power transmitter design. The following section presents a system functionality scenario, where the implantable transmitter is assumed to be in service acquiring real data from a glucose sensor, important performance figures are then estimated.

#### 4.6 System Functionality Scenario

As mentioned earlier, to achieve continuous glucose monitoring, measurements need to be taken every 10 minutes. Thus the external powering unit will supply power periodically i.e. at period of 10 minutes to the implantable transmitter. The sensor needs some time to settle to the right value. This settlement time depends on the type of terminology the sensor use to extract the glucose level e.g. oxygen based, etc. It also relies on the size of the sensor or implant in general, the smaller the implant, the faster the tissue surrounding it comes to stability. It also

---

becomes less susceptible to patients movement. Figure 5.57 below illustrates glucose monitoring system functionality.

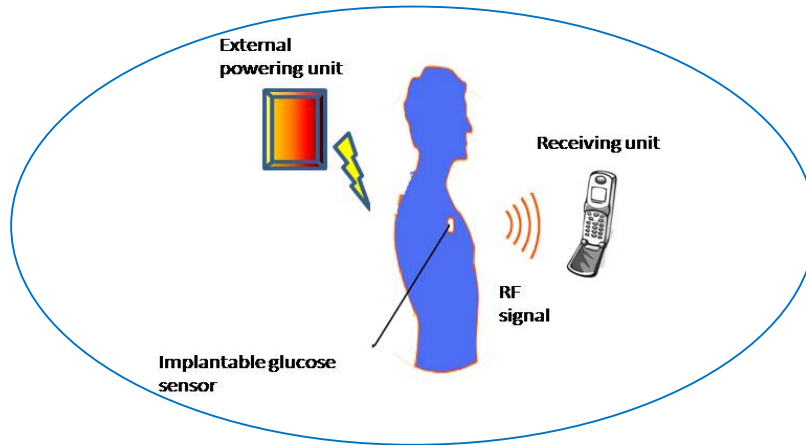


Figure 4.53: Monitoring System functionality diagram

In the following we define the state of the system in between transmission. This state is crucial for the system performance because the system will spend most of its time in this state. Thus minimizing the power consumption for this “inter-transmission” period is mandatory to achieve the desired goal of ultra low power consumption.

There are different low power states defined for system operation. The first one is sleep mode where the transmitter PA is in the off state but the clock generation circuitry is on. This mode of operation is recommended for applications that need ultrafast wake up times, complete state retention, or will only be inactive for short periods of time.

Deep Sleep mode is a state that achieves even lower power consumption with currents in the range of few nanoamperes. It is recommended for applications that are inactive for long periods of time, such as remote controls, input devices, sensors and thermometers. It is also ideal for applications that need to keep accurate time while consuming minimum power. The longer an application can stay in deep sleep mode, the lower the average current consumption of the device will be.

Depending on the wake up procedure from deep sleep mode, even clock generation circuitry can be turned off during this mode, theoretically, achieving zero power consumption.

The Ultra Low-Power Wake-Up (ULPWU) module, available on some deep sleep devices, allows a device to go into deep sleep for a certain period of time and

wake up, without using an oscillator. Because ULPWU is clock-less, it consumes less power than wake up sources that need an oscillator. Instead, ULPWU uses a slowly discharging capacitor voltage to trip a wake up after a period of time has passed [68].

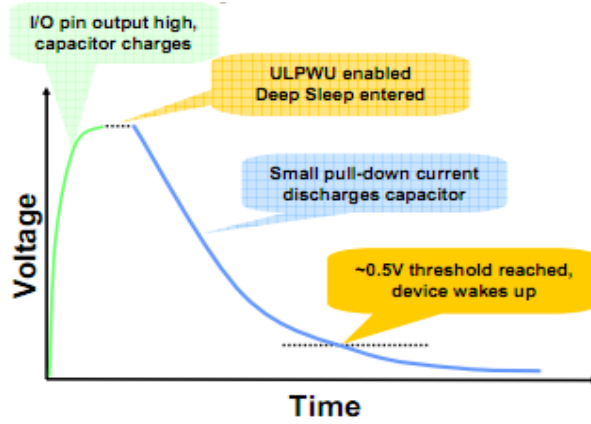


Figure 4.54: Ultra Low Power Wake-UP procedure [68]

Since the periodic transmitter wake up time is set, the time constant of this capacitor can be set to 10 minutes, which eliminates the need for a clock to provide periodic wake up. To calculate the time the system spends in deep sleep mode we need to calculate the system's duty cycle. The analysis followed in this calculation is provided below.

The sensor will be powered up first since it needs time to settle to its final value. The value reported in [3] is adopted to carry out these calculations i.e. 2 minutes. Then, the system will be powered up to transmit the measured glucose data, this includes powering up the entire system i.e. the clock generation and circuitry, data modulation circuitry, and PA.

In order to determine the time it takes to transmit the measured data, we need to know the data rate of the glucose sensor. For experimental purpose, the value given by the Dexcom Seven plus was used. The glucose sensor has a data rate of 8912 kbps.

The time it takes the implantable Bluetooth low energy transmitter which has a data rate of 1Mbps to transmit this data is:

$$T_{transmit} = \frac{Sensor_{output\ rate}}{Bluetooth\ low\ energy\ data\ rate} = \frac{8192}{1M} \approx 8ms \quad (4.32)$$

If we were to calculate the system duty cycle considering the major blocks responsible for the overall power consumption PA, clock generation and data modulation circuitries.

$$\text{system duty cycle} = \frac{.008}{10 \times 60} = 0.0013\% \quad (4.33)$$

With this very low duty cycle the ultra low power consumption goal can thus be achieved.

Wide detection range is an important figure for sensor applications. In the specific case of this transmitter design, the proposed receiver is the patient's cellular phone that supports Bluetooth low energy protocol. In this case the distance between the implantable transmitter and receiver is predicted to be small since the cellular phone is normally within the same vicinity of its owner. Yet it is still essential to know how far apart the patients can be from his/her phone while the transmitted sensor signal can be faithfully detected. An estimation of this figure is provided below.

#### 4.6.1 Maximum Detection Range

The one way maximum detection range can be defined is at the distance at which the receiver can faithfully detect and reproduce the transmitted signal. In order to calculate this range to a figure, merits needs to be calculated first, receiver sensitivity and the received signal strength.

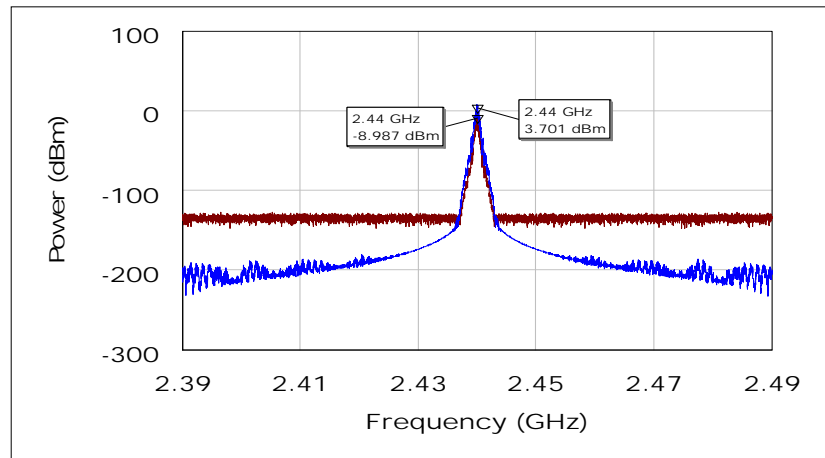


Figure 4.55: Signal after PA (-) and after attenuator (-)

Bluetooth low energy specifies a receiver sensitivity of -70 dBm or higher, thus we can calculate the loss we can tolerate given a certain transmitter output power level. Referring to Figure 4.55, the signal after the attenuator that resembles the skin

effect on the transmitted signal is approximately -9 dBm. From which we calculate the maximum power loss that can be tolerated as follows:

$$\begin{aligned} \text{Power loss} &= \text{Transmitted signal power} - \text{receiver sensitivity} \\ &= -9 - (-70) = 61 \text{ dB} \end{aligned} \quad (4.34)$$

In indoor environments where not only free space loss is encountered but multipath propagation as well, using Equation (4.35) below is more accurate to estimate the loss rather than the free space model.

$$L(\text{dB}) = P_{d0} + 10 \cdot n \cdot \log\left(\frac{d}{d0}\right) \quad (4.35)$$

Where  $L$  is the loss in dB,  $P_{d0}$  is the loss at  $d0$  which is the boundary between near and far field regions,  $n$  is the path loss exponent which depends on the environment and  $d$  is the distance at which the loss is to be estimated.

Referring to Section 4.3.1, the far field boundary at 2.4GHz is given by:

$$\frac{\lambda}{2\pi} = \frac{3 \times 10^8}{2.4 \times 10^9 \times 2\pi} = 1.98 \text{ cm} \quad (4.36)$$

The power loss at a distance  $d0$  ( $P_{d0}$ ) can be calculated using the free space path loss (FSPL) model given by Equation (4.37) below:

$$FSPL = 20 \log(d) + 20 \log(f) - 147.55 \quad (4.37)$$

Where  $d$  is the distance in m, and  $f$  is the frequency in Hz.

The loss at  $d0$  can then be calculated as follows:

$$P_{d0} = 20 \log(.0198) + 20 \log(2.4 \times 10^9) - 147.55 = 5.98 \text{ dB} \quad (4.38)$$

Applying this number to Equation (4.35) and solving for  $d$ , in indoor environments a typical value for  $n$  is 3 [69]:

$$\begin{aligned} 61 &= 5.98 + 10.3 \cdot \log\left(\frac{d}{0.0198}\right) \\ d &= 10^{\frac{61-5.98}{30}} \times 0.0198 = 1.35 \text{ m} \end{aligned} \quad (4.39)$$

Thus distance between the implantable transmitter and the receiver i.e. cellular phone is approximately in the range of 1.35 meters. This will not be hard to achieve if, for example, the patients were asked to keep their phones in their pockets all the time.

---

## CHAPTER 5

### CONCLUSION AND FUTURE WORK

In this research the design methodology and techniques for low power subcutaneous transmitter have been established. These design concepts introduced can serve as a base for implementation of miniaturized autonomous transmitter unit. This chapter starts by analyzing the results findings presented in the previous chapter. Then recommendations for alternative research methodologies and suggested future work are highlighted.

The RF signal interaction with the biological tissue has been characterized to estimate the amount of power gain needed from both the implantable transmitter and the external power unit PAs. Since the implantable is intended to be subcutaneous, the model used considered a single biological layer i.e. skin.

In Section 4.6, when calculating the system duty cycle, it is noticed that the settling time of the sensor is several orders of magnitude more than the time needed for data transmission, i.e. 2 minutes compared to 8 ms. This settling time adds an overhead power. It is crucial to reduce this settling time which can be considered as a setup time to be much less than the transmit time.

It is worth mentioning that the scope of this work is considerably large. The long term objective of this research is to build an implantable glucose monitoring system. It is recommended that the design of the complete system is divided into three major branches. Sensor and data acquisition, system architecture, and circuit design. This work is a mixture of the last two branches. Recommendations for work to be done in these three design lanes are given below:

As stated previously minimizing the sensor settling time is essential to achieve low duty cycles and consequently the goal of low power consumption. This time depends mainly on the technique of measurement i.e. to measure the glucose level or measure the interstitials fluid oxygen level through which the glucose level is estimated. Sensor miniaturization also helps to reduce this time, as sensor becomes less vulnerable to movement and displacement.

---

At the system level, a well defined scenario on how to operate the system must be set. When to operate the system, for how long, which units would be put to sleep and if enough power is being supplied to the system are all issues that need to be addressed. To reduce the work load on the implantable transmitter, we suggest putting a counter on the external power unit to provide periodic power supply. In that case the implantable transmitter clock can be turned completely off i.e. deep sleep in the inter-transmission time. This can be accomplished by using (ULWP) procedure described in Section 4.6.

As an elevation to the sensor long settling time, and to avoid powering the entire system while the sensor is still taking the measurement, we propose using a small internal capacitor in the implantable system. This capacitor charges while power is supplied inductively to the implantable transmitter. It serves as a local battery for the sensor, so as to enable it to take the measurement in advance. Thus the transmitter unit will be powered up once there is data ready for transmission.

Originally this work was based on ZigBee wireless protocol. One year later Bluetooth low energy was released. It was found to provide the least power consumption compared to other available wireless protocols at the time this work was conducted. Since wireless technology is continuously improving; in future work this point needs to be reinvestigated to ensure that the optimum wireless protocol is employed.

With regards to circuits, a differential design for both class E PA should be considered since differential design is less susceptible to noise and interference.

Once the goal of ultra low power consumption is achieved, energy scavenging techniques can be employed to make the implantable unit power autonomous. This field is an active area of research. Recent research trends show that power can be extracted from the blood sugar itself [70].

---

## REFERENCES

- [1] E. Lopelli, J. Van der Tang, A. Roermund, *System-level analysis of an Ultra-low power, low data-rate FHSS transceiver*, Nov., 2004. [Online]. Available: <http://www2.stw.nl/programmas/prorisc/proc2000/> [Accessed: Oct., 10, 2010]
- [2] Intensive blood-glucose control with sulphonylureas or insulin compared with conventional treatment and risk of complications in patients with type 2 diabetes, *UK Prospective Diabetes Group UKPDS 33 Lancet*, vol. 12, Sep. 1998, pp.837-853.
- [3] M. Ahmadi, G. Jullien, "A Wireless Implantable Microsystem for Continuous Blood Glucose Monitoring", *IEEE Trans. Biomed. Eng.*, vol. 3, no. 3, pp. 169-180, Jun., 2009.
- [4] SMSI® Glucose Sensor (in development), Jul., 2009. [Online]: Available: [http://www.s4ms.com/products\\_glucose.htm/](http://www.s4ms.com/products_glucose.htm/) [Accessed: Apr., 20, 2009]
- [5] K. Iniewski, *VLSI Circuits for Biomedical Applications*, 1<sup>st</sup> ed., Artech House, 2008.
- [6] A. Chi Wai Wong, Ganesh Kathiresan, Chung Kei Thomas Chan, Omar Eljamaly, Okundu Omeni, Declan McDonagh, Alison J. Burdett, and Christofer Toumazou, "A 1 V Wireless Transceiver for an Ultra-Low-Power SoC for Biotelemetry Applications", *IEEE J. Solid-State Circuits*, vol. 43, no. 7, pp. 1511-1520, Jul., 2008.
- [7] P. Bradley, "Implantable ultralow-power radio chip facilitates in-body communications," in *Semiconductor Technology*, 2007, pp. 20-24.
- [8] *TSI EN 301-839*, Parts 1 and 2 and *ETSI EN 301-489 Part 27*.
- [9] *Subparts E (95.601-95.673) and I (95.1201-95.1219) Personal Radio Services*, FCC Rules and Regulations 47 CFR Part 95, 2002.
- [10] M. D. Mey, C. Christensen, S. Blanchard, "Design concepts for wireless communication in implantable medical applications," in *Analog Circuit Design*, Springer, 2006, pp. 331–343.
- [11] Y. H. Chee , "Ultra Low Power Transmitter for Wireless Sensor Networks", Dept. of Elect. and Comput. Sci., Berkeley CA, 2006.
- [12] Y. H. Chee, A.M. Niknejad, J. Rabaey, "A 46% Efficient 0.8dBm Transmitter for Wireless Sensor Networks," *IEEE Symp. VLSI*, Jun., 2006.
- [13] B. J. Gilligan, M. C. Shults, R. K. Rhodes, P. G. Jacobs, J. H. Brauker, T. J. Pintar, and S. J. Updike, "Feasibility of continuous long-term glucose monitoring from a subcutaneous glucose sensor in humans," *Diabetes Technol. Ther.*, vol. 6, no. 3, pp. 378–386, 2004.
- [14] A. Johanson, "Wireless Communication with Medical Implants: Antennas and Propagation", Competence Centre for Circuit Design, Lund University, Lund, Sweden, June, 2004.
- [15] J. G. Webster, *Design of Cardiac Pacemakers*, IEEE Press, 1995.
- [16] Recommendation ITU-R SM.1056, *International Telecommunication Union*, 1994.
- [17] *SIG introduces Bluetooth low energy wireless technology, the next generation of Bluetooth wireless technology*, Dec, 2009. [Online]. Available: <http://www.businesswire.com/news/home/SIG-Introduces-Bluetooth-Energy-Wireless-Technology-Generation> [Accessed: Dec., 20, 2009]

- 
- [18] ZigBee Alliance, *ZigBee RF4CE Overview*, Mar, 2009. [Online]. Available: <http://www.zigbee.org/Specifications/ZigBeeRF4CE/Overview.aspx>
- [19] P. Heydari, "A study of low-power ultra wideband radio transceiver architectures", in *Wireless Communications and Networking Conf.*, 2005, pp. 758–763.
- [20] I. D. O'Donnell and R. W. Brodersen, "An ultra-wideband transceiver architecture for low power, low rate, wireless systems", *IEEE Trans. Veh. Technol.*, vol. 54, pp. 1623–1631, Sept. 2005.
- [21] R. G. Vaughan, N. L. Scott, and D. R. White, "The theory of bandpass sampling," *IEEE Trans. Signal Processing*, vol. 39, pp. 1973–1984, Sept. 1991.
- [22] B. Otis, Y. H. Chee, and J. Rabaey, "A 400  $\mu$ W-RX, 1.6 mW-TX super-regenerative transceiver for wireless sensor networks," in *International Solid-State Circuit Conf.*, 2005, pp. 396–397.
- [23] S. M. Schwartz, *Frequency Hopping Spread Spectrum (FHSS) vs. Direct Sequence Spread Spectrum (DSSS) in Broadband Wireless Access (BWA) and Wireless LAN (WLAN)*. [Online]. Available: [http://sorin-schwartz.com/white\\_papers/fhvsds.pdf](http://sorin-schwartz.com/white_papers/fhvsds.pdf) [Accessed: Apr., 6, 2010]
- [24] E. Lopelli, J. Van der Tang, A. Van Roermund, "A 1 mA Ultra-Low-Power FHSS TX Front-End Utilizing Direct Modulation With Digital Pre-Distortion," *IEEE J. Solid-State Circuits*, vol.42, no.10, pp.2212-2223, Oct. 2007.
- [25] R. D. Beach, F. V. Kuster, and F. Moussy, "Towards a miniature implantable in-vivo telemetry monitoring system dynamically configurable as a potentiostat or galvanostat for two- and three-electrode biosensors," *IEEE Trans. Instrum. Meas.*, vol. 54, no. 1, pp. 61–72, Feb. 2005.
- [26] M. Chaplin, C. Bucke, *Enzyme Technology*. [Online]. Available: <http://www.lsbu.ac.uk/biology/enztech/index.html> [Accessed: Jan., 23, 2011]
- [27] S. K. Garg, S. Schwarts, and S. V. Edelman, "Improved Glucose Excursions Using an Implantable Real-Time Continuous Glucose Sensor in Adults With Type1 Diabetes," *Diabetes Care*, Vol. 27, No. 3, 2004.
- [28] *Free Style Navigator Continuous Glucose Monitoring system*. [Online]. Available: <http://www.freestylenavigator.com> [Accessed: Oct., 23, 2010]
- [29] *The Guradian Real-Time Conitonus Glucose Monitoring System*. [Online]. Available: <http://www.minimed.com/products/guardian.html> [Accessed: Oct., 23, 2010]
- [30] V. Lodwig, L. Heinemann, "Continuous Glucose Monitoring with Glucose Sensors: Calibration and Assessment Criteria," *Diabetes Technol. Ther.*, vol. 5, no. 4, pp. 573–587, 2003.
- [31] (2010). *Continuous Glucose Sensors. children with Diabetes*. [Online]. Available: <http://www.childrenwithdiabetes.com/continuous.htm> [Accessed: Oct., 23, 2010]
- [32] *Interoperability*. [Online]. Available: <http://en.wikipedia.org/wiki/Interoperability> [Accessed: Nov., 12, 2010]
- [33] E. Lopelli, J.D van der Tang, A.H.M van Roermund, "Ultra low-power spread spectrum transmitters and receivers," in *Analog Circuit Design*, Springer, 2006, pp. 377–411.
- [34] G. Thoonen, "Ultra-low power wireless transmitters", M.S. thesis, Dept. Elect. Eng., Eindhoven Uni. Technology, Eindhoven, the Netherlands, 2004.
-

- 
- [35] Bluetooth SIG., *Bluetooth Low Energy Technology- Technical Info*. [Online]. Available: [http://www.bluetooth.com/Bluetooth\\_Low\\_Energy\\_Technology\\_Technical\\_Info.htm](http://www.bluetooth.com/Bluetooth_Low_Energy_Technology_Technical_Info.htm) [Accessed: Dec., 20, 2009]
- [36] A. More, *Reducing Health Care Costs with Bluetooth Low Energy Technology*. [Online]. Available: [http://www.bluetooth.com/Reducing\\_healthcare\\_costs.htm](http://www.bluetooth.com/Reducing_healthcare_costs.htm) [Accessed: Dec., 1, 2010]
- [37] P. Choi, "An experimental con-sized radio for extremely low power WPAN (IEEE 802.15.4) application at 2.4 GHz", *Tech Dig., Int. Solid State Circuits Conf.*, 2003, pp. 92-93
- [38] Texas Instruments, *2.4 GHz IEEE 802.15.4 / ZigBee-ready RF Transceiver*, 2007. [Online]. Available: <http://focus.ti.com/lit/ds/symlink/cc2420.pdf> [Accessed: Dec., 9, 2009]
- [39] S. Cho and A. P. Chandrakasan, "A 6.5 GHz energy efficient BFSK modulator for wireless sensor applications," *IEEE J. Solid-State Circuits*, vol. 39, pp. 731-739, May 2004.
- [40] V. Karam, P.H.R Popplewell, A. Shamim, J. Rogers and C. Plett, , "A 6.3 GHz BFSK Transmitter with On-Chip Antenna for Self-Powered Medical Sensor Applications," *IEEE Radio Freq. Integrated Circuits Symp.*, pp.101-104, 2007.
- [41] A. Yamagishi, M. Ugajin and T. Tsukahara, "A 1 V 2.4 GHz PLL synthesizer with a fully differential prescaler and low-off-leakage charge pump," *IEEE MTT-S Int Microw. Symp.*, pp. 733-736, Jun., 2003.
- [42] D. Banerjee, *PLL Performance, Simulation, and Design*, 4<sup>th</sup> ed., 2006, pp. 9-186.
- [43] D. Gough, K. Kertuz-Delgado, and T. Bremer, "Frequency characterization of blood glucose dynamics", *Ann. Biomed. Eng.*, vol. 31, no. 1, pp. 91-97, 2003.
- [44] K. Torvmark, *Bluetooth low energy frequency hopping* [Online]. Available: <http://www.bluetooth.com/SiteCollectionDocuments/Bluetoothlowenergyfrequencyhopping.pdf> [Accessed: Apr., 5, 2010]
- [45] M. Ali, L. Albasha, and H. Alnashash, "A system study of a wireless subcutaneous transmitter," *Int. Symp. Mechatronics and its Applications*, Sharjah, Apr. 2010.
- [46] S. C. Cripps, *RF power amplifiers for wireless communications*, 2<sup>nd</sup> ed., Artech House, 2006.
- [47] T. Dellsperger, "Device Evaluation for Current-Mode Class-D RF Power Amplifiers", Diploma Thesis, Dept. Info. Technology Elect. Eng., Swiss Federal Institute of Technology Zurich, Switzerland, Aug., 2003.
- [48] A. Shameli, P. Heydari, "A Novel Power Optimization Technique for Ultra-Low Power RFICs," *Proc. Int. sympos. Low power electronics and design*, Tegernsee, pp. 274-279, 2006.
- [49] P. Si, A.P Hu, J.W Hsu, M. Chiang, Y. Wang, S. Malpas, and D. Budgett, "Wireless Power Supply for Implantable Biomedical Device Based on Primary Input Voltage Regulation," *IEEE Conf. Ind. Electron. Apps.*, Harbin, pp.235-239, 23-25, 2007.
- [50] Journal of Energy Harvesting, *Solar powered implantable glucose sensor for diabetic*. [Online]. Available: <http://www.energyharvestingjournal.com/articles/solar-powered-implanted-glucose-monitor-for-diabetics-00002110.asp?sessionid=1> [Accessed: Dec., 10, 2010]
-

- 
- [51] S. Atluril, M. Ghovanloo, "A Wideband Power-Efficient Inductive Wireless Link for Implantable Microelectronic Devices Using Multiple Carriers," *Int. symps. Circuits and Systems*, Island of Kos, Greece, 2006, pp. 1131-1134.
- [52] Tutorial overview of inductively coupled RFID systems, 2003. [Online]. Available: <http://www.mobiusconsulting.com/papers/rfidsystems.pdf> [Accessed: Sept., 30, 2010]
- [53] B. Noureddine, M. Mohamed, and K. Smain, "Attenuation in Transferred RF Power to a Biomedical Implant due to the Absorption of Biological Tissue", in *Proc world academy of science, eng. technology*, Vol. 10, Dec. 2005.
- [54] C. Furse, D. Christensen, C. Dur, *Basic Introduction to Bioelectromagnetics*, 2<sup>nd</sup> ed., CRC Press, 2009.
- [55] F. Barnes, B. Greenebaum, "Chapter 3: Dielectric Properties of Biological Materials," in *Handbook of Biological Effects of Electromagnetic Fields*, CRC Press, 2007.
- [56] C. Gabriel, S. Gabriel, F. Corthout, "The dielectric properties of biological tissues: I. Literature Survey," in *Phys Med. Biol.*, vol. 41, 1996, pp 2231–2249.
- [57] S. Gabriel S, R. Lau, C. Gabriel, "The dielectric properties of biological tissues: II. Measurements in the frequency range of 10 Hz to 20 GHz," in *Phys. Med. Biol.*, Vol. 41, 1996, pp. 2251–2269.
- [58] Guidelines for limiting exposure to time varying electric, magnetic and electromagnetic fields (up to 300 GHz), in *Health Phys., Int. Commission on Non Ionizing Radiation Protection*, vol. 74, 1998, pp. 495–523.
- [59] *IEEE Standard for Safety Levels with Respect to Human Exposure to Radio Frequency Electromagnetic Fields*, 3 kHz to 300 GHz, pp. 1 – 238, 2006.
- [60] Glenn Elert et al., "Surface Area of Human Skin", *The Physics Factbook*, 2001. [Online]: Available: <http://hypertextbook.com/facts/2001/IgorFridman.html> [Accessed: Dec., 10, 2010]
- [61] Aurélie Laurent, Frédéric Mistretta, David Bottiglioli, Karima Dahel, Catherine Goujon, Jean François Nicolas, Anca Hennino and Philippe E. Laurent, "Echographic measurement of skin thickness in adults by high frequency ultrasound to assess the appropriate microneedle length for intradermal delivery of vaccines", *Vaccine*, vol. 25, no. 34, Aug., 2007, pp. 6423-6430.
- [62] J. Rogers, K. Plett, *Radio Frequency Integrated Circuit Design*, Artech House, 2003.
- [63] A. Laskovski , M. Yuce, and T. Dissanayake, *Practical Considerations for High Frequency Inductive Links*, University of New Castle, Australia, 2008. [Online]. Available: <http://www.eng.newcastle.edu.au/~mry122/spie2008.pdf> [Accessed: Sept., 30, 2010]
- [64] G. Bawa, A. Huang, M. Ghovanloo, "An efficient 13.56 MHz Active Back-Telemetry Rectifier in Standard CMOS Technology", In *proc. IEEE Int, circuits and systems Symps.*, Paris, pp. 1201-1204, May, 2010.
- [65] M. Ali, L. Albasha, H. Alnashash, "A Bluetooth low energy implantable glucose monitoring system", submitted for publication, *European Microwave Conf.*, Manchester, Oct., 2011.
- [66] D. Banerjee, D. Brown, K. Nguyen, Loop Filter Optimization. [Online]. Available: [http://www.national.com/AU/files/loop\\_filter\\_optimization.pdf](http://www.national.com/AU/files/loop_filter_optimization.pdf) [Accessed: Mar., 10, 2009]
-

- 
- [67] Bluetooth SIG, *Bluetooth specification version 4.0*. [Online]. Available:  
<http://www.bluetooth.com> [Accessed: Dec., 26, 2009]
- [68] Microchip web seminars, *Deep Sleep Lowest-Power Sleep Mode*. [Online]. Available:  
[http://techtrain.microchip.com/webseminars/documents/DeepSleep\\_121808.pdf](http://techtrain.microchip.com/webseminars/documents/DeepSleep_121808.pdf) [Accessed:  
Dec., 12, 2010]
- [69] J. Davis, *Indoor Wireless RF channels*, [Online]. Available:  
<http://www.wirelesscommunication.nl/reference/chaptr03/indoor.htm> [Accessed: Feb. 18, 2011]
- [70] *Energy Harvesting*, Aug., 2007. [Online]. Available:  
[http://en.wikipedia.org/wiki/Energy\\_harvesting#cite\\_note-22](http://en.wikipedia.org/wiki/Energy_harvesting#cite_note-22) [Accessed: Dec., 15, 2010]

---

## Appendix

### Bluetooth Low Energy Technical Details

- Data Transfers: supports very short data packets (8 octets minimum up to 27 octets maximum) that are transferred at 1 Mbps. All connections use advanced sniff-subrating to achieve ultra low duty cycles.
- Frequency Hopping: uses the adaptive frequency hopping common to all versions of *Bluetooth* technology to minimize interference from other technologies in the 2.4 GHz ISM Band.
- Host Control: places a significant amount of intelligence in the controller, which allows the host to sleep for longer periods of time and be woken up by the controller only when the host needs to perform some action. This allows for the greatest current savings since the host is assumed to consume more power than the controller.
- Latency: can support connection setup and data transfer as low as 3ms, allowing an application to form a connection transfer authenticated data in few milliseconds for a short communication burst before quickly tearing down the connection.
- Range: Increased modulation index provides a possible range for over 100 meters.
- Robustness: uses a strong 24 bit CRC on all packets ensuring the maximum robustness against interference.
- Strong security: Full AES-128 encryption using CCM to provide strong encryption and authentication of data packets.
- Topology: uses a 32 bit access address on every packet for each slave, allowing billions of devices to be connected. The technology is optimized for one-to-one connections while allowing one-to-many connections using a star topology.

---

## VITA

Mai Ali was born on Dec. 10, 1987, in Khartoum, Republic of Sudan. She was educated in government and private schools and graduated from Omdurman model Secondary School in 2003. She then got enrolled in University of Khartoum, Sudan from which she graduated with Honours in 2008. Her degree was Bachelor of Science in Electrical Engineering. Ms. Ali received a graduate teaching assistantship to join the master's program in Electrical Engineering at the American University of Sharjah.